AN ACCOUNT OF CHEMICAL AND MECHANICAL REGULATION OF TRPC6 CHANNELS IN PODOCYTES

A Dissertation

Presented to

the Faculty of the Department of Biology and Biochemistry

University of Houston

In Partial Fulfillment

of the Requirements for the Degree

Doctor of Philosophy

By

Marc Anderson

May 2013

AN ACCOUNT OF CHEMICAL AND MECHANICAL REGULATION OF TRPC6 CHANNELS IN PODOCYTES

_____

Marc Anderson

APPROVED:

_____

Dr. Stuart Dryer, Chairman

_____

Dr. Preethi Gunaratne

_____

Dr. David Sheikh-Hamad
Baylor College of Medicine

_____

Dr. Jokubas Ziburkus

_____

Dr. Mark A. Smith, Dean
College of Natural Sciences and Mathematics

PREFACE

The mind is its own place, and in itself

Can make a Heav'n of Hell, a Hell of Heav'n.

-John Milton, *Paradise Lost*

AN ACCOUNT OF CHEMICAL AND MECHANICAL REGULATION OF TRPC6 CHANNELS IN PODOCYTES

An Abstract of a Dissertation

Presented to

the Faculty of the Department of Biology and Biochemistry

University of Houston

In Partial Fulfillment

of the Requirements for the Degree

Doctor of Philosophy

By

Marc Anderson

May 2013

ABSTRACT

Podocytes play a dynamic role in regulating glomerular filtration. The focus here is on the regulatory mechanisms of podocyte expressed transient receptor potential 6 (TRPC6) channels, an ion channel implicated in certain forms of proteinuric kidney disease. TRPC6 channels are polymodal and can be activated by either chemical or mechanical stimuli. Chemical stimulation is mediated by surface-expressed receptors, and the roles of angiotensin II type 1 receptors (AT1R), insulin receptors, and N-methyl-D-aspartate receptors (NMDAR) on TRPC6 activity are studied here. In acutely isolated rat glomeruli, angiotensin causes an upregulation of TRPC6 activity, and this is mediated by the $G_{\alpha q}$ /PLC pathway. This angiotensin-evoked upregulation is partially dependent on the formation of reactive oxygen species (ROS). In mouse podocyte cell lines, insulin causes upregulation of TRPC6 through increasing ROS formation via NADPH oxidase 4 (NOX4). Similarly, NMDAR activation upregulates TRPC6, albeit through NOX2. The previously uncharacterized podocyte NMDAR has unusual properties with strong physiological implications. Specifically, podocyte NMDA receptors are essentially unresponsive to L-glutamate and L-aspartate and do not show glycine-mediated potentiation. These receptors respond to the agonists L-homocysteate and D-aspartate with large ionic currents that are potentiated by D-serine. Given their resistance to L-glutamate-induced activation, podocyte NMDA receptors likely do not act in a localized glomerular signaling system. However, their response to ligands that circulate in both the normal and pathological state suggests a role for podocyte NMDA receptors in normal

glomerular function. Receptor-driven upregulation of TRPC6 comprises a class of potential targets for prevention and treatment of multiple acquired kidney diseases. Independent of receptor-mediated response, TRPC6 channels are mechanosentive and can be activated by membrane deformation in both podocyte cell lines and isolated glomeruli. This mechanosensitivity is repressed by podocin, a cholesterol-binding, membrane-associated partner of the TRPC6 channel. In addition, podocin mediates diacylglycerol activation of TRPC6, suggesting that podocin determines the favored mode of TRPC6 activation in podocytes. It is possible that disruption of the podocin-TRPC6 complex at the slit diaphragm contributes to Ca^{2+} overload and eventual foot process effacement. Drugs that selectively target and suppress TRPC6 mechanosensitivity could potentially serve as treatments for glomerular diseases.

TABLE OF CONTENTS

LIST OF ILLUSTRATIONS AND FIGURES

LIST OF ABBREVIATIONS AND ACRONYMS

Abbreviation or Acronym	Full Name
ABD	agonist-binding domain
ACTN4	α-actinin 4
AMPA receptor	α-amino-3-hydroxy-5-methyl-4-isoxazole propionic acid receptor
AII / AngII	angiotensin II
AT1R	angiotensin II type 1 receptor
BK_{Ca} channel	large-conductance Ca^{2+}-activated K^+ channel
CD2AP	cluster of differentiation 2-associated protein
CRIB	calmodulin and IP3 receptor-binding
D609	tricyclodecan-9-xanthogenate
DAG	diacylglycerol
D-APV	D-2-aminophosphovaleric acid
DPI	diphenylene iodium
EC_{50}	half maximal effective concentration
FSGS	focal segmental glomerularsclerosis
$G\alpha_q$	heterotrimeric G protein alpha q subunit
GBM	glomerular basement membrane
GPCR	G-protein coupled receptor
GsMTx-4	*Grammostola spatulata* mechanotoxin-4
HC	L-homocysteine
HCA	L-homocysteate
IP_3	inositol 1,4,5-trisphosphate
KAR	kainate receptor
L689,560	trans-2-carboxy-5,7-dichloro-4-phenylaminocarbonyl amino-1,2,3,4-tetrahydroquinoline
MK-801	dizocilpine

MMP	matrix metalloproteinase
MnTBAP	manganese (III) tetrakis (4-benzoic acid) porphyrin chloride
NFAT	nuclear factor of activated T-cells
NMDAR	N-methyl-D-aspartate receptor
NOX	nicotinamide adenine dinucleotide phosphate-oxidase
NTD	N-terminal domain
OAG	1-oleoyl-2-acetyl-sn-glycerol
ONO-RS-082	2-(p-amylcinnamoyl) amino-4-chloro benzoic acid
PIP_2	phosphatidylinositol 4,5-bisphosphate
PKC	protein kinase C
PKG	protein kinase G
PLA	phospholipase A
PLC	phospholipase C
ROS	reactive oxygen species
SKF-96365	1-[2-(4-methoxyphenyl)-2-[3-(4-meth oxyphenyl)propoxy]ethyl-1H-imidazole hydrochloride
TRPC	transient receptor potential canonical
U73122	1-[6-[((17β)-3-Methoxyestra-1,3,5[10]-trien-17-yl)amino]hexyl]-1H-pyrrole-2,5-dione

1 INTRODUCTION

1.1 Glomerular Filtration and Podocytes:

The kidneys are responsible for the removal of toxins and waste products from the blood, and the functional unit of the kidneys is the nephron. The nephron itself is further divided into the renal corpuscles, located in the cortex of the kidney, and the renal tubules that descend into medulla of the kidneys (24, 35). The human kidneys possess approximately 2.5 million renal corpuscles that serve as the initial site of blood filtration. The renal corpuscle is comprised of glomerular capillaries and the glomerular capsule (24, 73). Blood enters the renal corpuscle via the afferent arteriole and passes into the glomerular capillaries. Here, water and small molecules from the plasma pass through the capillary wall and into the urinary space where they become known as the ultrafiltrate (93). At the same time cells and proteins are retained in the capillary loop and exit the corpuscle through the efferent arteriole. With a normal filtration rate of approximately 125 ml per minute, the kidneys filter about 180 liters in a 24-hour period. Of this, only 1.5 liters is excreted in the form of urine while the remaining majority is reabsorbed by the renal tubules. Protein loss is minimal, with greater than 99.99% of the plasma proteins prevented from ever entering the ultrafiltrate (46, 93). It is the capillary wall that ultimately acts as the filtration barrier of the glomerulus, and it is composed of three main components. First, the capillaries have an endothelial layer with many pore-like openings known as fenestrations that allow for the filtration of the blood plasma. Surrounding the endothelial layer is the glomerular basement membrane (GBM). The GBM is an acellular matrix of proteins that acts as both a size and charge selective filter to prevent passage of

proteins into the ultrafiltrate (46, 93). Typically, the GBM has a thickness of 300 to 350 nm, and it is composed of type IV collagen, laminin, heparan sulfate proteoglycan, and other extracellular proteins (43). The components of the GBM are largely produced by the third layer of the glomerular filtration barrier, specialized epithelial cells known as podocytes. In addition to the podocytes, mesangial cells provide structural support for the capillary wall and serve a phagocytic function (2, 73). Mesangial cells may play a role in altering glomerular filtration rate by controlling the blood flow through the glomerular capillaries, but it is now thought that the podocytes that play the more significant role of regulating the contents of the ultrafiltrate (73, 93). Podocyte structural abnormalities, specifically foot process effacement, invariably lead to proteinuric pathologies and are an indicator of most glomerular diseases (24, 34, 43).

Podocytes are terminally differentiated cells that surround the glomerular capillaries within the kidney (73, 93). When functioning properly, podocytes prevent the loss of most plasma proteins by producing the acellular components of the GBM and acting as a physical barrier by sheathing the capillaries with structures known as foot processes (43, 73). In addition to the structural components of the GBM, podocytes also produce matrix metalloproteinases (MMPs) that are important for remodeling and maintaining the GBM (43). The basement membrane domain of podocyte foot processes is anchored to the GMB via integrin- and dystroglycan-based adhesion complexes. These complexes facilitate contact mediated signaling, and podocyte-GMB contacts are necessary for maintaining podocyte structure. The foot processes of neighboring podocytes regularly interdigitate to form filtration slits with a uniform width of approximately 40 nm that act as a size-selective filtration barrier (35).

Spanning these filtration slits is the slit diaphragm, a mesh-like network of membrane-bound proteins that physically couple adjacent podocytes (4, 24). Many of the proteins that make up the slit diaphragm have been identified, including nephrin, CD2-associated protein (CD2AP), podocin and neph 1-3 (Illustration 1) (4, 46, 56, 57). These adhesion and cytoplasmic adapter proteins are thought to play a role in detecting cell membrane deformation and initiating signaling pathways that regulate the dynamic properties of podocyte foot processes (4). Nephrin has an extracellular domain that extends between neighboring foot processes and interacts with itself in *trans*. By spanning the slit diaphragm, nephrin is positioned to detect alterations in glomelular filtration pressure and can internally convey this signal via its intracellular domain (54, 56). Defects of the nephrin gene are linked with a severe form of congenital nephrotic syndrome, indicating its essential role in normal renal function (8, 47, 56). Podocin is a cholesterol-binding, membrane-associated protein that thought to localize many components of the slit diaphragm. Similar to nephrin, mutations of the podocin gene result in early onset focal segmental glomerularsclerosis (FSGS) (27, 56). As will be discussed, evidence suggests that podocin plays a role in modulating mechanosensitivity in the foot process (58).

1. 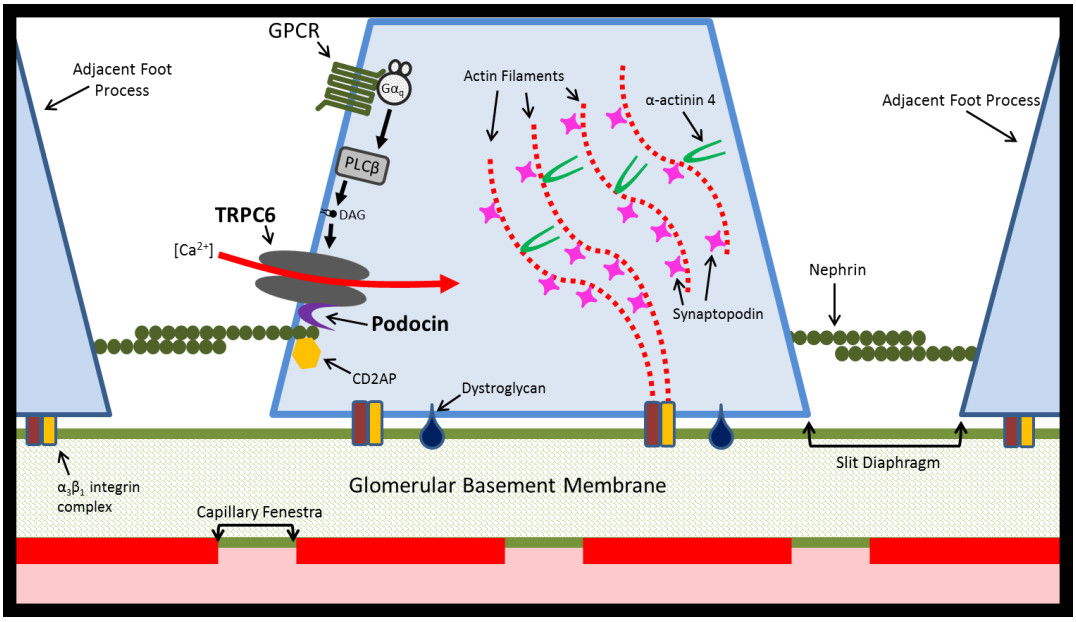

Illustration 1: Simplified model of podocyte foot process in cross section. Nephrin from adjacent podocyte foot processes span the slit diaphragm. Transient receptor potential (canonical) channels 6 (TRPC6) are thought to interact with CD2-associated protein (CD2AP), podocin and nephrin. Calcium influx can lead to alterations in the actin cyctoskeleton. Multiple forms of G protein–coupled receptors (GPRC) can influence TRPC6 activity and other intracellular proteins. One such mechanism is through $G\alpha_q$-Phospholipase Cβ (PLCβ) mediated generation of diacylglycerol (DAG). Synaptopodin is an actin-associated protein that influences podocyte shape and motility and can influence α-actinin 4(ACTN4), an actin bundling protein. Dystroglycan and the α3β1 integrin complex serve to anchor foot processes to the underlying glomerular basement membrane.

By their very location, podocytes are exposed to hydrodynamic forces that at minimum require them to possess a certain structural rigidity, and more likely necessitate the ability for podocytes to actively contract (31, 34). Experimental findings conducted on cultured cells have supported the hypothesis that podocytes contract in response to mechanical stimulation. Specifically, actin rearrangement and tyrosine kinase activation have been observed in podocytes exposed to fluid shear stress (31). Furthermore, Ca^{2+} -influx-dependent and Rho kinase-mediated stress fiber formation can be induced in podocytes exposed to linear strain (31, 32, 69). Maintenance of a contractile apparatus

appears to be essential for podocyte function, in that disruption of the podocyte actin cytoskeleton portends foot process effacement and is closely associated with proteinuric kidney diseases. In addition, mutations of several actin-interacting proteins have been causatively tied to FSGS (31, 34, 60). It is speculated that cytoskeletal rearrangement and contractility may be necessary in order to periodically flush the filtration slits in order to remove blockages accrued during the filtration process (86, 87).

Coupled with the structural proteins of the slit diaphragm, podocyte dynamics and function appear to also be greatly influenced by the interplay between ligand-gated receptors and ion channels (4, 20, 27). This subject will be expanded upon further in the following sections, but a general overview will be discussed here. Podocytes are known to express a number of surface receptors, including insulin receptors, angiotensin II type 1 receptors (AT1R), and both ionotropic and metabotropic glutamate receptors (25, 45, 49, 88, 106). Many of these receptor initiated signaling cascades result in the activation of other Ca^{2+} -permeable channels at the cell surface and the release of internal Ca^{2+} stores that can then alter cytoskeletal dynamics. One such class of these surface expressed channels is the transient receptor potential (TRP) family of channels. Previous studies have shown that multiple types of TRP channels are associated with the slit diaphragm complex and play a role in podocyte function and glomerular filtration (4, 20, 27, 41). Following a 2005 study, it was found that a subset of familial FSGS is caused by mutations in the TRPC6 channel, it became subject to further investigation (98). As the TRPC6 channel is one of the main points of focus of this study, only a brief introduction will be given here; the next section is dedicated to describing the TRPC6 channel, its regulation, and its role in podocyte physiology. That stated, overexpressing either wild

type TRPC6 or gain-of-function mutant TRPC6 in mice is sufficient to induce proteinuric kidney disease analogous to FSGS (72). In addition, activation of the AT1R results in TRPC6 upregulation and TRPC6-mediated Ca^{2+} influx; it is suspected that other receptors can mediate similar responses. As I show, this is in fact the case, with both insulin receptor- and NMDAR-driven signaling cascades converging on the TRPC6 channel. Although it is known that the AT1R can influence TRPC6 activity, the precise mechanism behind this action has, until now remained elusive (25, 49, 88). Here, using isolated rat glomeruli, I show that angiotensin causes an upregulation of TRPC6 through a $G_{\alpha q}$ /PLC pathway, and that this effect is at least partially dependent on NADPH-oxidase (NOX) and the formation of reactive oxygen species (ROS).

While TPRC6 channels are located in the podocyte cell body, major processes and foot processes, the TRPC6 channels only associate with podocin at the slit diaphragm and, as a result, may play a particularly important role in podocyte dynamics (4, 27, 34). As part of the podocin dependent, megadalton signaling complex at the slit diaphragm, TRPC6 can serve as a potential conduit for Ca^{2+} entry and thereby induce cyctoskeletal rearrangement. More intriguingly, the podocin-TRPC6 interaction suggests a mechanosensitive function (56, 58). It has been shown that podocin can regulate TRPC6 channel activity when coexpressed in *Xenopus* oocytes. Due to its homology with MEC-2 and other proteins involved in regulating channel sensitivity to stretch, it has been proposed that podocin acts in similar fashion on TRPC6 channels in podocytes (53, 58). This theory is supported by my findings that siRNA knockout of podocin causes an increased mechanosensitive response in mouse podocytes. In addition, I found that

podocin is necessary for diacylglycerol activation of podocyte TRPC6 channels, indicating a dual regulatory role for podocin.

As stated, podocytes express N-methyl-D-aspartate (NMDA) receptors, but their function has not been fully characterized (1, 38). I show that NMDAR activation causes an increase in TRPC6-mediated currents, a process that was found to be NOX2-ROS dependent. TRPC6 channels aside, in cultured podocytes, antagonism of the NMDA receptor has been reported to cause significant cytoskeletal remodeling and redistribution of nephrin (38). Again, some nephropathies are associated with compromised nephrin function, and there are reports of nephrin downregulation in diabetes (4, 38, 43, 95). These observations implicate a potential role for NMDA receptors in these diseases. Furthermore, podocytes have been shown to possess glutamate containing vesicles and other components necessary for localized glutamatergic signaling (38). Any role for NMDA receptors in any localized signaling system is questionable, as will be explained by our most recent findings. Nonetheless, our group has shown that sustained activation of NMDA receptors causes activation of secondary signaling cascades in podocytes, including protein kinases Erk and Akt and the small GTPase Rho (1, 67). Given the implications of NMDA receptors being essential for maintaining podocyte structure and function, characterizing their physiological properties may herald new therapeutic methods for treating various nephropathies.

1.2 TRPC6 channels:

The mammalian Transient Receptor Potential (TRP) superfamily of channels consists of six loosely related families of cation channels that show marked divergence in

their mode of activation, function, and selectivity (7, 17). TRP channels obtained their moniker from the *trp* mutation in *Drosophila* that was required for photoreceptors to exhibit transient voltage responses to continuous light. All TRP genes encode channel subunits that co-assemble as tetramers to form a functional ion channel (30). These tetramers can be comprised of either one type of subunit (homotetramers) or a combination of familial subunit types (heterotetratmers). All TRP channel subunits possess six-spanning membrane α-helical domains, with the pore-forming region found between S5 and S6, and intracellular NH_2 and COOH termini (17). Of the mammalian TRPs, the TRP canonical (TRPC) family is the most structurally similar to the *Drosophila* TRP channel (7). The TRPC family is composed of 7 known members (TRPC1-7), six of which are expressed in humans (TRPC2 being a pseudogene). All TRPC channels have similar intracellular domains, and TRPC NH_2-termini are characterized by a variable number of ankyrin repeats. On the COOH-terminus is a highly conserved 25-residue TRP domain that contains a sequence known as TRP box 1, followed by a proline-rich sequence referred to as TRP box 2. A calmodulin and IP3 receptor-binding (CIRB) region follow the TRP domain. The remaining COOH-terminus is more variable among TRPC members, but at least one coiled-coil domain is present (17, 27). Based on additional similarities in sequence and function, the TRPC family is commonly divided into two subgroups; TRPC1/4/5 and TRPC3/6/7 (20). Both subgroups can be activated by phospholipase C (PLC), although the downstream pathways diverge. Recall that PLC is an enzyme that cleaves phosphatidylinositol 4,5-bisphosphate (PIP_2) into diacylglycerol (DAG) and inositol 1,4,5-trisphosphate (IP_3). DAG remains membrane bound and acts as a second messenger for signaling. IP_3 on the other hand, is a

freely soluble entity that can diffuse into the cytoplasm where it initiates additional signaling cascades. The TRPC1/4/5 subgroup can be activated by IP_3-mediated release of intracellular Ca^{2+}, while the TPC3/6/7 group is directly activated by diacylglycerol (DAG) (7, 17, 20, 51).

There are many additional forms of TRPC activation, but they often depend on cell context and the tetrameric make-up of the functional channels. Lysophospholipids, generated by phospholipase A_2 (PLA_2), and oxidized phospholipids, accumulated with the formation of ROS, can stimulate TRPC5 (30, 51, 99). Arachidonic acid, another product of PLA_2, and its metabolites can stimulate TRPC6 (61). In addition, TRPC6 is redox sensitive and can be directly activated by ROS (40). Tyrosine phosphorylation can also activate some types of TRPC channels (50). Apart from chemical modification, some TRPC channels display sensitivity to membrane stretch and shear force (29, 39). This mechanosensitivity may depend on both TRPC binding proteins and the lipid domain surrounding the channel. It is thought that tension on the cell membrane results in thinning of the bilayer, thereby inducing a conformational change of the TRPC channel from the closed to the open state (107). The toxin from the Tarantula spider, GsMTx-4, is believed to disrupt this membrane-channel tension and is extensively used to study putative mechanosensitive channels (9, 108).

TRPC3, TRPC5, and TRPC6 have been detected in immortalized podocyte cell lines. In addition to TRPC5 and TRPC6, TRPC1 and TRPC2 have been detected in mouse glomeruli and have an expression pattern indicative of being podocyte specific (20, 48, 112). Of these, TRPC6 has been subject to the greatest degree of study due to its association with familial and acquired glomerular diseases. In 2005, a gain-of-function

mutation of the TRPC6 channel was associated with a hereditary form focal segmental glomerulosclerosis (FSGS) (112). It was later shown that overexpression of either wild-type or mutant TRPC6 induces foot process effacement and glomerular disease in mice (72). Related to this, wild-type TRPC6 upregulation has been detected in a subset of acquired proteinuric kidney diseases, including membranous nephropathy and minimal change disease (82). Many additional FSGS causing mutations of TRPC6 have been identified, and while all are located on the NH_2 and COOH terminals, not all mutations result in an overt gain of function (20, 48, 102).

As with all TRPC channels, TRPC6 is a non-specific cation channel. However, its permeability to Ca^{2+} is voltage-dependent, and at more depolarized membrane potentials, TRPC6 effectively becomes a monovalent cation channel (6, 33). It seems that by itself, TRPC6 is a limited carrier of Ca^{2+} into podocytes and is unlikely to generate significant changes in intracellular Ca^{2+} concentrations beyond a small nanodomain surrounding the channel. Nevertheless, such localized effects may be sufficient to activate other closely associated ion channels (20, 27). It was discovered that large-conductance Ca^{2+}-activated K^+ channels (BK_{Ca} channels) are also expressed in podocytes, and they closely associate with TRPC6 channels (27, 65, 69). It is theorized that TRPC6-mediated Ca^{2+} entry may be sufficient to activate BK_{Ca} channels, which would then drive the cell to a more negative potential. This model sets up a possible feedback system whereby BK_{Ca} channels maintain the sufficiently negative voltage necessary to enable calcium influx through the TRPC6 (27, 65). Sustained Ca^{2+}-influx could trigger cytoskeletal rearrangement and altered gene transcription in the short term; in the long term, excessive Ca^{2+} levels could result in podocyte effacement and apoptosis. Based on this proposed

model, one can see how increased TRPC6 activity can easily become detrimental to podocytes and may partly explain the pathologies associated with many TRPC6 mutations (20, 27).

As stated, TRPC6 channels can be activated by products of PLC. Many receptor types that are found on podocytes can stimulate PLC and potentially influence TRPC6 function (4, 47, 54). Additional signaling cascades that lead to the formation of ROS can also activate TRPC6 (40, 120). Both PLC and ROS pathways can be initiated by the same receptor and both components may be necessary for full activation of TRPC6. It is known that angiotensin II type 1 receptors (AT1R) are expressed by podocytes, and angiotensin activates TRPC6 in these cells. However, to date, the precise mechanism responsible for this activation is unknown. AT1R is a serpentine G-protein coupled receptor that can activate both PLCβ and multiple isoforms of NOX (Illustration 2) (16, 29, 49, 76). I show that both pathways are involved in AT1R mediated TRPC6 activation, and blocking either of them results in a diminished effect of angiotensin.

The insulin receptor is another receptor type expressed in podocytes (4, 66, 68). Prior to our work, it remained unknown if insulin affects TRPC6 activity in podocytes. As a receptor tyrosine kinase, the insulin receptor can activate both PLCγ and NOX4, so it is reasonable to assume that insulin signaling may influence TRPC6 activity. It is already known that insulin signaling is necessary for normal glomerular function (27). As with many other cell types, insulin stimulates podocytes to take up glucose by increasing the surface expression of glucose transporters (66). Research carried out by other members of our group found that insulin also increases surface expression of BK_{Ca} channels in podocytes (68). Similarly, we found that insulin causes a rapid increase in

TRPC6 surface expression, and I show here that there is a functional increase of TRPC6 in response to insulin. I also show that the effects of insulin on TRPC6 are dependent on the production of ROS.

NMDA receptors are also expressed on podocytes, and I show that they can activate TRPC6 in a NOX2 dependent manner (1, 67). Because such a large body of my work involves this receptor, I will reserve further comment on the NMDA receptor for the section dedicated to its discussion.

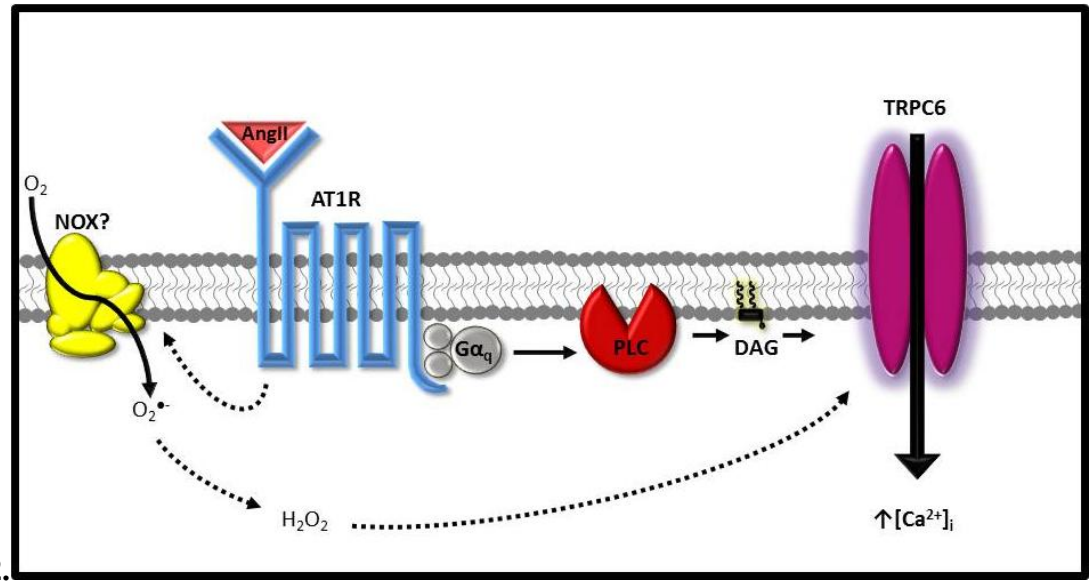

2.

Illustration 2: Simplified model of angiotensin II type 1 receptor (AT1R) activation of TRPC6. Activation of AT1R leads to simultaneous activation of NADPH-oxidase (NOX) and the $G\alpha_q$ subunit of a heterotrimeric G-protein. The NOX isoform remains unknown in podocytes. $G\alpha_q$ triggers phospholipase C (PLC) to generate diacylglycerol (DAG) and inositol 1,4,5-trisphosphate (IP_3). DAG directly activates TRPC6. In addition, NOX generates H_2O_2 which activates the redox-sensitive TRPC6 channel. Solid-line arrows represent direct pathways that are known to occur. Dashed-line arrows represent pathways that are either indirect or the exact mechanism remains to be determined.

TRPC6 channels are expressed on the podocyte cell body, along the major processes, as well as the foot processes, where its function at the slit diaphragm is of particular importance (27). TRPC6 interacts with both podocin and nephrin at the slit diaphragm and is thought to act as part of a signaling complex that regulates cytoskeletal dynamics (4, 54). In nephrin-deficient mice, there is increased expression of TRPC6 and alteration in its localization at the slit diaphragm (4, 56). Nephrin also initiates signaling pathways that directly effect TRPC6 activity. Specifically, Fyn-kinase can be activated by nephrin and it directly alters TRPC6 activation by tyrosine phosphorylation. Fyn-kinase can also recruit and activate PLCγ, leading to the production of DAG and subsequent TRPC6 activation (4, 47).

Podocin seems to regulate TRPC6 by binding directly to the channel and other slit diaphragm proteins and by creating a cholesterol-rich microdomain that surrounds the channel (4, 54, 101). Altering the lipid profile of the cell membrane effects membrane pliability; the addition of cholesterol decreases membrane elasticity (101). Podocin therefore creates a more rigid membrane around the TRPC6 complex, and it has been found that podocin-dependent activation of TRPC6 requires cholesterol (58). In transfected *Xenopus* oocytes, it was found that podocin increased TRPC6 sensitivity to OAG, a DAG analogue, i.e. OAG caused greater activation of TRPC6 in cells coexpressing podocin than in cells expressing TRPC6 alone. As stated in the previous section, podocin is homologous to the MEC-2 protein found in *C. elegans* (58). In the nematode, MEC-2 forms part of a multiprotein channel complex and is necessary for touch sensitivity (53, 58). These facts have led to the hypothesis that podocin regulates the mode of activation of the TRPC6 channel at the slit diaphragm. I show that podocin

suppresses TRPC6 stretch-sensitivity and enhances OAG activation of TRPC6 in both cultured and glomerular-attached podocytes. Furthermore, I show that the TRPC6 stretch response is increased after cholesterol depletion, indicating that the podocin-TRPC6 interaction is dependent on podocin binding to cholesterol.

1.3 NMDA receptors:

Ionotropic glutamate receptors are a major class of heteromeric ligand-gated ion channels that are divided into three subclasses based on their pharmacological specificity to selected agonists. These subclasses are N-methyl-D-aspartate (NMDA) receptors, α-amino-3-hydroxy-5-methyl-4-isoxazole propionic acid (AMPA) receptors, and kainate (KA) receptors (78). Among the three, NMDA receptors are unique in that they are highly permeable to Ca^{2+} ions, are tonically inhibited at normal cell resting potential by a Mg^{2+} block of the channel pore, and typically require the binding of coagonist for channel opening (62, 79, 80).

NMDA receptors are heteromeric tetramers that incorporate a combination of NR1, NR2 and NR3 subunits (90). A single gene, subject to alternative splicing, generates eight functional NR1 subunits. Four genes encode for NR2 A, B, C, and D, and the NR3 A and B subunits are also distinct transcripts (12, 78, 90, 116). Prototypically, NMDA receptors are formed from two dimers of the NR1 and NR2 subunits, with at least one NR1 subunit obligatory for functionality. While the NMDA receptor subunits all share the same basic topology, they differ in their binding sites. L-glutamate, the canonical agonist for NMDA receptors, binds to NR2 subunits on their extracellular agonist-binding domain (ABD) (78, 90). Other agonists such as L-aspartate, L-

homocysteine (HC), and L-homocysteate (HCA) also bind to the ABD and share a similar structure with glutamate. In addition to their ABD, NR2 subunits posses an allosteric modulator site located on their N-terminal domain (NTD). Allosteric inhibitors such as Zn^{2+} bind to this site, preventing channel activation. The NR1 subunits contain the co-agonist binding site. Informally known as the "glycine site," the co-agonist binding site can also be activated by endogenous D-serine (84, 90). Occupation of this co-agonist site is thought to be necessary for channel opening, and antagonists of the site prevent NMDA receptor activity. Less is known about the NR3 subunit, but it has also been found to bind both glycine and D-serine, albeit with much higher affinity than the NR1 subunit (12, 90). In addition, the presence of the NR3 subunit reportedly lowers NMDA receptor sensitivity to Mg^{2+} and significantly reduces Ca^{2+} permeability. It follows that NR1/NR3 heteromers do not form glutamate activated receptors, as they lack an ABD. Interestingly, NR1/NR3 heteromers do form glycine-activated cationic channels. It is believed that functional NMDA receptors are assembled in vivo from NR1/NR2 heteromers and NR1/NR2/NR3 triheteromers (12).

First identified in neurons, NMDA receptors have been found to play a crucial role in mediating excitatory synaptic transmission and changes in synaptic strength (95, 116). Outside of the nervous system, NMDA receptors have been detected in a multitude of tissue types, including heart, parathyroid, bone, pancreas, immune cells, erythrocytes, and kidney (19, 75, 76, 77). In erythrocytes, NMDA receptor activation facilitates the formation of nitric oxide (76), while in proximal tubule cells there is evidence that NMDA receptor subunits play a role in Na^{+} reabsorption (19). Apart from these and a

few other instances, the function of many of these peripheral NMDA receptors remains largely uncharacterized.

Functional neuronal NMDA receptors are permeable to K^+, Na^+, and Ca^{2+}, with permeability contingent upon prior depolarization of the cell. At the cellular resting potential, Mg^{2+} blocks the pore, and although NMDA receptors can be activated, no current is permitted (78, 80). The opening of non-NMDA, glutamatergic channels results in depolarization of the cell that is sufficient to remove the Mg^{2+} from the pore site (80). NMDA receptors display relatively slow activation kinetics, with current reaching a peak 10 to 20 ms post-activation (75). The degree that NMDA receptors are permeable to Ca^{2+} is determined by the subunit composition of the NMDA receptor, but at typical extracellular concentrations, the selectivity for Ca^{2+} exceeds that for Na^+ 10-fold in most NMDA receptors (78, 116). As a result NMDA receptors are ideally suited to initiate Ca^{2+} dependent signaling cascades, while at the same time posing a risk for Ca^{2+}-induced exitotoxicity. In neurons, over-stimulation of NMDA receptors triggers cellular death via the production of reactive oxygen species (ROS), the excessive activation of Ca^{2+}-dependent kinases and proteases, and disruption of Ca^{2+}-dependent ion channel functionality (15). It has been shown both in vivo and in neuronal cultures that NMDAR activation can trigger NADPH oxidase 2 (NOX2)-dependent ROS production (10, 116, 117). The precise mechanism of this process remains unclear, but one theory holds that Ca^{2+}-influx through the NMDA triggers the activation of nitric oxide synthesis, the subsequent generation of nitric oxide, leading to the eventual activation of protein kinase G (PKG). PKG is thought to then activate Rac1, a small (~21 kDa) signaling GTPase, that is an essential component of the active NOX2 complex (10). The ROS generated by

NOX2 can not only directly affect the redox sensitive NMDAR, but cause further downstream effects. As I show, this NMDAR-mediated signaling cascade can have a detrimental impact on podocytes.

Recently, NMDA receptors have been identified in human and rodent glomeruli (96). While not definitive, there is some evidence that systemic inhibition of these receptors results in a tendency to develop proteinuria, although our group has been unable to confirm this. Here, evidence is presented that the negative effects of NMDA receptor activation may in part be the result of TRPC6 upregulation. I found that NMDAR activation causes an upregulation of TRPC6 through increasing ROS formation via NOX2 in mouse podocyte cell lines. It is of note that the TRPC6 effects of both angiotensin and insulin also depend on the formation of ROS, albeit through slightly different mechanisms. Previously, it was hypothesized that NMDAR signaling may occur in a very localized manner (19, 38, 96). Podocyte foot processes have both glutamate containing vesicles and glutamate transporters, and it seems plausible that glutamate release from adjacent foot process could serve as a limited range signal (38, 96). However, as will be shown further below, our findings do not suggest a role for NMDA receptors in a signaling pathway that involves localized release of glutamate.

Here I show that podocytes from cell lines and primary cultures express functional NMDA receptors with a set of properties that distinguishes them from previously characterized NMDA receptors. While readily activated by NMDA, podocyte NMDA receptors are essentially unresponsive to L-glutamate and L-aspartate and are not potentiated by glycine. Despite their resistance to the classical agonists, podocyte NMDA receptors are inhibited by typical competitive and non-competitive antagonists. In

addition, these receptors respond to both L-homocysteate and D-aspartate with large ionic currents that are significantly mediated by calcium influx. D-serine acts as a potentiator of the evoked currents, and antagonists of the D-serine binding site inhibit NMDA receptor current.

1.4 Summary of objectives:

The purpose of this research is to study polymodal activation of TRPC6 channels in podocytes, i.e. chemical and mechanical stimuli. Chemical activation is mediated by surface-expressed receptors, so it is necessary to identify and characterize the signaling pathways that can influence TRPC6 channel activity in podocytes. I focused on three specific receptors that are known to be expressed in podocytes; the angiotensin II type 1 receptor (AT1R), the insulin receptor, and the NMDA receptor (Illustration 3A).

Based on previous research, it is hypothesized that AT1R-mediated activation of TRPC6 is $G\alpha_q$-PLC dependent and may involve reactive oxygen species (ROS). Using whole cell current recordings obtained from glomeruli-attached podocytes, I tested these assumptions. Less was known about the role of the insulin receptor in TRPC6 activation. Our preliminary data suggested that insulin increases surface expression of TRPC6, and I set out to determine if insulin has a functional effect on TRPC6 channel activity. There are multiple downstream effects from the insulin receptor and the production of peroxide and other ROS are implicated in normal insulin receptor signaling. Given that TRPC6 channels are redox-sensitive, I investigated the role of ROS in regulating TRPC6 channels. The final receptor studied was the NMDA receptor. Again, the physiological role of podocyte NMDA receptors remains unclear. I began by further characterizing the

NMDA receptor itself. I sought to determine the ligands, both agonists and antagonists, as well as channel permeability properties of the NMDA receptor. There is speculation that the NMDA receptor may facilitate TRPC6 channels in podocytes. I wanted to determine whether this is actually the case, and by what mechanism it may occur.

Finally, there has been much conjecture over TRPC6 mechanosensitivity in podocytes (Illustration 3B, C, D, and E). I tested the hypothesis that TRPC6 channels are activated by membrane stretch and other forms of membrane deformation. Membrane cholesterol levels were altered in order to determine the how membrane fluidity affects TRPC6 mechanosensitivity. I also investigated the potential role of podocin in regulating TRPC6 mechanosensitivity, and whether podocin has any additional regulatory roles.

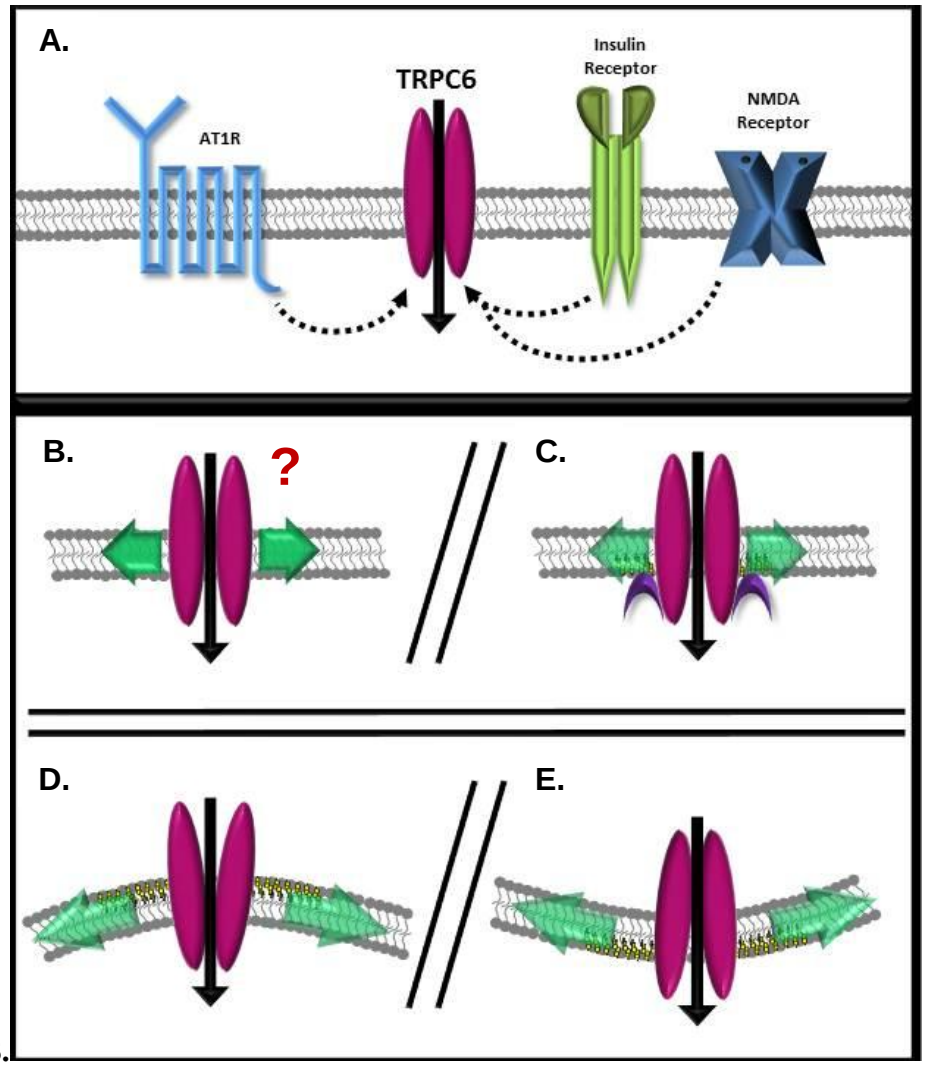

3.

Illustration 3: Illustration of objectives. The research presented is focused on polymodal activation of TRPC6 channels in podocytes. ***A:*** Multiple forms of receptor-mediated activation are examined. The mechanism of angiotensin II type 1 receptor (AT1R) mediated activation is studied as well as TRPC6 activation by insulin receptor and NMDA receptor-mediated signaling. ***B:*** Prior to this work, it was uncertain if podocyte TRPC6 channels are mechanosensitive. It will be determined whether this is the case, and what, if any, role podocin plays in regulating TRPC6 mechanosensitivity (***C***). Altering cholesterol levels can cause membrane deformation, and will be used to study the mechanosensitivity of TRPC6 channels. ***D:*** Addition of cholesterol to the outer leaflet of the plasma membrane is thought to cause an outward curvature of the membrane. ***E:*** Selective removal of cholesterol from the outer leaflet is thought to cause an inward deflection of the membrane. The methods used to alter cholesterol levels is described in the text.

2 MATERIALS AND METHODS

2.1 Cell culture and glomerular isolation:

Immortalized mouse and human podocyte cell lines (obtained from Dr. Peter Mundel then at the University of Miami Miller School of Medicine, now at Harvard Medical School) were maintained as described in detail previously (90). Cell lines were propagated at 33°C in the presence of mouse γ -interferon (10 U/ml; Sigma). Removal of γ-interferon and raising the temperature to 37°C for 2 weeks induced differentiation and expression of podocyte markers (90). To prepare primary cultures of podocytes, 6-week old mice were anesthetized with pentobarbital and sacrificed according to procedures approved by the University of Houston Institutional Animal Care and Use Committee and kidneys were excised and placed in ice cold PBS. The capsule and adhering fat were removed, and the cortex was carefully dissected and chopped into 1 mm^3 pieces using a razor blade. A preparation enriched in glomeruli was made using a standard sequential sieving procedure using three stainless steel sieves with mesh sizes of 190 µm, 140 µm and 104 µm. A fourth mesh screen of 73.7 µm was used as a final barrier, and glomeruli were collected at this stage. A similar procedure was used for isolating glomeruli from rats, however the mesh size for the sieves were 230 µm, 190 µm, 140 µm, and the final barrier sieve was 104 µm. For acutely isolated podocytes, glomeruli were then collected by brief centrifugation and incubated at 37°C in a saline free of divalent cations containing 0.5 mg ml/ml Sigma type II collagenase for 20 min. The glomeruli were transferred to cell culture medium and gently dissociated by 10 passes through a fire-polished Pasteur pipette (tip diameter 0.5 mm), and the cell suspension was plated onto

poly-D-lysine-coated or collagen-coated glass coverslips. Recordings were made 72 hr after plating, at which time glomerular cells were adherent and podocytes could be readily identified by their primary processes extending from the cell body, which were easily seen under Hoffman modulation contrast optics. Intact rat glomeruli were first isolated by the described sieving procedure and then collected by pipette, spun down, and directly plated on collagen-coated coverslips. Recordings were carried out 24-72 hours post plating in order to allow for sufficient adherence. Panels of siRNAs directed against TRPC6 and podocin, and non-targeted siRNAs for use in control experiments, were obtained from Santa Cruz Biotechnology and transfected into podocytes using Oligofectamine™ (Invitrogen) in serum-reduced medium according to the manufacturer's directions. Experiments were carried out 24-hr after transfection with siRNA.

2.2 Whole-cell recordings and data analysis:

Whole-cell recordings were made at room temperature (21-23°C) using standard techniques. For TRPC6 recordings, the control bath solution (100%) contained 150 mM NaCl, 5.4 mM CsCl, 0.8 mM $MgCl_2$, 5.4 mM $CaCl_2$, and 10 mM HEPES, pH 7.4. To prepare a 70% hypoosmotic solution, 700 ml of the control solution was simply diluted to a volume of 1 L. In experiments using pressure pulses as a mechanical stimulus, the external solution was the same as the normoosmotic 100% control except that the external Ca^{2+} was reduced to 0.8 mM to facilitate detection of inward currents at more negative membrane potentials (63). Pipette solutions in all experiments contained 10 mM NaCl, 125 mM CsCl, 6.2 mM $MgCl_2$, 10 mM HEPES, and 10 mm EGTA, pH 7.2.

For experiments on hypoosmotic stretch, the bath was perfused at a constant flow rate (0.3 ml/min) and outwardly rectifying currents were periodically evoked by ramp voltage commands (-80 to + 80 mV over 2.5 sec) from a holding potential of -40 mV. This was done in normal and 70% hypoosmotic solutions, which in some experiments also contained drugs or inhibitors, as indicated. Whole-cell currents were quantified at +80 mV as described previously (90). To evoke inward deformations of the membrane, glass micropipettes with tip diameters of ~ 1 μm were filled with normal external saline containing 60% sucrose, and were positioned 40-50 μM from a podocyte cell body under whole-cell clamp. Pressure pulses of 34 kPa (5 p.s.i) were applied using a Picrospritzer™ pressophoresis system, which, with optimal placement of the micropipette, resulted in visible and highly reproducible deformation of the plasma membrane. This stimulus was applied in a constantly flowing bath while the cell membrane potential was held at -60 mV. To examine effects of shear force, whole-cell recordings from rat podocytes in isolated glomeruli were made in a static 0.5 ml bath, and mechanical stimulation was applied by briefly initiating a flow at 0.3 ml/min while the cell was held at -60 mV. In these experiments, we only recorded from cells in which large primary processes could be seen emanating from the cell body, and we choose cells on the outer margin of the glomerulus that would be directly exposed to the flowing bath. For pharmacological experiments, recombinant human insulin, 1-oleoyl-2-acetyl-*sn*-glycerol (OAG), U73122, ONO-RS-082, angiotensin II, apocynin, losartan, suramin, chelerythrine, diphenylene iodium (DPI), and cytochalasin D were obtained from Sigma. SKF-96365 was from Calbiochem. Manganese (III) tetrakis (4-benzoic acid) porphyrin chloride (MnTBAP) was from Percipio Biosciences. GsMTx4 was from Smarttox.

For NMDAR recording, the external bath normal external saline contained (mM): 150 NaCl, 5.4 KCl, 0.8 $MgCl_2$, 5.4 $CaCl_2$, and 10 HEPES-NaOH, pH 7.4. In experiments designed to examine relative ionic permeability, $CaCl_2$ was increased to 10 mM in the control solution and nominally decreased to 0 mM in the experimental solution and NMDA responses obtained over a range of membrane potentials in both solutions. Recording electrodes were filled with a solution containing (mM): 120 KCl, 10 NaCl, 10 HEPES-KOH, and 10 EGTA, pH 7.2. In some experiments $MgCl_2$ was increased to 5 mM in internal or external solutions, as indicated (in which case EGTA was omitted from the internal solution). The resistance of filled recording electrodes was 4-6 MΩ. In pilot studies we used recording electrode solutions in which KCl was replaced with CsCl, and identical results were obtained. Because recordings lasted longer with KCl, we used those solutions for the rest of these studies. It was possible to compensate 80-90% of the series resistance without introducing oscillations into the current output of the clamp amplifier (Axopatch 1D, Molecular Devices, Sunnyvale, CA). Agonists (NMDA, L-glutamate, L-aspartate, D-aspartate, L-homocysteate, or glycine) were obtained from Sigma and dissolved in extracellular saline at various concentrations and applied by pressure injection (4 lb/in^2 = 27.6 kPa for 1-60 sec duration) from a second micropipette (~2 μm tip diameter) positioned 30-40 μm from the cell body of the podocyte. The amplitudes and waveforms of responses to agonists showed some variability from cell to cell depending in part on injection pipette placement relative to the podocyte cell body, and the bath perfusion rate. However, once the pressure injection pipette was placed, amplitudes and waveforms of responses in individual cells were highly reproducible and could often be maintained for up to 30 min with little variation. With this apparatus,

only a single concentration of agonist could be applied to any given cell. The antagonists MK-801 and D-2-aminophosphovaleric acid (obtained from Sigma), and L689,560 (obtained from Tocris) and allosteric modulators (glycine or D-serine) were dissolved in extracellular saline and applied to cells by bath superfusion. Macroscopic currents were digitized with a Digidata 1322A interface (Molecular Devices) and stored for off-line analysis with pCLAMP software (Molecular Devices). Curve fitting was carried out using the non-linear least squares algorithms implemented in Origin v 6.0 software (Microcal Software Inc., Northhampton, MA).

2.3 Immunoblot analysis, cell-surface biotinylation assays, and nuclear localization of NFAT:

Immunoblot analysis and cell-surface biotinylation were carried out using standard methods as described in detail previously (65, 66, 67, 68, 69). The primary antibodies were rabbit anti-TRPC6 (Alomone), rabbit anti-p47(phox) and rabbit anti-NOX2 (Santa Cruz), rabbit anti-NOX4 (Epitomics), rabbit anti-podocin (Santa Cruz), rabbit anti-nephrin (Abcam), and mouse monoclonal anti-β-actin (Millipore). For cell-surface biotinylation assays, intact podocytes were treated with a membrane impermeable biotinylation reagent, sulfo-*N*-hydroxy-succinimidobiotin (Pierce Biotechnology, Rockford, IL) (1 mg/ml) for 1 h. The reaction was stopped, cells were lysed, and biotinylated proteins from the cell surface were recovered by incubation with immobilized streptavidin-agarose beads. A sample of the initial cell lysate was retained for analysis of total proteins, and in some experiments of β-actin. These samples were quantified by immunoblot analysis followed by densitometric analysis using Image J™

software. Bar graphs describing these data were constructed from 3-5 repetitions of each experiment. NFAT localization in podocyte nuclei was measured using a commercial assay (Active Motif) and a nuclear extract kit purchased from the same manufacturer. In this assay we also used a mouse monoclonal anti-histone and a mouse monoclonal anti-β-actin (Millipore). In separate experiments on NFAT localization, podocytes were subjected to various treatments and fixed in 4% paraformaldehyde at room temperature for 10 minutes. Fixed cells were permeablized, blocked and incubated with rabbit anti-NFATc1 (Active Motif) and nuclei were counterstained with 4'-6-diamidino-2-phenylindole (DAPI) for 1 hour at 37°. After washing, cells were treated with AlexaFlour 488-conjugated anti-rabbit IgG (Molecular Probes), and then rinsed, mounted, and images were collected on an Olympus FV-1000 inverted stage confocal microsope using a Plan Apo N 60X 1.42NA oil-immersion objective, and processed by FluoView™ software.

3 RESULTS

3.1 Angiotensin modulates TRPC6 channels in isolated rat glomeruli:

It is known that podocytes express functional angiotensin II type 1 receptors (AT1R), and it has been shown that angiotensin causes increased expression of TRPC6 and TRPC6-mediated Ca^{2+}-influx (25, 49, 90). Additional studies have shown that AT1R-mediated upregulation of TRPC6 transcription is dependent on the calcineurin/NFAT pathway(88), but this pathway does not explain the observed, acute effects of angiotensin on TRPC6 functionality. Using isolated rat glomeruli, I was able to further characterize the signaling pathways required for AT1R facilitation of TRPC6 function. I obtained whole cell recordings from cells located at the peripheral surface of the glomeruli. The cells' location and morphology were used to identify them as podocytes. In these experiments, K^+ ions that would normally be present in physiological solutions were replaced by Cs^+ in both the bath and pipette solutions. In addition, external Ca^{2+} was raised to 5.4 mM to improve the stability of whole cell recordings. Macroscopic currents were evoked by 2.5s voltage ramps from -80 to +80 mV, and currents at +80 mV were quantified for analysis.

I found that angiotensin has a dose dependent effect on cationic current evoked by voltage ramps (Fig. 1, A). Angiotensin had a noticeable effect at concentrations as low as 0.1 nM, with the largest effects observed at concentrations of 100 nM. At larger concentrations ($\geq$1 mM), angiotensin had an inhibitory effect. The maximum observed outward current occurred at +80 mV, and this value was used to plot the dose-dependency curve. There was an increase in both inward and outward current, and (Fig.

1, B). At a negative holding potential (-60 mV), 10 nM angiotensin evoked a substantial increase in inward current when measured from baseline (Fig. 1, C).

In order to substantiate that the increased current was mediated by AT1R, I applied the AT1R inverse agonist, losartan (100μM), prior to angiotensin wash-on. Losartan effectively inhibited any increase in measured current (Fig. 2, A and B), thereby further implicating AT1R.

Cationic current could potentially be mediated by channels other than TRPC6 (41). In order to verify the identity of the channel facilitated by AT1R, I utilized two known inhibitors of TRPC6. SKF-96365, is an agent that blocks cationic channels in the TRPC family (81). At micromolar concentrations, lanthanum (La^{3+}) blocks TRPC6 while at the same time activating TRPC5 (64). Angiotensin-evoked currents were effectively blocked by the SKF-96365 compound (10 μM) (Fig. 3, A and B), indicating that the current was TRPC mediated. La^{3+} (50 μM) had similar effects (Fig. 4, A and B), indicating that the current was specifically TRPC6 mediated. Furthermore, the La^{3+} trials convincingly negated the possibility of any involvement of TRPC5. As final substantiation that angiotensin is upregulating TRPC6 specifically, I used siRNA to knockdown TRPC6. Transfected cells, showed a significantly reduced response to angiotensin compared to control cells transfected with a scrambled siRNA sequence (Fig. 5, A - C).

I next determined the signaling pathways involved in AT1R activation of TRPC6. It is known that AT1R is a $G\alpha_q$ –coupled receptor, and $G\alpha_q$ can activate PLCβ (25,46). No angiotensin-evoked activation of TRPC6 was observed whe suramin (100 μM), a $G\alpha_q$ inhibitor, was included in the pipette solution (Fig. 6, A). D609 is a selective competitive

inhibitor of PLC and chelerythrine is a cell permeable PKC inhibitor. Addition of D609 (100 μM) to the bath solution blocked a significant portion of angiotensin mediated increase in TRPC6 current (Fig. 7, A and B). On the other hand, chelerythrine (10 μM) did not inhibit the effects of angiotensin (Fig. 7, C). Taken together, these results indicate that AT1R activation of TRPC6 is PLC dependent, but does not require PKC.

TRPC6 is a redox-sensitive channel, and it is known that AT1R signaling can generate ROS (27, 40, 46). I used multiple methods in order to determine if the generation of ROS plays a role in AT1R activation of TRPC6. The effects of angiotensin were blocked by concurrent treatment with 100μM of MnTBAP, a membrane permeable mimetic of superoxide dismutase and catalase (Fig. 8, B). ROS can be generated via NADPH-oxidases (NOX), and AT1R is reported to activate NOX2 and NOX4 (16). Both apocynin and DPI are inhibitors of NOX enzymes. Separately, apocynin (10 μM) and DPI (10 μM) greatly inhibited the effects of angiotensin (Fig. 8, C and D), though a statistically significant effect of angiotensin remained. Nonetheless, these findings indicate that AT1R is promoting free radical formation via NOX activation, and this process is in part necessary for angiotensin activation of TRPC6.

Figure 1: Angiotensin II activates cationic currents in glomerular attached podocytes. ***A:*** angiotensin II has a dose dependent effect on cationic currents recorded from rat glomerular attached podocytes. Whole-cell currents were evoked by ramp voltage commands (-80 mV to +80 mV in 2.5 seconds) before and after addition of angiotensin to the bath solution. Dose response was measured by subtracting the maximum outward current obtained in the normal bath solution from the maximum outward current obtained in the presence of angiotensin, as shown in *B*. Angiotensin doses ranged from 0.1nM to 1µM, with doses increasing by a factor of 10. Angiotensin had the greatest effect at 100nM, with higher doses resulting in reduced current. Each data point is the average of 5 cells (n = 5). Error bars indicated ±SE. ***B:*** example of traces obtained using ramp voltage command both before and after application of angiotensin (1nM). ΔI indicates the value used to plot the dose response curve. ***C:*** angiotensin (100nM) evokes inward cationic current when cell is held at -60mV. Inward current was sustained in the presence of angiotensin.

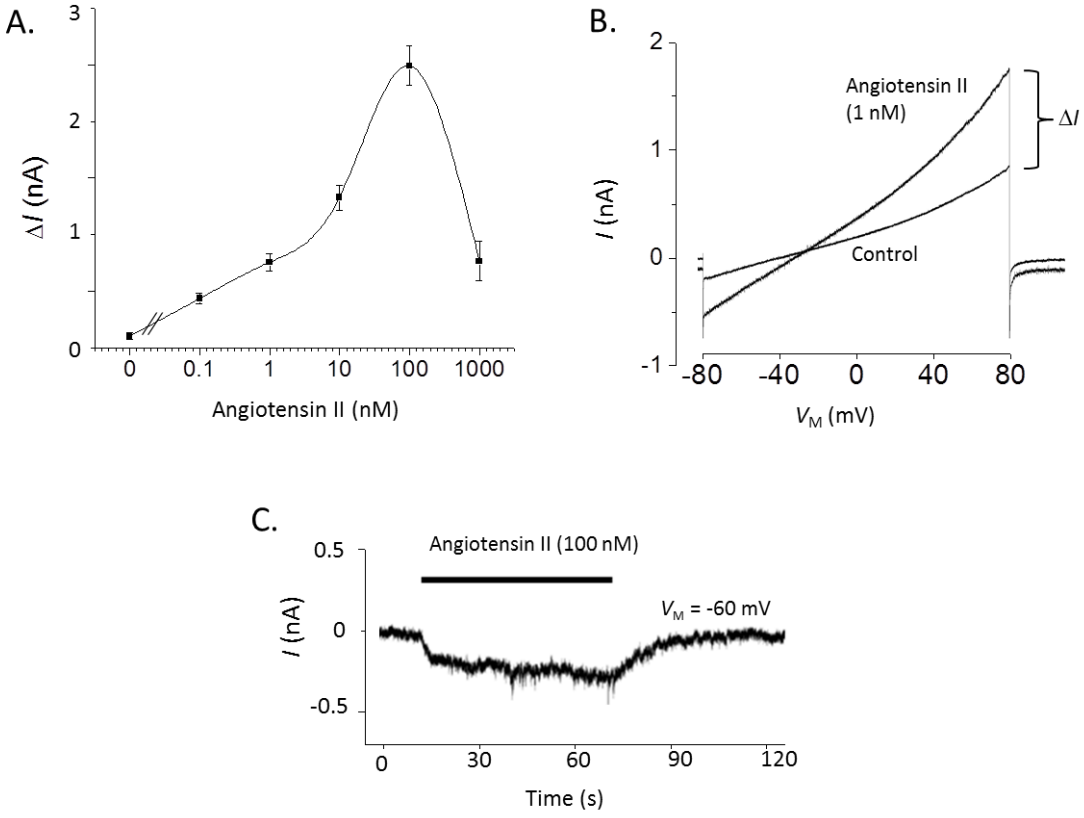

Figure 1.

Figure 2: Losartan inhibits angiotensin activation of cationic current. ***A:*** example of traces showing that pre-application of losartan (100μM) prevented angiotensin (1nM) (abbreviated as AII) evoked activation of cationic current. ***B:*** no significant (n.s.) ($P < 0.0001$, Student's unpaired t-test, $n = 5$) increase in either inward or outward current was observed when angiotensin (1nM) was applied in the presence of losartan (100μM).

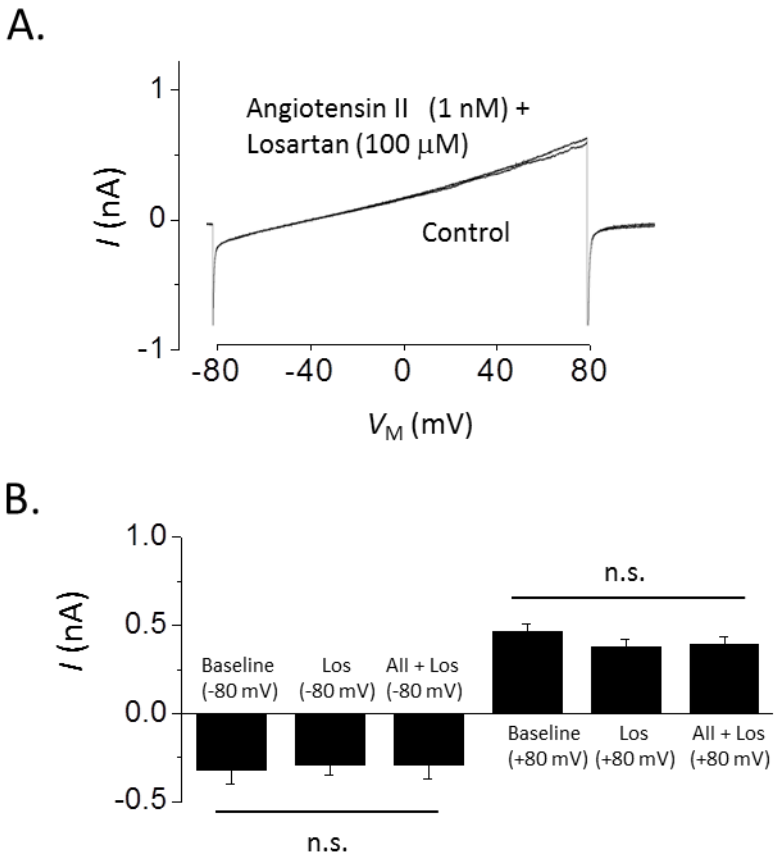

Figure 2.

Figure 3: Angiotensin-activated current is sensitive to TRPC blocker, SKF-96365. ***A:*** example of traces showing that angiotensin (1nM) evoked currents were effectively blocked by SKF compound (10µM) in a single cell. ***B:*** angiotensin resulted in a significant increase in both inward and outward current ($P < 0.0001$, Student's unpaired t-test, $n = 5$) compared to currents measured in control conditions. Angiotensin (1nM) activated current was significantly inhibited by SKF compound (10µM).

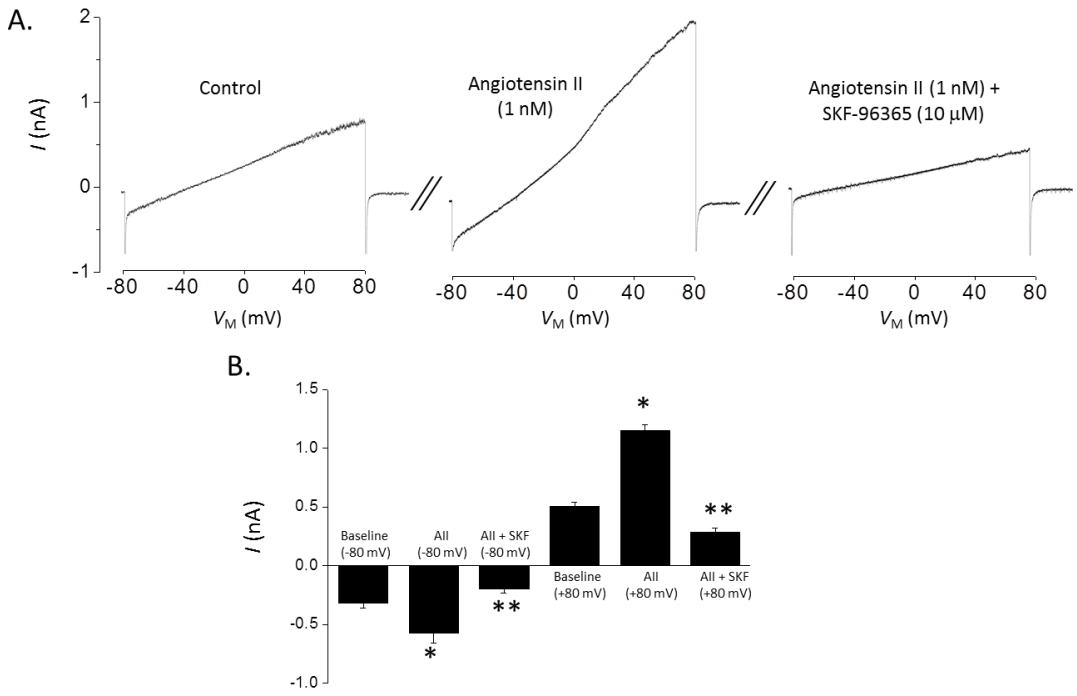

Figure 3.

Figure 4: Angiotensin-activated current is sensitive to TRPC6 blocker, Lanthanum (La^{3+}). ***A:*** example of traces showing that angiotensin (1nM) evoked currents were effectively blocked by La^{3+} (50µM) in a single cell. ***B:*** angiotensin resulted in a significant increase in both inward and outward current ($P < 0.0001$, Student's unpaired t-test, $n = 5$) compared to currents measured in control conditions. Angiotensin (1nM) activated current was significantly inhibited by La^{3+} (50µM).

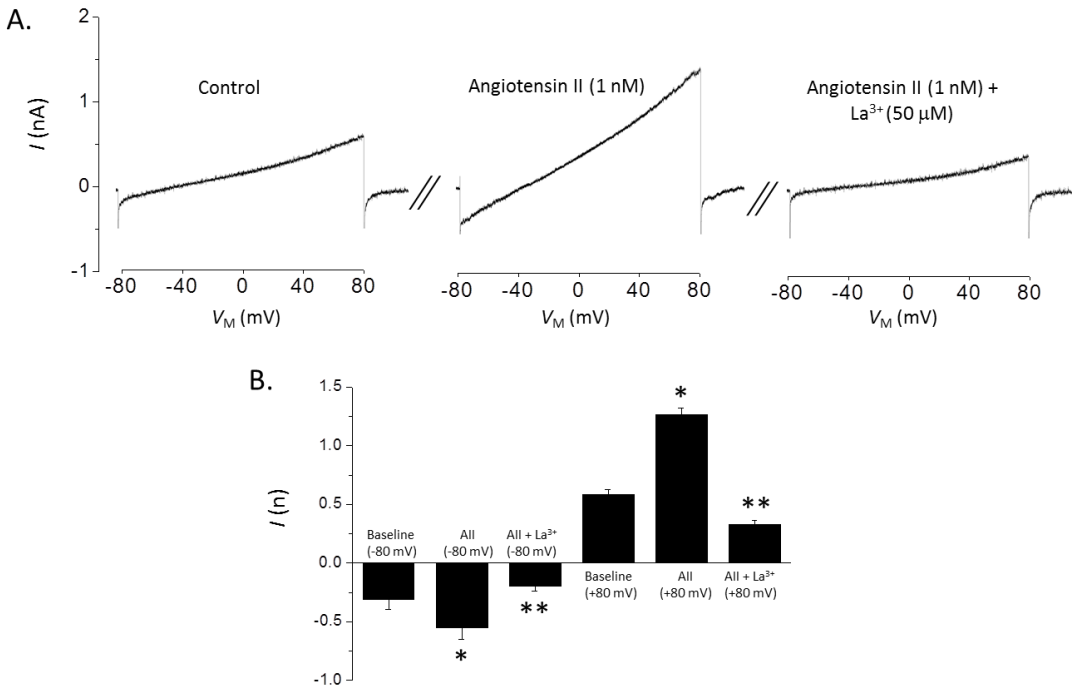

Figure 4.

Figure 5: Angiotensin does not increase current in TRPC6 knockdown cells. ***A:*** example of traces obtained from cells treated with control siRNA both before and after angiotensin application (1nM). ***B:*** example of traces obtained from cells treated with TRPC6 siRNA both before and after angiotensin application (1nM). ***C:*** mean currents at ±80 mV recorded in cells treated with vehicle or TRPC6 siRNA (each group n = 5). Data were analyzed by 2-way ANOVA, which showed that TRPC6 knockdown had a significant ($P < 0.005$) effect on cell sensitivity to angiotensin activation.

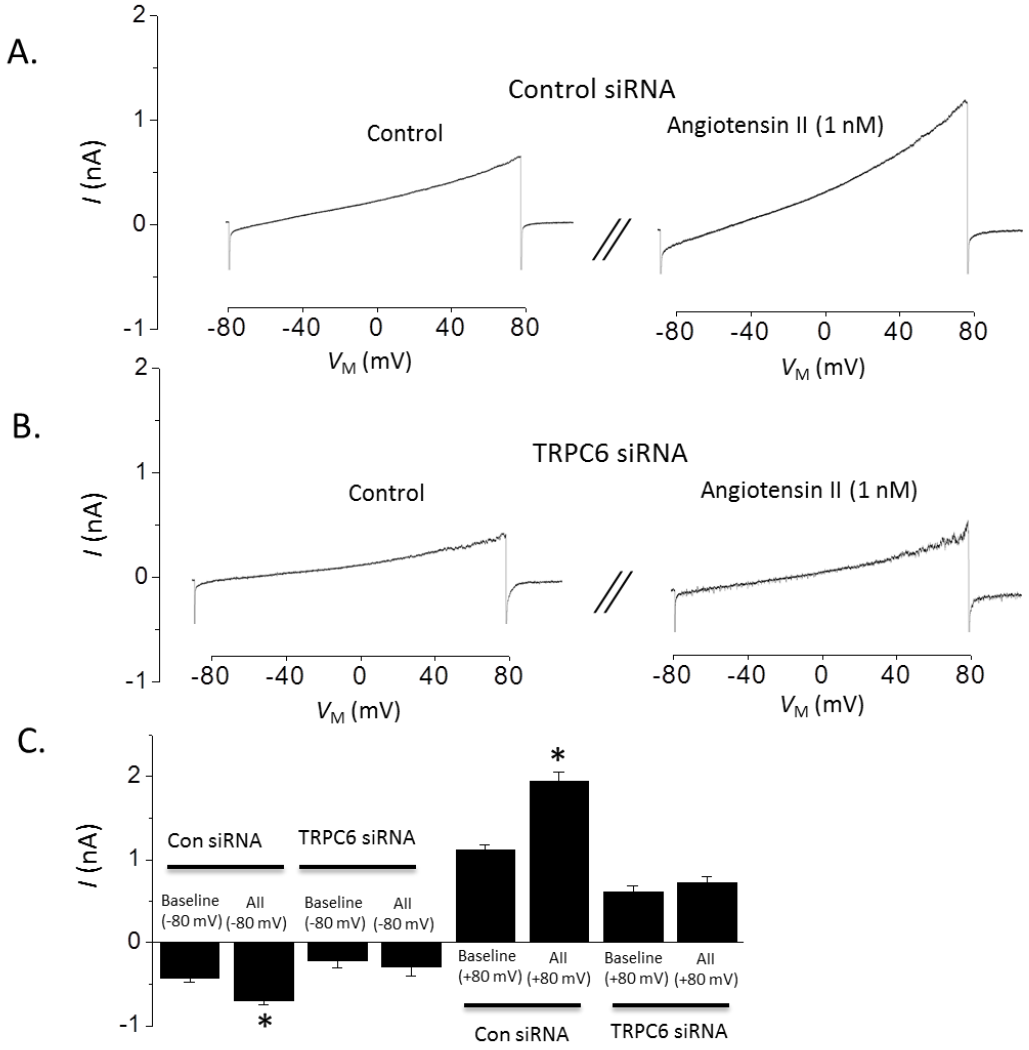

Figure 5.

Figure 6: Suramin, a $G\alpha_q$-protein inhibitor, prevents angiotensin activation of cationic current. ***A:*** example of traces showing that inclusion of suramin (100µM) in recording pipette solution prevented angiotensin (1nM) evoked activation of cationic current. ***B:*** no significant (n.s.) ($P < 0.0001$, Student's unpaired t-test, $n = 5$) increase in either inward or outward current was observed in response to angiotensin (1nM) when suramin (100µM) was present in the recording pipette solution.

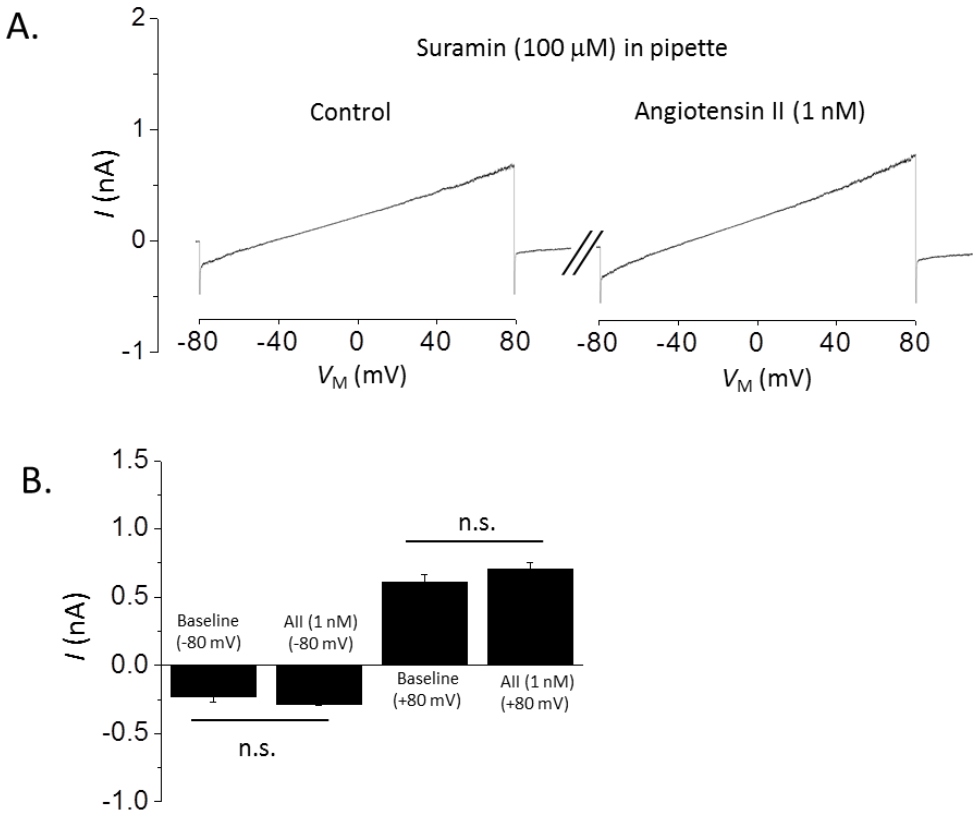

Figure 6.

Figure 7: Inhibition of PLC but not PKC prevents angiotensin activation of cationic current. ***A:*** example of traces showing that pre-application of the PLC inhibitor, D609 (100µM) prevents angiotensin (1nM) evoked activation of cationic current. ***B:*** no significant (n.s.) ($P < 0.0001$, Student's unpaired t-test, $n = 5$) increase in either inward or outward current was observed in response to angiotensin (1nM) when D609 (100µM) was present in the bath solution. ***C:*** pre-application of the PKC inhibitor, chelerythrine (10µM) did not inhibit angiotensin (1nM) activation of cationic current ($P < 0.0001$, Student's unpaired t-test, $n = 5$).

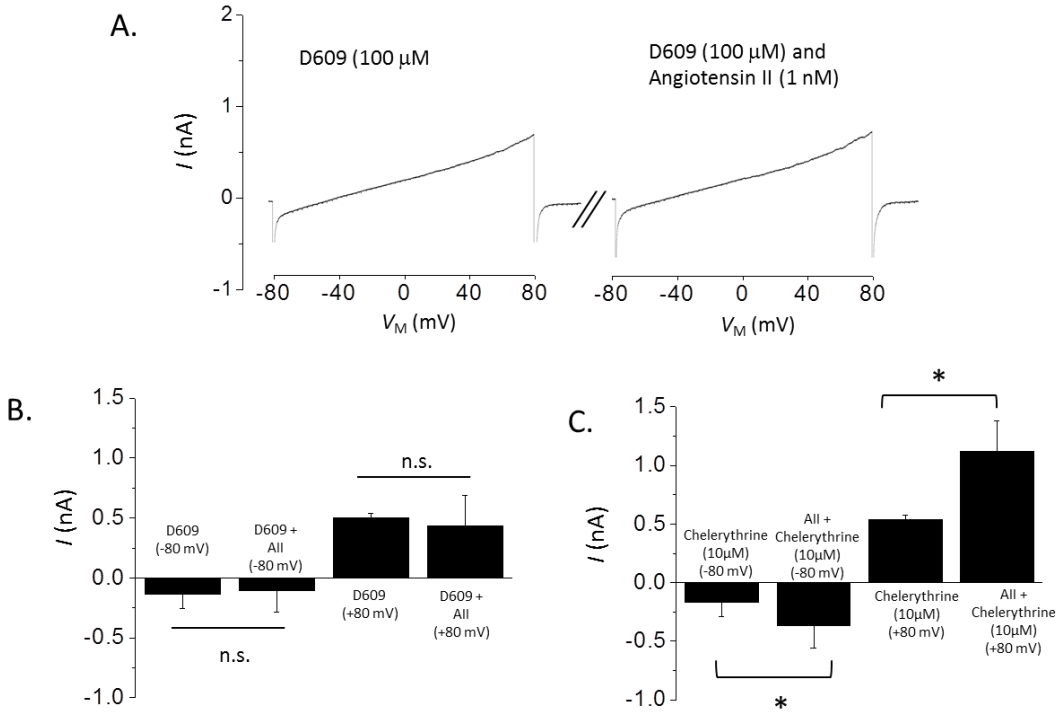

Figure 7.

Figure 8: Angiotensin activation of cationic current is greatly dependent on NOX activity and the presence of reactive oxygen species. ***A:*** mean effects of angiotensin (1nM) on group of control cells (n = 5 for all groups) showing significant increase in inward and outward current ($P < 0.0001$, Student's unpaired t-test). ***B:*** mean effects of angiotensin (1nM) on group of cells pretreated (12hr) with MnTBAP (100μM) showing no significant increase current ($P < 0.0001$, Student's unpaired t-test). ***C:*** mean effects of angiotensin (1nM) on group of cells pretreated (12hr) with apocynin (10μM) showing reduces effect of NOX inhibition on current activation ($P < 0.0001$, Student's unpaired t-test). ***D:*** mean effects of angiotensin (1nM) on group of cells with pre-application of DPI (100μM) showing reduces effect of NOX inhibition on current activation ($P < 0.0001$, Student's unpaired t-test).

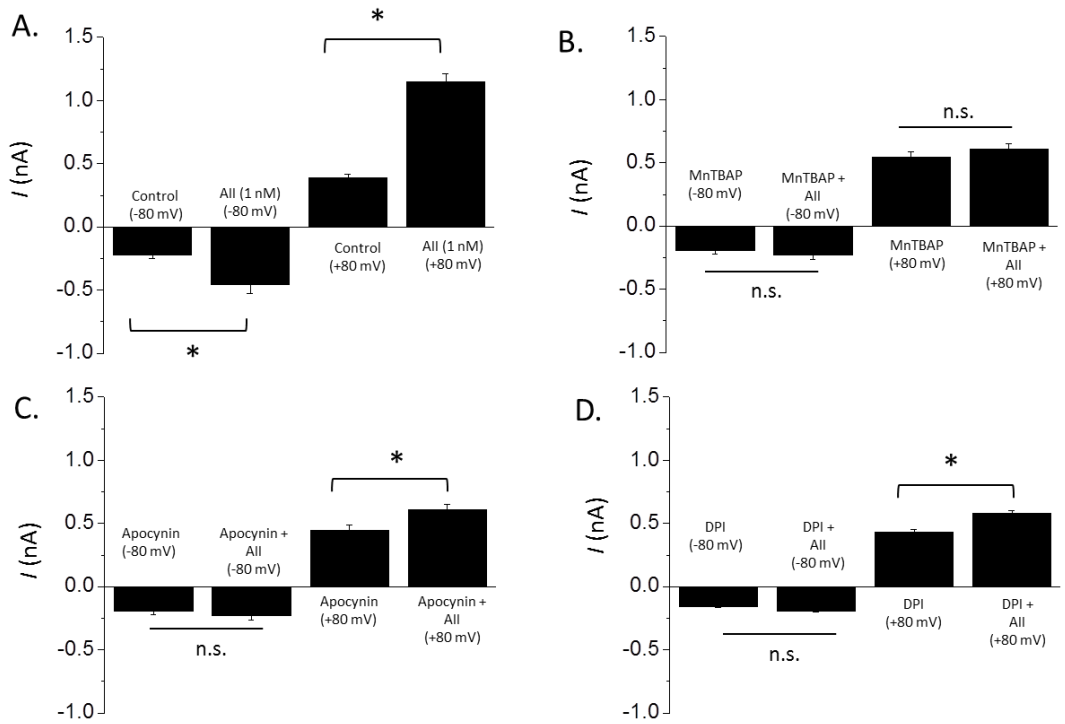

Figure 8.

3.2 Insulin modulates podocyte TRPC6 channels:

Previous studies on TRPC6 channels in heterologous expression systems showed that their activation gives rise to outwardly rectifying macroscopic cationic currents that are much larger in the presence of DAG analogs (20, 51) and that are reduced in the presence of millimolar external Ca^{2+} (33). I observed macroscopic currents with these characteristics by means of conventional whole cell recordings from differentiated podocytes derived from mouse cell lines (Fig. 9). In these experiments, K^+ ions that would normally be present in physiological solutions were replaced by Cs^+ in both the bath and pipette solutions. In addition, external Ca^{2+} was raised to 5.4 mM to improve the stability of whole cell recordings. Macroscopic currents were evoked by 2.5-s voltage ramps from -80 to +80 mV, and currents at +80 mV were quantified for statistical analysis. I observed that cationic currents evoked by voltage ramps under these conditions had an average reversal potential of -4 mV under the recording conditions used in these experiments (N = 18 cells). These currents were substantially larger in cells exposed for 5 min to 100 μM OAG, a membrane-permeable analog of DAG that can activate TRPC6, TRPC3, and TRPC7 channels (20). Moreover, these cationic currents were markedly reduced after superfusion of 10 μM SKF96365, an inhibitor of nonselective cation channels of the TRPC family (81) (Fig. 9, A and B). They were also blocked by superfusion of 100 μM La^{3+}, which blocks TRPC6 channels (64), but increases activation of TRPC5 channels (22, 48, 56) (Fig. 9, C and D). Using a similar design, I observed that treating podocytes with 100 nM insulin could also evoke a significant increase in cationic currents in podocytes that could be instantly blocked by

bath superfusion of either 10 μM SKF-96365 (Fig. 10, A and B) or 100 μM La^{3+} (Fig. 10, C and D).

More than one functional member of the TRPC family is expressed in podocytes (27, 41, 109). Because of the lack of perfectly selective inhibitors, there is no single experimental design that would allow for completely unambiguous isolation of whole cell currents or, for that matter, any functional responses that are mediated by endogenously expressed TRPC6 channels. However, I performed two other experiments that suggest that most or all of the insulin-stimulated current is due to modulation of TRPC6 channels. In one set of experiments, I examined the effects of OAG in control cells and in podocytes previously treated with insulin for 24-hr, and I analyzed the results using a two-way ANOVA (Fig. 11, A). Currents were recorded from 10 cells in each group (for a total of 40 cells in this experiment). There was a significant effect of both insulin ($F1 = 199.38$, $P < 0.0001$) and OAG ($F2 = 26.35$, $P < 0.0005$) in the overall data set. Importantly, there was also a statistically significant interaction between these two treatments ($F1,2 = 37.74$, $P < 0.0002$). This last result indicates that the response to OAG depends on whether cells were previously treated with insulin. Post hoc analysis indicated that both OAG and insulin were effective when applied by themselves, but that applying OAG to cells immediately after 24-hr exposure to insulin treatment did not produce any additional effect. In other words, insulin appears to completely occlude the response to OAG, an observation that is consistent with the hypothesis that OAG and insulin are modulating the same population of channels in podocytes.

Previous studies showed that the set of channels that can be activated by OAG is comprised of TRPC3, TRPC6, and TRPC7 (20). Therefore, in another set of experiments,

I examined the effects of OAG and insulin in wild-type podocytes and in a subclone of the same cell line stably expressing siRNA targeting TRPC6 channels. I observed a nearly complete loss of both OAG-evoked cation currents and insulin-stimulated cation currents in the TRPC6 knockdown cells compared with controls (Fig. 11, B), even though the knockdown is less than 100%. Currents were recorded from 10 cells in each group (for a total of 60 cells in this experiment). Analysis of these data by two-way ANOVA revealed significant effects of the TRPC6 knockdown ($F1 = 17.18$, $P < 0.005$), as well as significant effects of insulin or OAG treatment ($F2 = 66.21$, $P < 0.0001$). Most importantly, there was a highly statistically significant interaction between these two classes of independent variables ($F1,2 = 55.47$, $P < 0.0001$). I found that TRPC6 knockdown abolished the ability of podocytes to increase cationic currents in response to either insulin or OAG. Fluorometric assays, conducted by Dr. Eun Young Kim, indicated that insulin increases H_2O_2 production, and it is known that TRPC6 channels are redox sensitive. I observed that treatment of podocytes with H_2O_2 at 250μM for 30 minutes resulted in significant increase of TRPC6-mediated current (Fig. 11, C and D). Pretreatment with the free radical scavenger MnTBAP inhibited the effects of H_2O_2.

Figure 9: Properties of podocyte cationic currents activated by the diacylglycerol analog oleoyl-2-acetyl-*sn*-glycerol (OAG). ***A***: examples of currents recorded during 2.5-s ramp voltage commands as indicated above the traces in cells treated with vehicle (*top* traces) or after 5-min exposure to 100 µM OAG (*bottom* traces) for 5min. Superimposed traces to the *left* are from single cells before and after bath application of 10 µM SKF96365. The traces on the *right* show SKF96365-sensitive currents obtained by digital subtraction. The dotted lines running through the subtracted traces denote the zero-current level. Note that SKF96365-sensitive currents are much larger after OAG treatment. ***B***: summary of results of several repetitions of the experiment shown in *A*. Ordinate is the amount of mean SKF96365-sensitive current measured at +80mV. *Significant ($P < 0.001$, Student's unpaired *t*-test) increase in current after OAG treatment ($n = 10$ cells in each group). Note that these are group means. The cells exposed to vehicle were not exposed to OAG. ***C***: as in *A* except that currents in vehicle- or OAG-treated cells were blocked by bath superfusion of 100 µM La^{3+}. ***D***: summary of several repetitions of the experiment shown in *C*, showing that La^{3+}-sensitive currents are significantly larger in OAG-treated cells ($P < 0.001$, Student's unpaired *t*-test, $n = 5$ cells in each group).

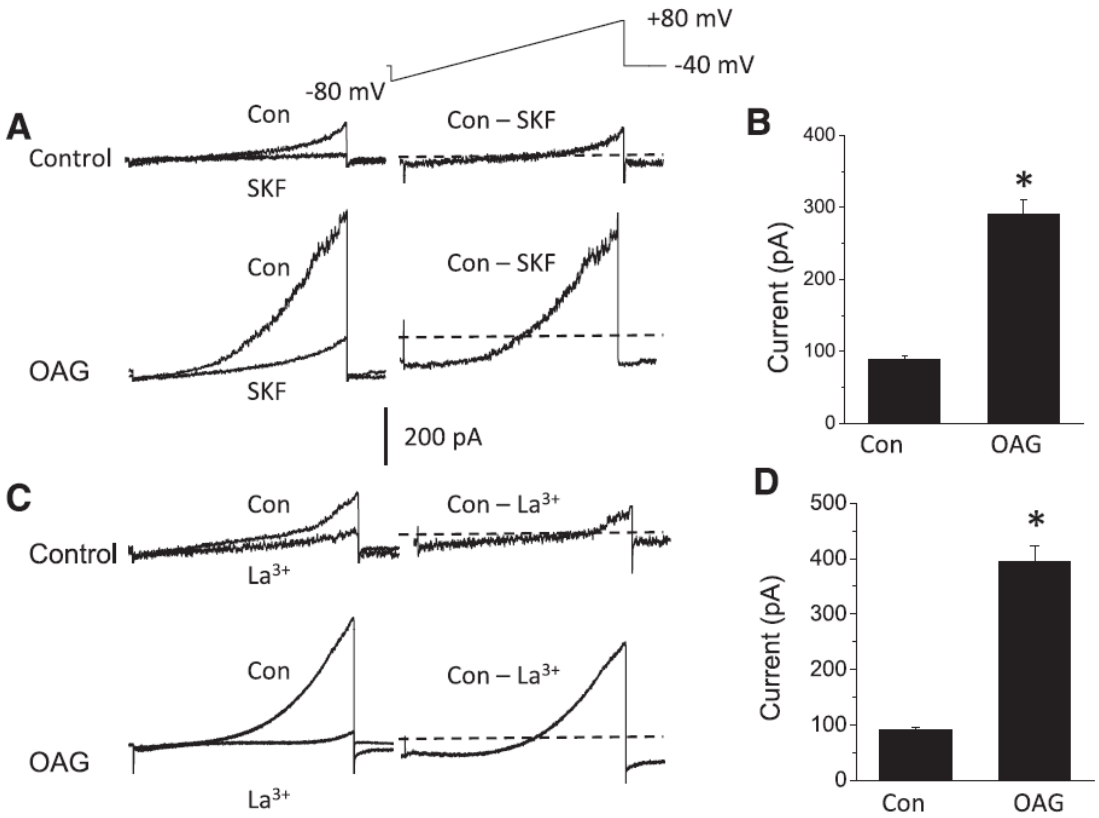

Figure 9.

Figure 10: Insulin increases cationic currents in podocytes. ***A***: currents evoked during voltage ramps in control podocytes (top traces) and in podocytes treated with 100 nM insulin for 12 h (bottom traces), as indicated. Superimposed traces to the left are from the same cell before and after bath application of 10 µM SKF96365. The traces on the right show SKF96365-sensitive current calculated by digital subtraction. The dotted lines running through the subtracted traces denote the zero-current level. Note that SKF96365-sensitive currents are much larger in cells treated with insulin. ***B***: summary of results of several repetitions of the experiment shown in A. Ordinate is the mean SKF96365-sensitive current measured at +80 mV. *Significant ($P < 0.0001$, Student's unpaired t-test) increase in current after insulin treatment ($n = 10$ cells in each group). ***C***: as in A except that currents in control or insulin-treated cells were blocked by bath superfusion of 100 µM La^{3+}. ***D***: summary of several repetitions of the experiment shown in C, showing that La^{3+}-sensitive currents are significantly larger in insulin-treated cells ($P < 0.001$, Student's unpaired t-test, $n = 5$ cells in each group).

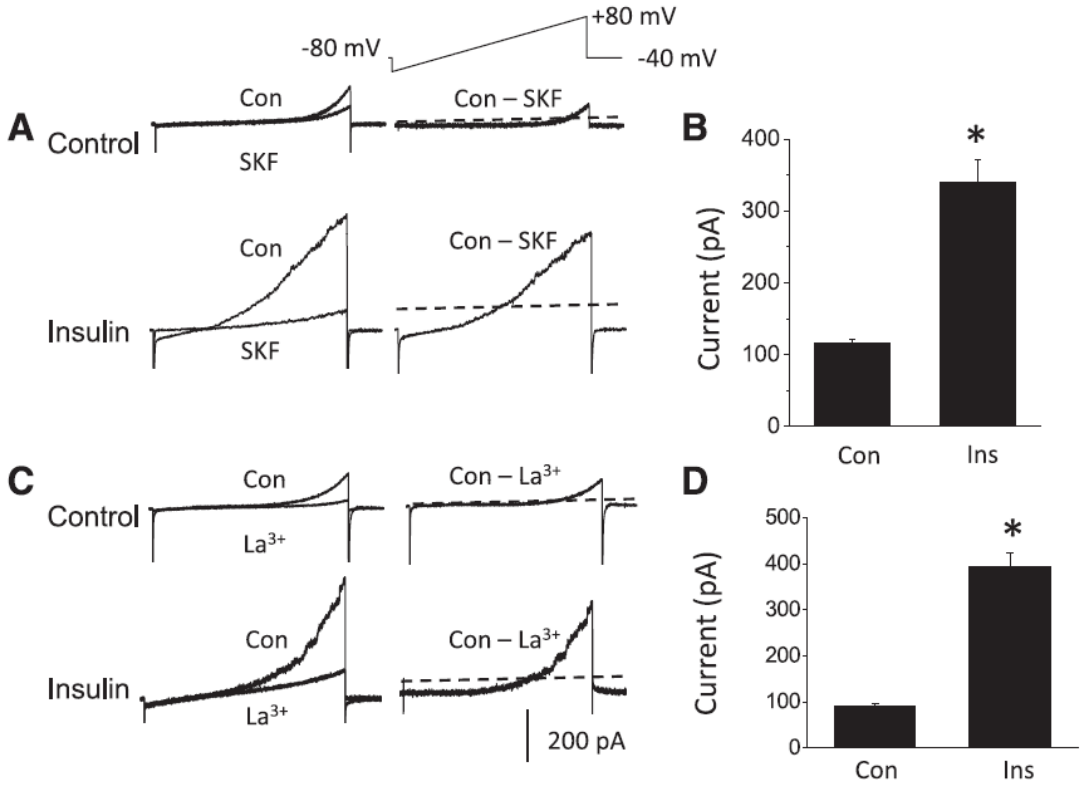

Figure 10.

Figure 11: Insulin activates OAG-sensitive currents in podocytes that are eliminated by TRPC6 knockdown, and H_2O_2 activates TRPC6. ***A***: insulin treatment occludes electrophysiological responses to OAG in podocytes. Control podocytes, or podocytes treated with 100 nM insulin for 12 h, were exposed to vehicle or 100 μM OAG for 5 min, and whole cell quantification of currents at +80 mV was carried out as in Figs. 2 and 3. Bars represent means ± SE for 10 cells in each group. Data were analyzed by 2-way ANOVA and Tukey's post hoc test. The effect of a combination of insulin and OAG was not significantly different from those evoked by either OAG or insulin alone. ***B***: mean currents at +80 mV recorded cells treated with vehicle, with 5 min of OAG, or 24-hr of insulin in wild-type podocytes or in TRPC6 knockdown podocytes, as indicated. Data were analyzed by 2-way ANOVA, which showed that TRPC6 knockdown had a significant ($P < 0.005$) interaction effect on responses to OAG and insulin. Post hoc analysis indicated that responses to OAG and insulin were eliminated in TRPC6 knockdown cells. ***C:*** mean currents at +80 mV recorded from control cells, cells pretreated with MnTBAP with and without H_2O_2, and cells treated with H_2O_2 (250μM) for 30 minutes (for all groups n = 10, P < 0.001, Student's unpaired t-test). ***D:*** representative traces of currents obtained from cells in *C*.

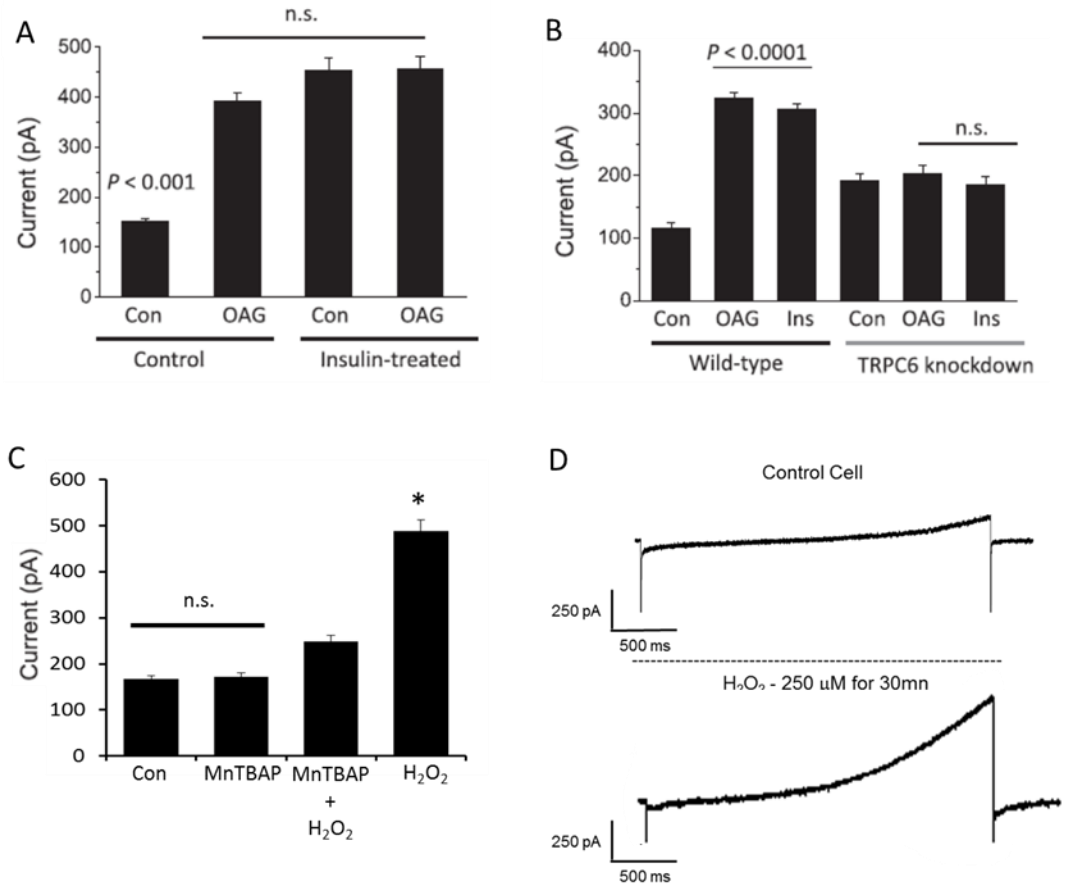

Figure 11.

3.3 NMDAR activation modulates podocyte TRPC6 channels in a ROS dependent manner:

I observed an increase in functional macroscopic currents with pharmacological properties of TRPC6 after treating podocytes with NMDA receptor agonists (Fig. 12). In these experiments, podocytes were treated with NMDA receptor agonists and antagonists for 24-hr. It is known that TRPC6 channels are activated by the diacylglyercol analogue OAG. In order to maximize the observed effects of NMDA receptor activation on TRPC6 channels, cells were then treated with 100μM OAG for 15 min prior to whole-cell recordings. I have previously shown that the OAG-evoked macroscopic currents in podocytes are eliminated by TRPC6 knockdown (66). Whole-cell currents were evoked by 2.5-s duration ramp voltage commands (-80 to +80 mV) before and after application of 50μM La^{3+} (Fig. 12, A), which blocks TRPC6 channels but not TRPC5 channels in podocytes (64). The La^{3+}-sensitive components of the currents were obtained by digital subtraction in each cell and then quantified (Fig. 12, B). I observed that La^{3+}-sensitive currents (measured at +80 mV) in cells previously exposed to NMDA were nearly 3-fold larger than those observed in untreated cells, and the effects of NMDA were blocked by concurrent treatment with either 10μM MK-801 or 100μM MnTBAP (Fig. 12, A and B). In addition, I observed that the currents recorded using these protocols were almost completely inhibited by 50μM SKF-96365 (Fig. 12, C), an agent that blocks cationic channels in the TRPC family, and which nearly eliminates TRPC6 currents in podocytes at this concentration (66). In order to determine the mechanism of NMDA receptor activation of TRPC6, multiple fluorometric and surface biotinylation assays were carried out by Dr. Kim (67). Dr. Kim observed increased surface expression of p47(phox) after

24-hr of NMDA treatment, and inhibition of NMDA effects by a ROS scavenger. By contrast she did not see marked increases in steady-state surface expression of NO2 or NOX4. Recall that p47(phox) is one of two cytosolic auxiliary subunits of NOX2, and its translocation to the cell surface is an essential step leading to activation of NOX2 catalytic activity (10). These findings indicate that NMDA receptor activation triggers NOX2 generation of H_2O_2. I have already shown that peroxide treatment activates TRPC6 channels in podocytes. Using surface biotinylation assays, Dr. Kim found that a 24-hr treatment with 50 or 100μM NMDA caused a robust increase in the steady-state surface expression of podocyte TRPC6 channels. This effect was blocked by concurrent application of MK-801 or MnTBAP. It is known that sustained activation of NMDA receptors in podocytes can engage functionally significant pathways that are downstream of TRPC6. One such pathway entails activation of nuclear factor of activated T-cells (NFAT) (67). Highly phosphorylated NFAT normally resides in the cytosol. However, TRPC6-mediated activation of calcineurin results in dephosphorylation of NFAT, causing some of it to translocate to the nucleus where it can regulate gene expression (67). Dr. Kim looked at NMDA's effect on NFAT mobilization (Fig. 13). Using an assay based on cell fractionation, Dr. Kim observed that 100 μM NMDA treatment for 24 hours caused a marked increase in the amount of NFAT that is located in nuclei (a cell fraction enriched in histone), but did not produce a substantial effect on cytosolic NFAT (a much larger pool in a cell fraction in which actin is abundant). This effect of NMDA was blocked by concurrent exposure to either 10 μM MK-801 or 50 μM SKF-96365.

Figure 12: NMDA treatment increases TRPC6-like cationic currents in podocytes. All cells were treated with 100 μM OAG for 15 min before recordings were made. ***A***: Examples of whole-cell currents evoked by ramp voltage commands (-80 mV to +80 mV in 2.5 seconds) made from a holding potential of -40 mV. Traces on left show currents before and after bath superfusion of 50 μM La^{3+}, and traces on right are digital subtractions (control - La3+). Examples shown are from control cells and from cells treated for previous 24-hr with 100 μM NMDA in presence and absence of 10 μM MK-801 or 100 μM MnTBAP, as indicated. NMDA was not present at the time recordings were made. Note increase in La^{3+}-sensitive currents in NMDA-treated cells, and inhibition of this effect by MK-801 and MnTBAP. ***B***: Summary of results of recordings with n = 10 cells in each group. Ordinate represents La3+-sensitive current measured at +80 mV. Asterisk indicated $P < 0.05$ as determined by one-way ANOVA followed by Tukey's post hoc test. ***C***: As in panel A except that traces show currents evoked before and after application of 50 μM SKF-96365.

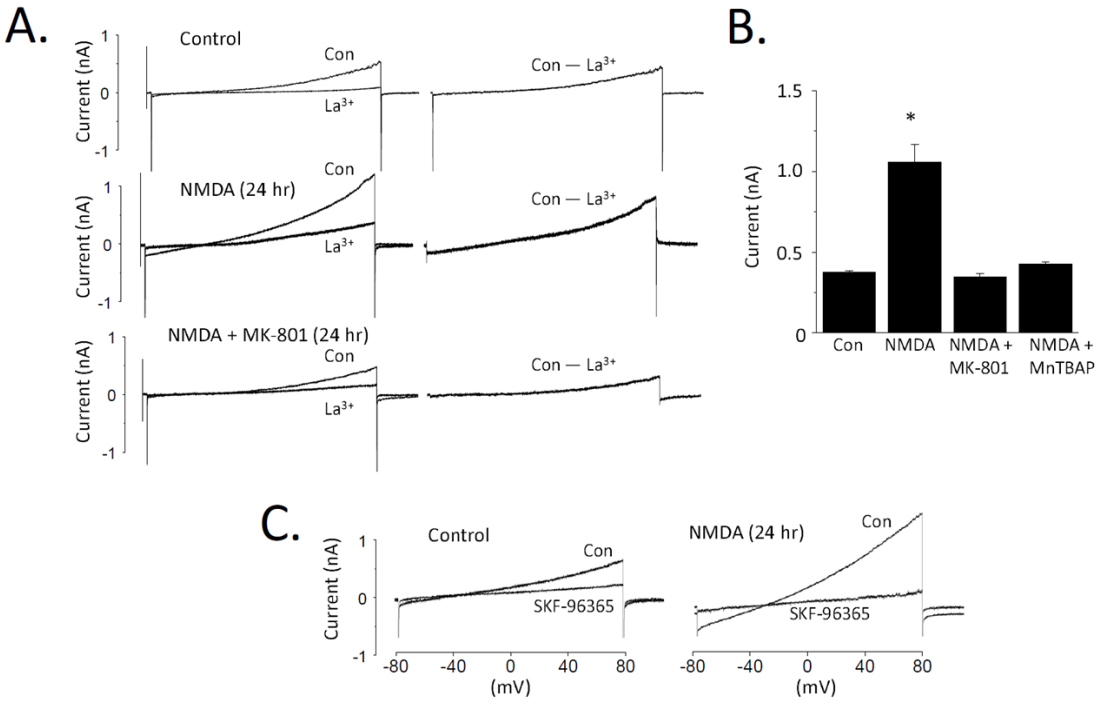

Figure 12.

Figure 13: NMDA increases nuclear localization of NFAT in podocytes. Experiments were carried out by Dr. Eun Young Kim. ***A:*** NMDA treatment for 24-hr increases the amount of NFAT detected by immunoblot in a nuclear extract of podocytes. ***B:*** Histone expression was used to monitor loading. There was no change in NFAT expression in the cytosolic fraction in which actin expression was used to monitor loading. The effects of NMDA were blocked by either 10 μM MK-801 or 10 μM SKF-96365, an inhibitor of TRPC6 channels.

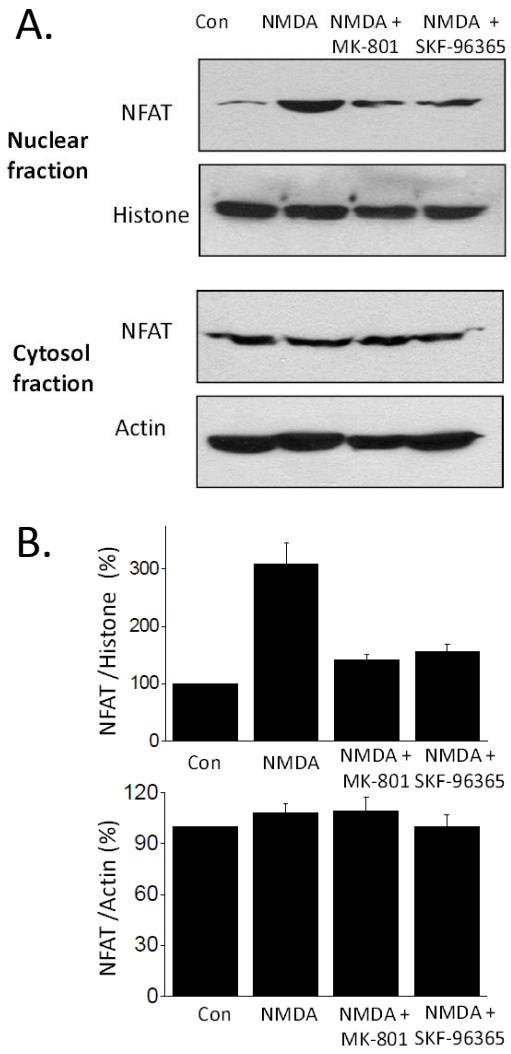

Figure 13.

3.4 Podocyte TRPC6 channels are mechanosensitive:

In my initial studies I examined whether mechanical stimuli could evoke activation of endogenously expressed TRPC6 channels of differentiated immortalized podocyte cell lines. In my experiments, membrane stretch was evoked by changing from a 340 mOsm/L bath saline (100%) to a hypoosmotic saline diluted to 70% of control (238 mOsm/L). The amplitudes of cationic currents were monitored by periodic application of ramp voltage commands (from -80 mV to + 80 mV over 2.5 sec). I observed a marked increase in cationic currents in podocyte cell lines during application of 70% hypoosmotic extracellular solutions. This increase in current was fully reversible when the bath was returned to the original 100% saline (Fig. 14, A). Hypoosmotic stretch produces a highly reproducible response, resulting in a current typically about 2-fold greater than control at +80 mV, based on recordings from more than 80 immortalized podocytes. The effect of hypoosmotic stretch on cationic current was blocked by pretreating cells with 10 μM SKF-96365, a pore-blocking inhibitor of TRP superfamily channels (Fig. 14, B). I observed that the effect of membrane stretch on cationic currents in podocytes was completely blocked by pretreatment with 50 μM La^{3+} (Fig. 14, C), suggesting that currents activated by hypoosmotic stretch are mediated primarily by TRPC6. To confirm this more directly, I used siRNA to selectively reduce expression of TRPC6. Transfecting podocytes with a panel of siRNAs directed against TRPC6 reduced total expression to <20% of that observed in cells transfected with a control siRNA (Fig. 15, A). This treatment nearly abolished the hypoosmotic stretch-evoked increase in cationic current (Fig. 15, B and C), confirming that this response requires functional

TRPC6 channels, as I previously observed with La^{3+}- and SKF-96365-sensitive currents activated by analogs of DAG (66, 67).

I was also able to activate these cationic currents using other mechanical stimuli in podocyte cell lines. In one set of experiments, a micropipette with a tip diameter of ~1 μm was placed adjacent to the podocyte cell body, and was used to eject extracellular saline containing 60% sucrose using a pressure pulse of 5 p.s.i. (34 kPa) (Fig. 16, A). The sucrose was included mainly to increase the density of the solution and thus the efficacy of the mechanical stimulus. These pressure pulses evoked a localized slight inward deformation of the plasma membrane that could be readily observed using Hoffman modulation contrast optics. This stimulus also evoked a transient inward current at -60 mV that could be evoked repeatedly. This response was completely blocked after perfusion of saline containing either 50 μM La^{3+} (Fig. 16, B) or 10 μM SKF-96365. Based on these experiments, it is clear that the TRPC6 channels expressed in immortalized mouse podocytes can be activated by stimuli that cause deformation of the plasma membrane.

I next examined if similar responses could be observed in podocytes in a more intact preparation. To do this, I made whole cell recordings from rat podocytes in explanted glomeruli. Briefly, rat glomeruli were isolated using a sieving procedure and allowed to adhere to a collagen-coated glass coverslip. After 24-72 hr, glomeruli adhere sufficiently tightly to allow stable whole-cell recording from cells on the outer margins of the glomeruli. These cells were chosen because it is possible to see the initial segments of primary processes extending from the podocyte cell body under Hoffman modulation contrast optics with a 40x objective. Note that in this preparation, the podocytes are still

attached to the glomerular capillary. In my initial experiments, I observed a robust increase in cationic currents after application of a hypoosmotic stretch using the same recording and pipette salines used in the experiments on immortalized cell lines. The resulting cationic currents are qualitatively similar to those in immortalized podocyte cell lines, and the percentage increase in current evoked by membrane stretch was similar. However, both basal and stretch-evoked currents in the explanted glomerulus preparation were substantially larger than those observed in podocyte cell lines. As with immortalized cell lines, the stretch-evoked currents in explanted glomeruli were blocked by bath application of 50 μM La^{3+} or 10 μM SKF-96365 (Figs. 17, A and B). I also used the explanted glomerulus preparation to apply a shear force evoked by fluid flow over the surface of the cell. In these experiments, whole cell recordings were made from podocytes in a static bath. Simply introducing a flow of saline over the podocytes in this preparation was sufficient to evoke an inward current which reversed as soon as the flow was halted (Fig. 17, C). These responses could be evoked repeatedly. Moreover, this response was almost completely blocked when the flow stimulus was applied in a bath solution containing 50 μM La^{3+} (Fig. 17, D).

Previous investigators working in other cell types have demonstrated that TRPC6 channels show changes in gating in response to various mechanical stimuli (29, 39, 91). However the mechanisms that underlie these responses are controversial (39, 107) and may be cell-type specific. In cerebral arteries there is evidence that TRPC6 channels become active as a result of stretch-evoked activation of signaling cascades that act through various phospholipases. As a result, stretch responses on those cells can be blocked by phospholipase inhibitors (107). This type of phenomenon does not appear to

explain the mechanical activation of podocyte TRPC6 channels, as I observed that normal hypoosmotic stretch activation could be recorded from podocytes treated with the pan-phospholipase C inhibitor U73122 or the pan-phospholipase A2 inhibitor ONO-RS-082 (Fig. 18, A and B). Moreover, the mechanical forces that lead to activation of TRPC6 appear to propagate through the plasma membrane, rather than through underlying cytoskeleton. Thus, treating podocytes with 1 μM cytochalasin D (Cyto D) for 20 min caused a marked disruption of filamentous actin networks in podocytes, based on phalloidin staining (Fig. 19, D). This treatment also increased the mean amplitude of hypoosmotic stretch-evoked currents but had no effect on basal currents (Fig. 18, A and B), suggesting that actin filaments are not required to evoke a mechanical response, and that they actually constrain the expansion of the plasma membrane during hypoosmotic stretch. By contrast, stretch-activation of podocyte TRPC6 was completely inhibited by GsMTx4, a peptide toxin originally isolated from the Chilean tarantula spider *Grammostola spatulata* (9, 108). GsMTx4 can inhibit the mechanical activation of a wide range of structurally dissimilar mechanosensitive channels, although notably it does not block mechanical activation of TRPC6 in cerebral vascular smooth muscle, which is thought to be a secondary response to phospholipase activation (9). Because both enantiomers of GsMTx4 are equally effective, this toxin is thought to act at the lipid-protein interface to prevent transmission of force to key residues in mechanosensitive channels (9, 107, 108). I observed that pretreatment of podocytes with 2.5 μM GsMTx4 completely eliminated responses to hypoosmotic stretch in podocytes. Moreover, perfusion with GsMTx4 caused complete inhibition of a fully developed hypoosmotic stretch response in less than 3 min (Fig. 19, C). Collectively these experiments are

consistent with a model in which various mechanical forces are transmitted directly to TRPC6 channels through the leaflets of the podocyte plasma membrane (9). Membrane deformation can be induced chemically by insertion of anionic amphipaths into the cell membrane. The addition of trinitrophenol increases cationic current in podocyte cell line with a significant increase in maximum outward current (Fig. 20, A and B). Membrane fluidity, or its ability to stretch, can be influenced by membrane cholesterol levels (14). Methyl-β-cyclodextran (MβCD) can be used to remove cholesterol from the cell membrane, or MβCD can be preloaded with cholesterol and used to insert additional cholesterol into the membrane (14, 101). For cholesterol depletion, cells were treated for 24 hours with 10mM MβCD. Treated cells displayed increased hypoosmotic stretch response (Fig. 21). Conversely, after addition of cholesterol by a 24 hour treatment of a 10mM MβCD-cholesterol complex, podocytes showed markedly reduced hypoosmotic stretch response (Fig. 22).

3.5 Podocin differentially modulates chemical and mechanical activation of podocyte TRPC6 channels:

Podocin is selectively expressed in the SD domain of podocyte foot processes in vivo, and Huber and coworkers showed that podocin and TRPC6 can co-immunoprecipitate when they are co-expressed in heterologous expression systems (58). Dr. Eun Young Kim in our group used co-immunoprecipitation of proteins endogenously expressed in the immortalized mouse podocyte cell line to confirm this interaction. This interaction could be easily detected regardless of which protein was targeted for the initial precipitation. To assess which portions of the proteins are involved in the

interaction, constructs encoding the soluble NH_2- and COOH-terminals of TRPC6 with HA tags (HA-TRPC6-N and HA-TRPC6-C) were expressed in HEK293 cells. Dr. Kim found that direct interactions between podocin and TRPC6 occur at the cytosolic COOH-terminals of these proteins.

To establish a physiological role for podocin in regulation of endogenously expressed TRPC6 channels, I utilized a transient siRNA protocol that reduced podocin expression to <10% of that observed in podocytes transfected with a control siRNA (Fig. 23, A). This procedure did not affect the total expression of TRPC6 channels as assessed by immunoblot. Importantly, I observed a very large increase in the amplitude of cationic currents evoked by hypoosmotic stretch in podocin knockdown cells compared to controls treated with a non-specific siRNA (Fig. 23, B). Indeed, this manipulation evoked the largest TRPC6 currents that we have ever seen in these cells, regardless of the stimulus used for their activation. We should also note that the large stretch-evoked currents in podocin knockdown cells were completely blocked by bath application of 50 μM La^{3+} or 10 μm SKF-96365, and currents were eliminated after siRNA knockdown of TRPC6 itself. Thus, podocin knockdown is not uncovering a pharmacologically distinct mechanosensitive channel. By contrast to its effects on stretch responses, podocin knockdown largely suppressed the increases in cationic current normally evoked by 100 μM of the membrane-permeable DAG analog 1-oleoyl-2-acetyl-*sn*-glycerol (OAG) (Fig. 23, C). We have previously shown that those responses are entirely mediated by TRPC6 in mouse podocyte cell lines (66). In addition, siRNA knockdown of TRPC6 in podocin KD cell lines prevents an increase in whole cell current in response to hypoosmotic

stretch (Fig. 24, A and B). Collectively this data indicate that in podocytes the presence or absence of podocin affects the preferred mode of activation of TRPC6 channels.

Figure 14: Hypoosmotic stretch activates currents through TRPC6 channels in immortalized mouse podocyte cell lines. ***A***: Representative example of currents in a single cell evoked by ramp voltage commands (-80 mV to +80 mV over 2.5. s from a holding potential of -40 mV) in normal external saline (100%), in hypoosmotic saline (70%) and after return to normal saline (100%, right). Note reversible increase in ourwardly rectifying cationic currents. ***B***: Examples of hypoosmotic stretch responses in a control cell (left) and in a different cell in the presence of 10 μM SKF-96365 (right). Currents recorded in normal and hypoosmotic solutions are superimposed. ***C***: Examples of hypoosmotic stretch responses in a control cell (left) and in a different cell in the presence of 50 μM La^{3+} (right). ***D***: Summary of results from several cells. The ordinate is the mean difference current ± s.e.m. (70% saline – 100% saline) at +80 mV in control conditions and in the presence of 10 μM SKF-96365 or 50 μM La^{3+} as indicated. *N* = 10 cells in each group.

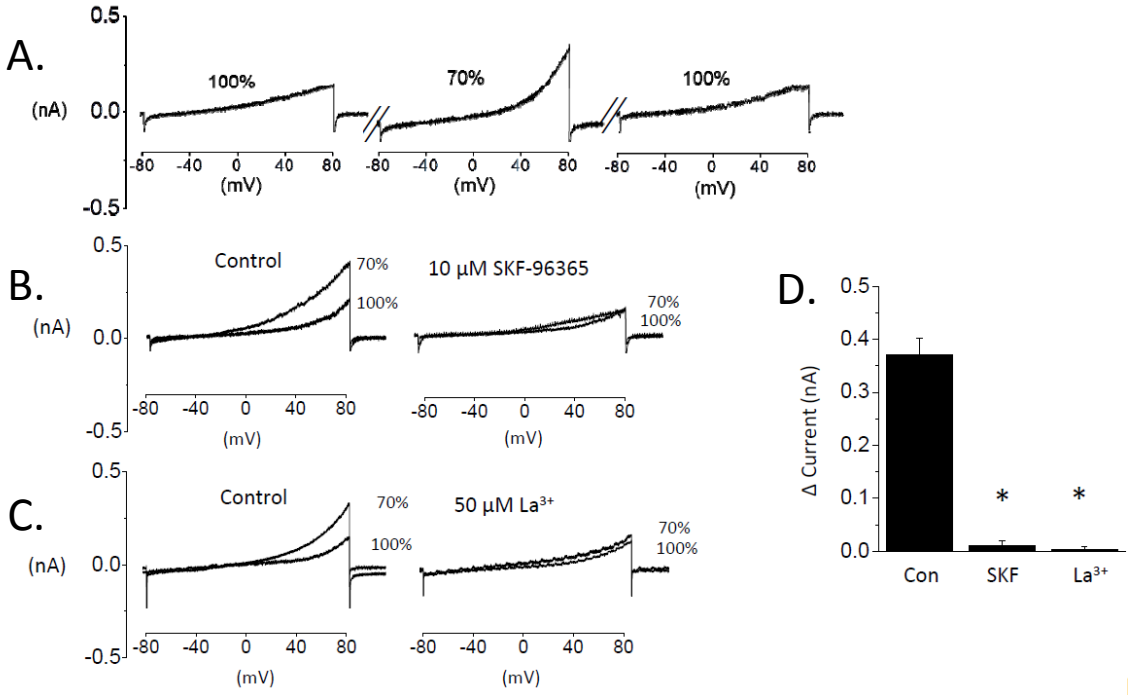

Figure 14.

Figure 15: Stretch induced currents are primarily TRPC6 mediated. ***A:*** Western blot results of TRPC6 siRNA knockdown on total TRPC6 levels. ***B:*** Summary of effects of TRPC6 knockdown with N = 10 cells in each group. Asterisk indicates $P < 0.05$ compared to control. ***C:*** Representative examples of hypoosmotic stretch-evoked currents in TRPC6 knockdown and control cells.

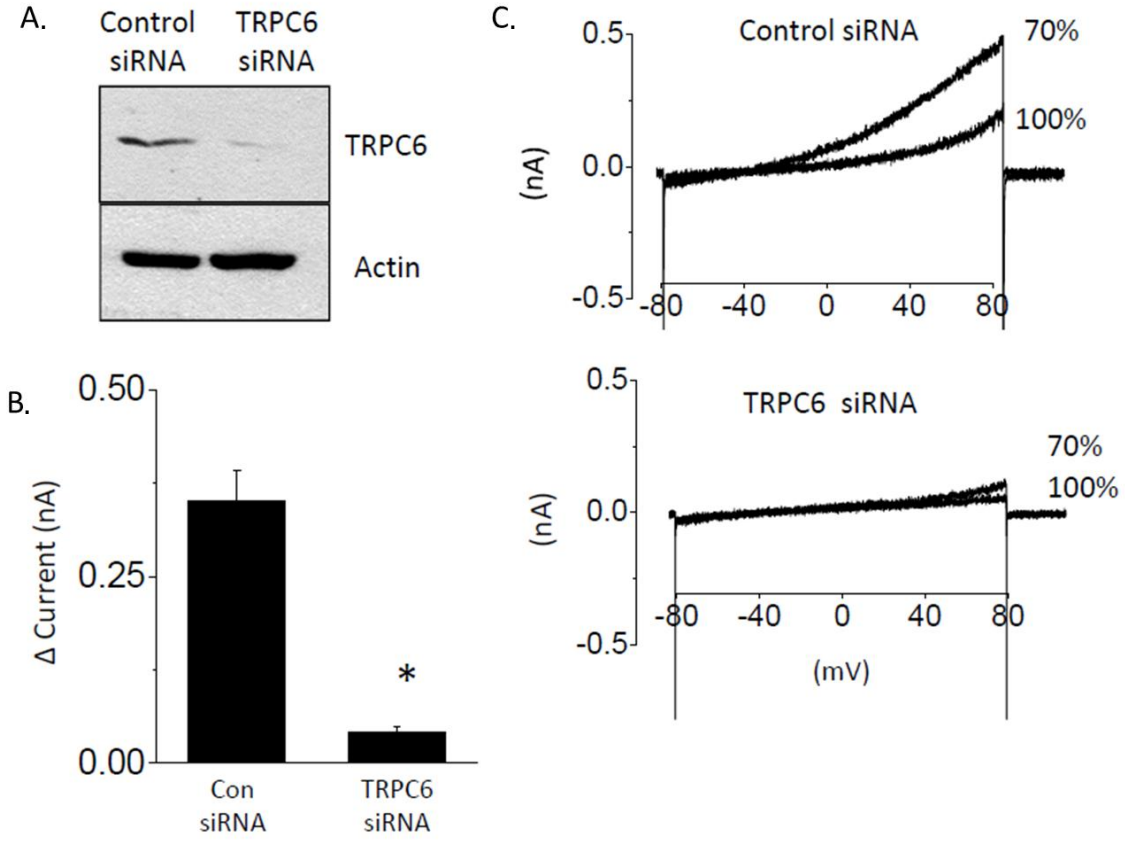

Figure 15.

Figure 16: Currents evoked by pressure pulses in mouse podocyte cell lines. ***A***; Schematic diagram showing experimental design. Normal saline containing 60% sucrose to increase viscosity is applied to the cell body by pressophoresis from an adjacent micropipette. ***B***: This stimulus produces a distinct inward current in normal saline, but not after application of external saline containing 50 μM La^{3+}. In this figure, two responses from the same cell are shown superimposed. Holding potential was -60 mV. Similar responses were seen in eight other cells.

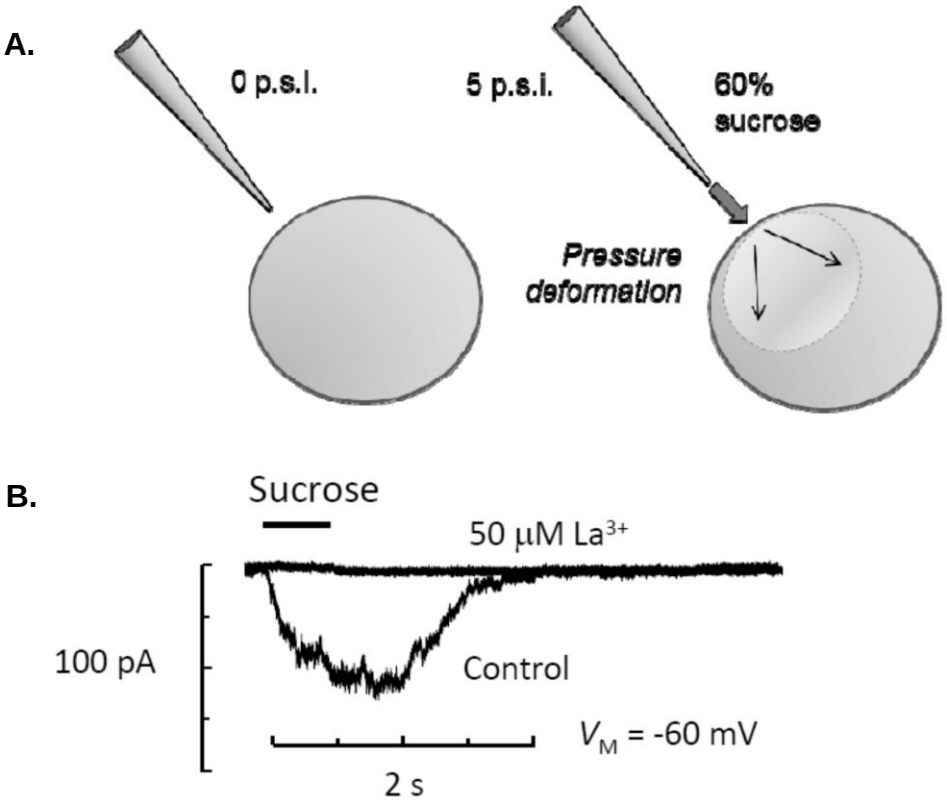

Figure 16.

Figure 17: Hypoosmotic stretch evokes cationic currents in primary rat podocytes in glomerular explants. Whole-cell recordings are from podocytes on the external margin of the preparation. These cells could be identified by larger primary processes emanating from the cell body. ***A***: Representative recording from a single cell showing currents evoked by ramp voltage commands in normal saline (left), in hypoosmotic saline (center) and in hypoosmotic saline containing 50 μM La^{3+}. ***B***: Representative recordings from a single cell showing complete inhibition of hypoosmotic stretch response after application of 10 μM SKF-96365. ***C:*** Examples of cationic currents repeatedly evoked by flow of bath saline in podocyte on the external margin of isolated glomerulus. ***D***: Example of recording showing complete block of flow-evoked currents after introducing 50 μM La^{3+} into the bath.

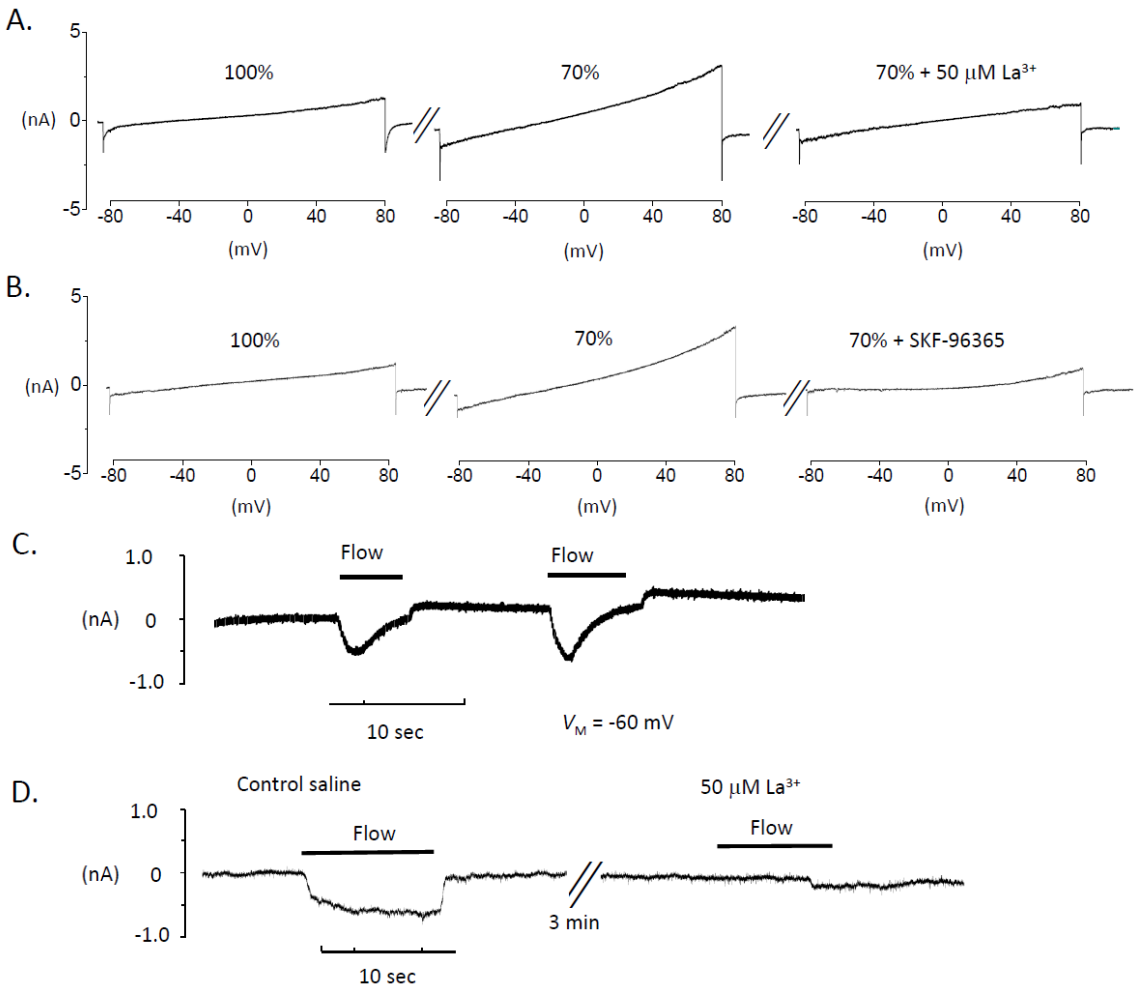

Figure 17.

Figure 18: Hypoosmotic stretch responses persist after inhibition of phospholipases in mouse podocyte cell lines. ***A***: Representative responses to hypoosmotic stretch in control cells (left), in cells treated with the pan-phospholipase A2 inhibitor ONO-RS-082 (middle) and in cells treated with the pan-phospholipase C inhibitor U73122 (right). ***B***: Summary of several repetitions of these experiments, with $N = 8$ cells in each group. No statistically significant differences were observed.

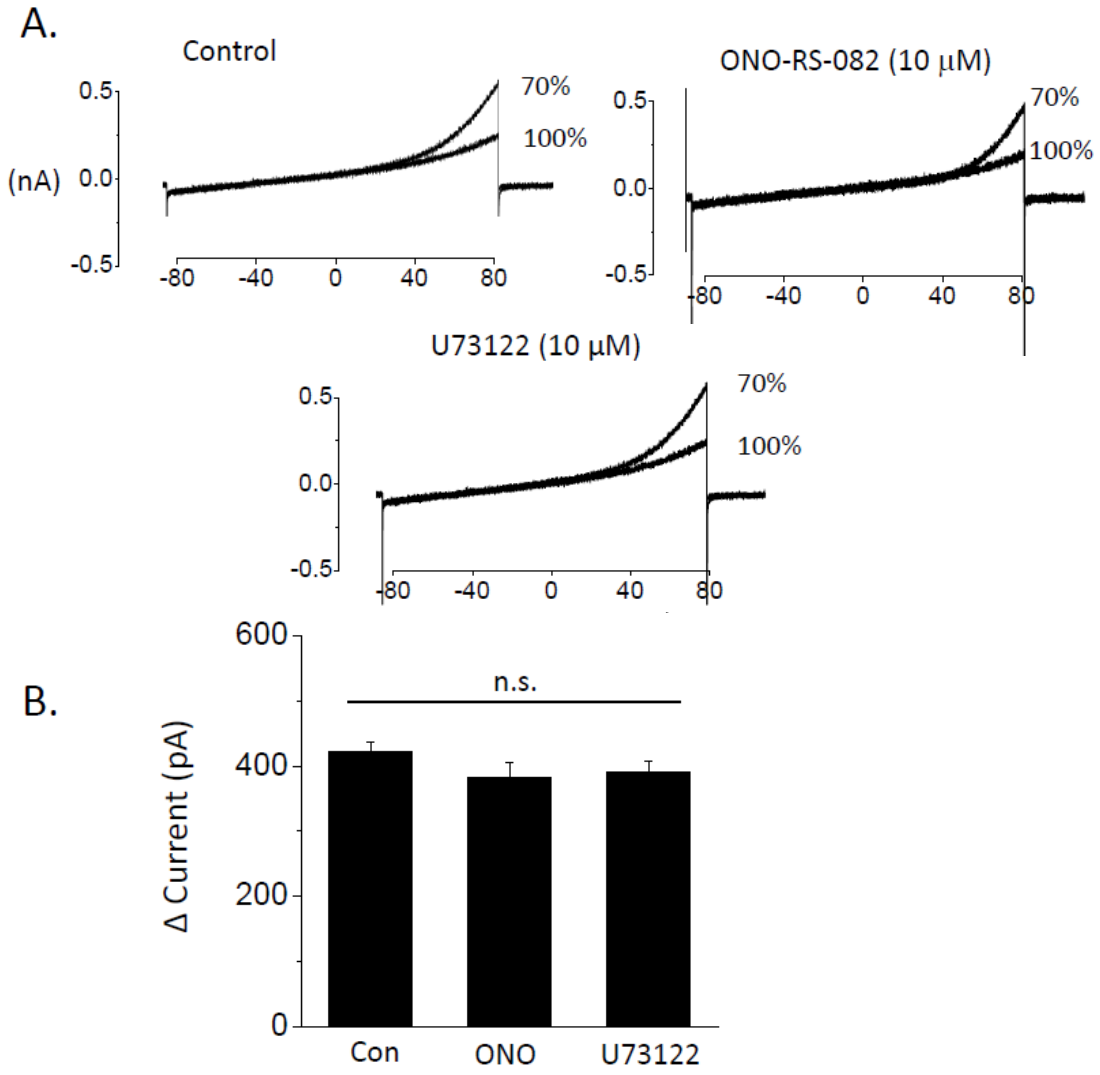

Figure 18.

Figure 19: Evidence that forces are transmitted to TRPC6 channels through the lipid bilayer in mouse podocyte cell lines. ***A:*** Representative examples of stretch-evoked cationic currents in a control cell (left) and in a different podocyte that had been treated with cytochalasin D for 20 min (right). ***B***: Summary of several repetitions of this experiment. Note marked increase in stretch-evoked currents after cytochalasin D, $N = 8$ cells in each group. ***C:*** Recording from a single cell in control saline (right), during hypoosmotic stretch (middle) and complete blockade of the hypoosmotic response within minutes of adding 2.5 μM GsMTx4 (right). ***D:*** Actin filament staining of podocytes before and after cytochalasin D treatment.

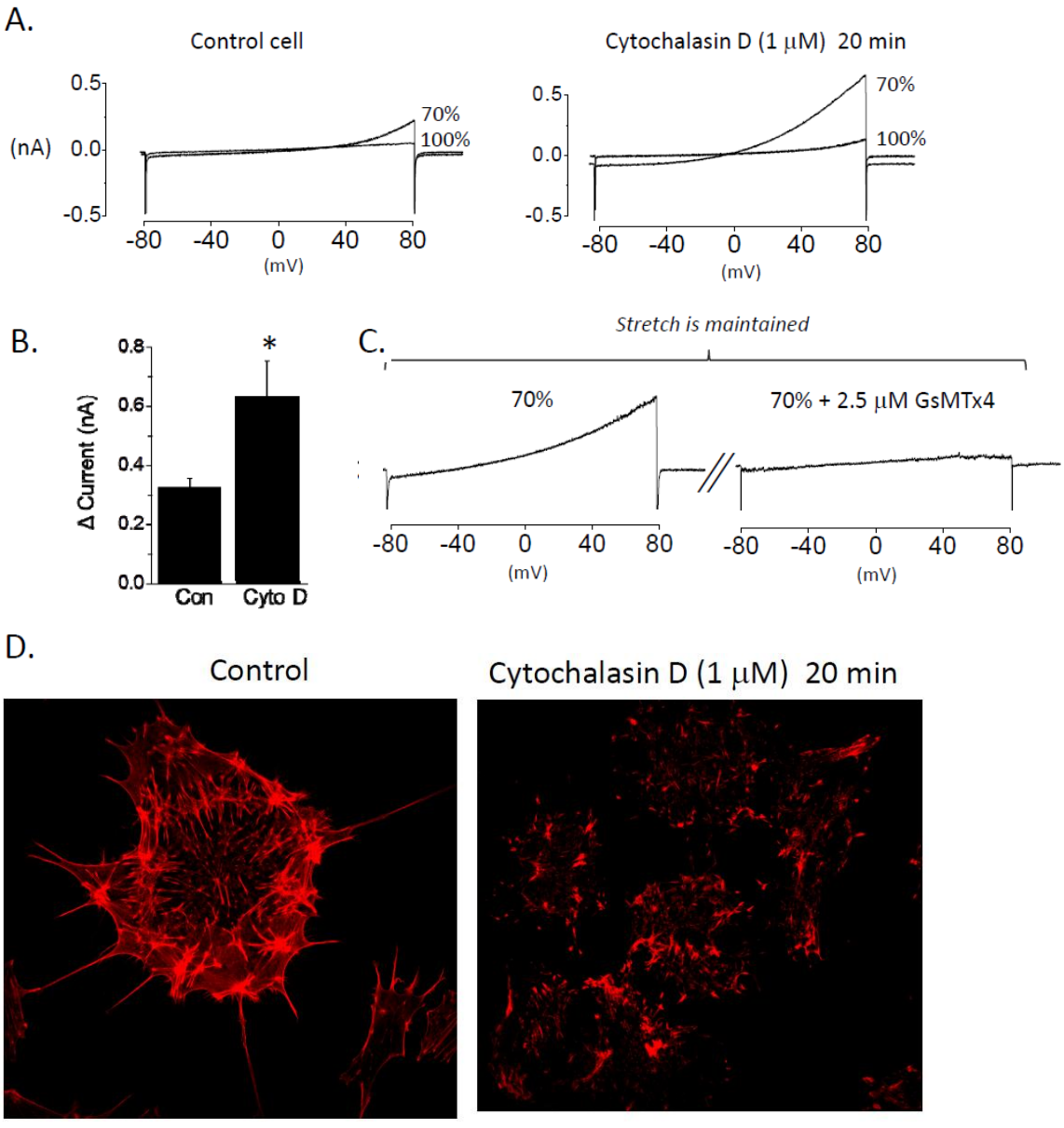

Figure 19.

Figure 20: Deformation of cell membrane with an anionic amphipath increases cationic current in podocyte cell line. ***A:*** representative traces showing the effects of washing on trinitrophenol (500µM). ***B:*** mean effects of trinitrophenol on a group of cells (n = 9). TNP caused a significant increase in maximum outward current ($P < 0.0001$, Student's unpaired t-test).

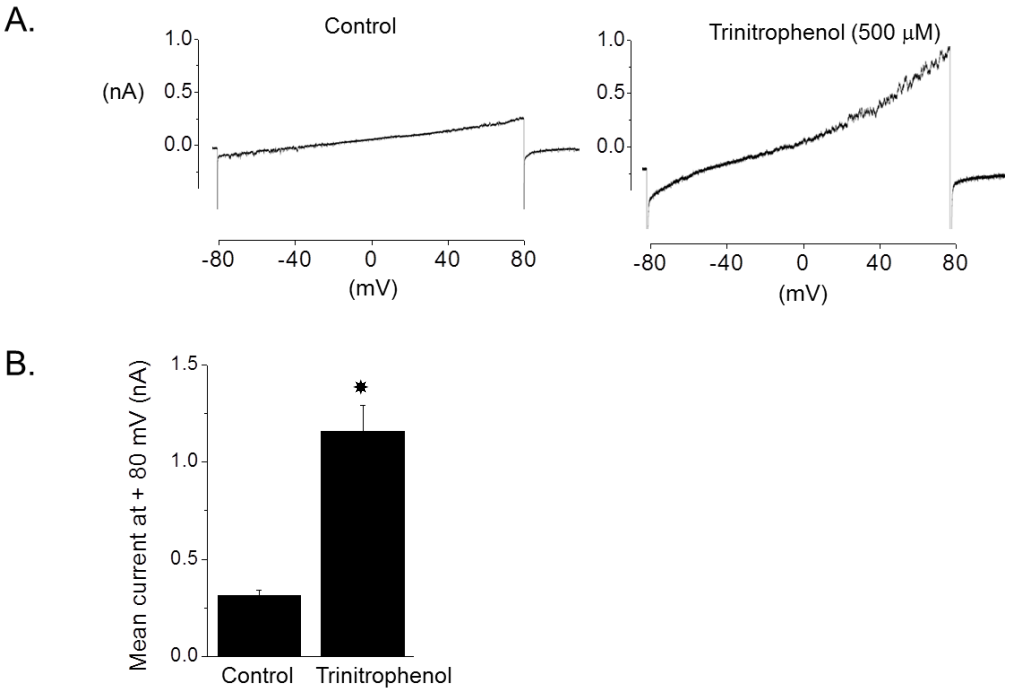

Figure 20.

Figure 21: Sustained depletion of membrane cholesterol increases stretch-activated currents in podocytes. ***A:*** representative tracings from two cells treated for 24hr. with 10mM MβCD. Treated cells displayed increased hypoosmotic stretch response. ***B:*** representative traces obtained from a control cell. Stretch response was measured as a reference for the cholesterol depleted cells.

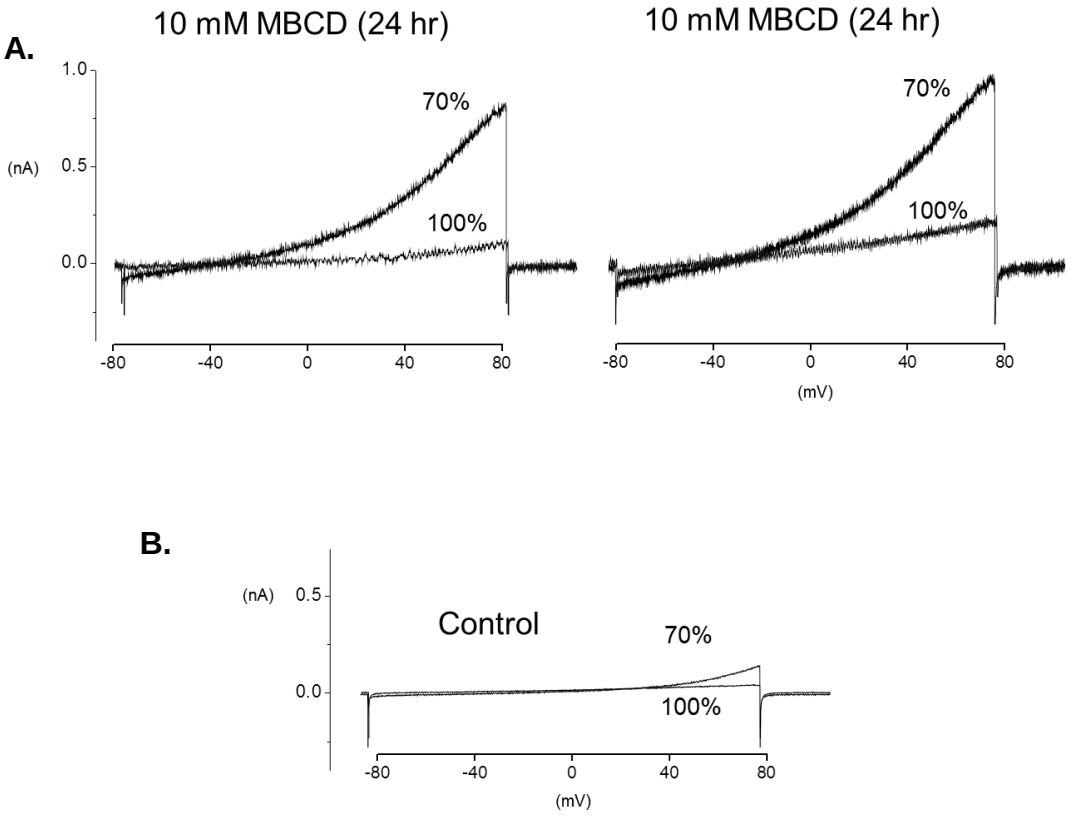

Figure 21.

Figure 22: Addition of membrane cholesterol suppresses stretch activation in podocytes. ***A:*** representative tracings from two cells treated for 24hr. with 10mM MβCD-cholesterol complex. Treated cells displayed limited hypoosmotic stretch response. ***B:*** representative traces obtained from a control cell. Stretch response was measured as a reference for the cholesterol depleted cells.

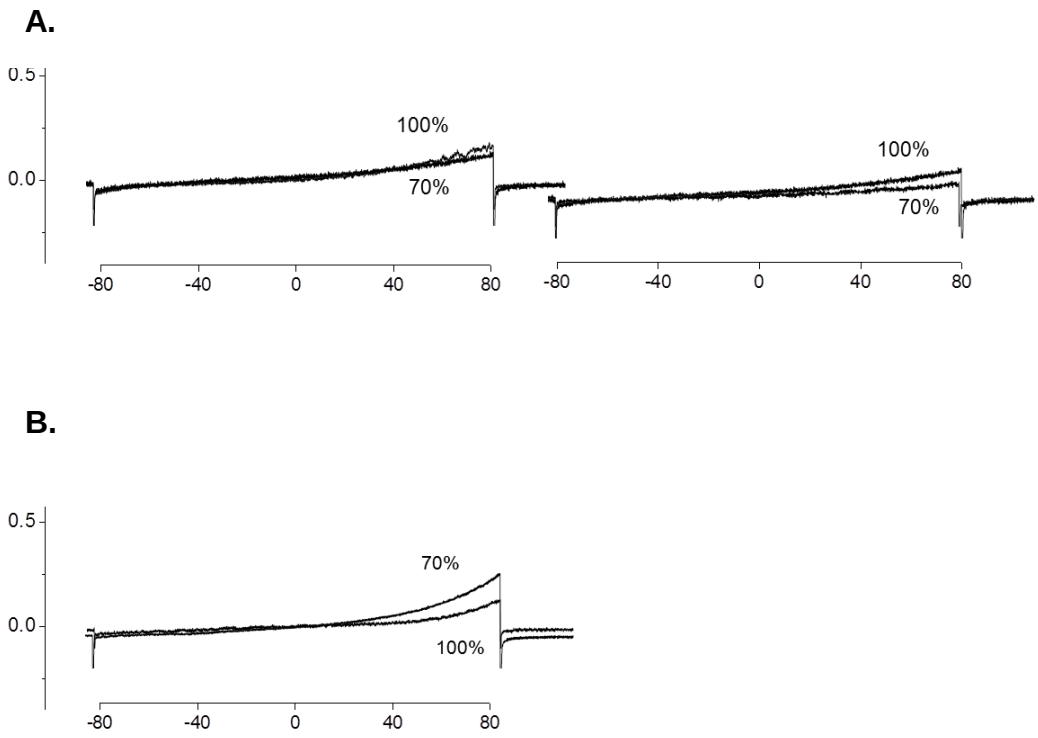

Figure 22.

Figure 23: Podocin knockdown affects mechanical and chemical activation of podocyte TRPC6 channels. ***A:*** Immunoblot results of siRNA knockdown of podocin showing no effect on TRPC6 levels. ***B***: Representative examples of hypoosmotic stretch responses in control cells (left) and in podocin knockdown cells (right). Note very large amplitude of currents after podocin knockdown. ***C***: Summary of several repetitions of this experiment showing 4-5 fold increase in difference currents, *N* = 12 cells in each group. ***D***: Typical responses to the membrane-permeable DAG analog OAG (100 μM) in control (top) and podocin knockdown cells (bottom). Traces show currents in single cells before and after bath application of OAG. In control cells, OAG evokes a marked increase in cationic currents, but these responses are nearly eliminated after podocin knockdown. ***E***: Summary of several repetitions of this experiment, showing nearly complete block of OAG responses in podocin knockdown cells (N = 8 cells in each group, P < 0.0001, Student's unpaired t-test).

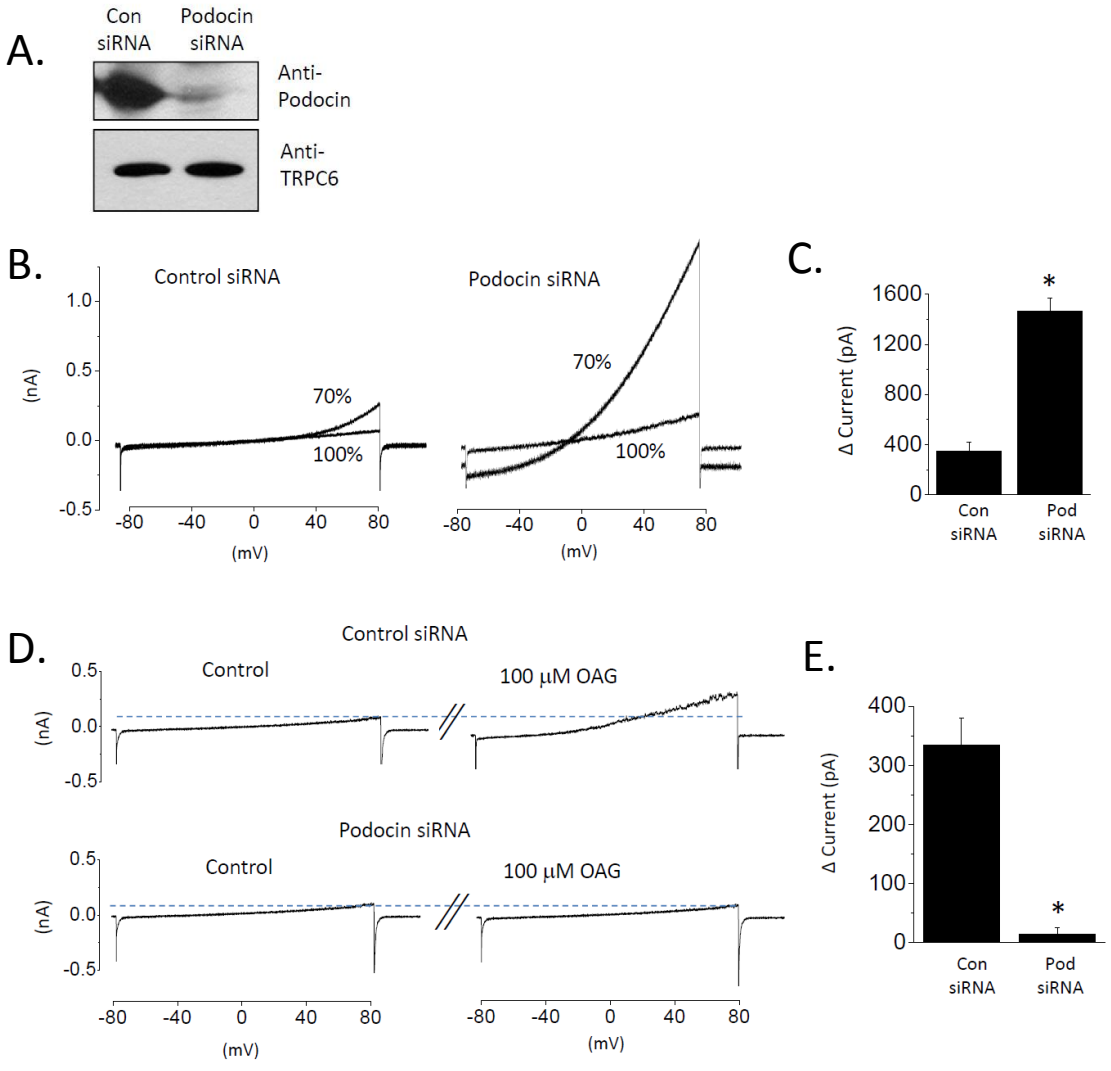

Figure 23.

Figure 24: Podocin effects TRPC6-mediated current. ***A:*** Representative traces obtained from podocin KD cells treated with control siRNA and TRPC6 siRNA. TRPC6 knockdown significantly reduces hypoosmotic stretch activated current. ***B:*** Summary of several repetitions of this experiment, showing TRPC6 knockdown significantly reduced inward and outward current. (n = 8 cells for both groups, $P < 0.0001$, Student's unpaired t-test).

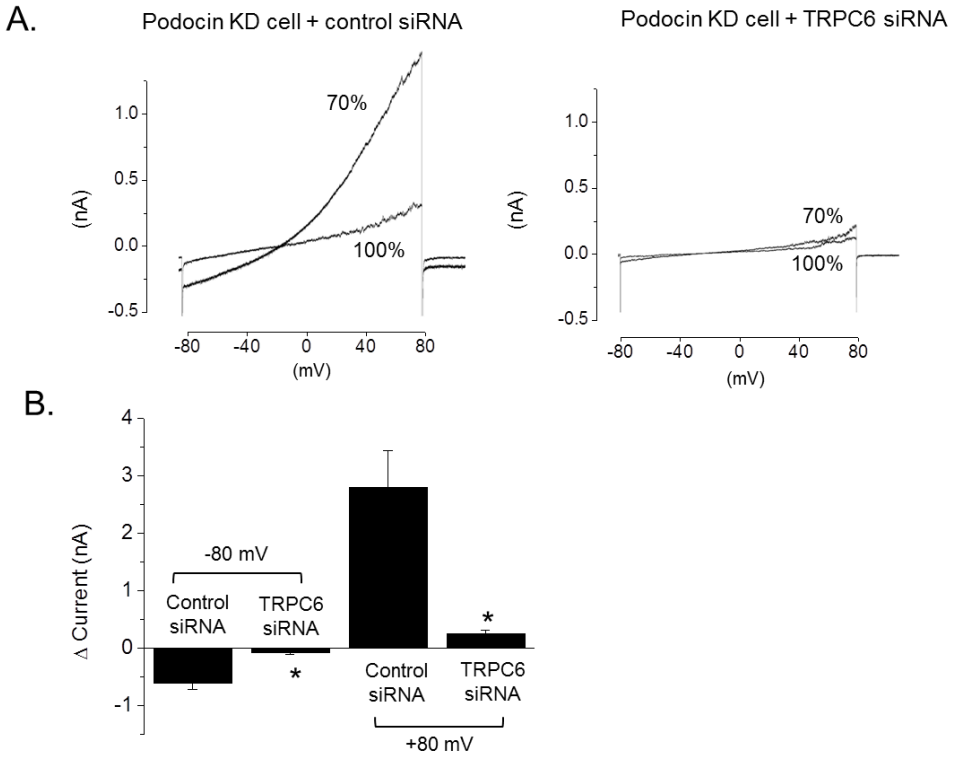

Figure 24.

3.6 Application of NMDA evokes inward current in podocytes:

Whole-cell recordings were first obtained from differentiated cells of an immortalized mouse podocyte cell line. Pressure injection of NMDA onto podocytes voltage clamped at -60 mV consistently evoked inward currents. Each cell displayed evoked currents that were internally similar in amplitude and reproducible with repeated applications of NMDA (Fig. 25, A). NMDA application evoked currents in all of the 86 podocytes tested in normal physiological conditions. As a control, bath saline was sprayed onto 10 cells using the same pressure injection method, and no effect was observed (data not shown). Regardless of the number of applications or the duration of the application, the cells displayed no appreciable desensitization to NMDA (Fig. 25, B). The amplitudes of the NMDA-evoked currents were concentration dependent. I was limited to applying a single concentration of NMDA to an individual cell, so each concentration from a range of 1 μM to 1 mM was tested in a separate group of four cells. 100 μM NMDA was sufficient to elicit a maximal response (Fig. 25, C). Using a non-linear least squares algorithm, the concentration-response curve could be fitted with the equation $I = I_{Max} / \{1 + (EC_{50}/NMDA)^n\}$ where I is the mean current evoked by a given concentration of NMDA, I_{Max} is the mean response to a saturating concentration of NMDA, EC_{50} is the concentration of NMDA that yields half-maximal mean responses, and n is the Hill coefficient, which describes the steepness of the dose-response curve. The fitted curve has an EC_{50} of 36 μM NMDA, and a Hill coefficient n of 1.98. These values are similar to NMDA sensitivities measured in cultured telencephalic neurons, which have an estimated EC_{50} for NMDA of 25-40 μM and Hill coefficients of 1.3-1.4 (92, 94).

3.7 Podocyte NMDA receptors display high permeability to Ca^{2+}:

Under physiological conditions, the reversal potential for NMDA-evoked currents was slightly positive to 0 mV (Fig. 26, A and B). Relative Ca^{2+} permeability of podocyte NMDA receptors was determined by obtaining current-voltage characteristics and reversal potentials in external solutions containing 10 mM free $Ca^{2+}$and in the same cells after bath perfusion with Ca^{2+} free-external solutions (Fig. 26, C and D). No other divalent cations were present in the extracellular solutions. In Ca^{2+}-free bath solution evoked-inward currents were appreciably reduced between -60 and -20 mV. In addition, outward rectification at potentials positive to +20 mV were increased (Fig. 26, C). Further clarification of the reversal potentials were obtained by recording at a range of membrane potentials between -20 and +20 mV. After switching to Ca^{2+}-free external saline, we observed a shift in reversal potential of -4.1 ± 0.2 mV (mean ± S.E.M., n = 4 cells) (Fig. 26, D). The mean shift in reversal potential was used to estimate relative ionic permeabilities according to the following equation:

$$\frac{P_{Ca}}{P_M} = \frac{M_o\,(1 - \{\exp\,[2(\Delta E_R)/(RT/F)]\,\})}{\exp\,[2(\Delta E_R)/(RT/F)][4Ca_0]}$$

Here P_{Ca} is the permeability to Ca^{2+}, P_M is the permeability to monovalent cations, M_o is the total activity of external monovalent cations, ΔE_R is the change in reversal potential after perfusion with Ca^{2+}-free solution, Ca_o denotes the activity of Ca^{2+} used in the control extracellular solution, and R, T, and F have their usual meanings. Published activity coefficients for Na^+ (110) and Ca^{2+} (11) were used to estimate the P_{Ca}/P_M of

NMDA receptors in podocytes. We found that at room temperature, podocyte NMDA receptor P_{Ca}/P_M = 2.11. While this value is less than the P_{Ca}/P_M of 4-5 that was measured for NMDA receptors of cultured hippocampal neurons using similar methods (62, 79), it still represents significant Ca^{2+} permeability. At high external concentrations, Ca^{2+} can act as a partial pore blocker (79) and I observed similar effects on NMDA-evoked currents in differentiated cells of a human immortalized podocyte cell line (data not shown) and also in primary cultures of mouse podocytes examined 72 hr after their preparation from isolated glomeruli (Fig. 27).

3.8 NMDA-evoked currents in podocytes are inhibited by Mg^{2+} and recognized NMDA receptor antagonists:

Consistent with other NMDA receptors (90, 100), evoked currents in mouse podocyte cell lines were inhibited by superfusing external salines containing elevated (5 mM) Mg^{2+} (Fig. 28, A and B). When recording pipettes filled with a solution containing 5 mM Mg^{2+}, NMDA application failed to evoke currents in any of 6 cells tested (Fig. 27, C). Additionally, NMDA-evoked currents were also inhibited by both the uncompetitive inhibitor MK-801 (10 μM) (Fig. 29, A and C) and by the competitive antagonist D-2-aminophosphonovaleric acid (D-APV) (10 μM) (Fig. 29, B and D). While I was unable to observe a recovery from MK-801 inhibition even after 30 min of washout (data not shown), the effect of D-APV was at least partially reversible over a period of 10-20 min (Fig. 29, B).

3.9 Podocyte NMDA-evoked current is potentiated by D-serine:

Either glycine or D-serine can act as obligatory co-agonists for neuronal NMDA receptors (113, 114), but I observed that superfusion of glycine at concentrations up to 10 mM had no significant effect on the amplitude of NMDA-evoked currents in podocytes (Fig. 30, A and B). To test if glycine could evoke currents by itself, 10 mM glycine was pressure injected onto podocytes. Again, no evoked-current was observed (Fig. 30, C). Despite these findings, bath superfusion of 1 mM D-serine caused a marked and statistically significant increase in the amplitude of NMDA responses in podocytes (Fig. 31, A and B). This effect was almost completely blocked after application of 100 nM L689,560, a potent inhibitor of the NR1 allosteric site (42) (Fig. 31, C). The fact that such inhibition occurs in the presence of D-serine suggests that occupation of the co-agonist binding site by an allosteric modulator is necessary for receptor activation.

3.10 Podocyte NMDA receptors have a highly atypical agonist activity profile:

In more than 30 cells tested, I was unable to detect robust responses to L-glutamate. This lack of effect occurred even at concentrations as high as 10 mM. Rarely, I observed responses of around 10-20 pA (Fig. 32, A), but in the majority of cells no evoked currents were observed. Tests of glutamate application were carried out in the presence and absence of glycine or D-serine, and a range of glutamate concentrations were tried. All of these conditions yielded essentially no response from the differentiated cells of an immortalized mouse podocyte cell line. These findings were replicated in primary cultures of podocytes (data not shown), further verifying that podocytes typically

do not respond to glutamate. I also found that podocytes do not respond to L-aspartate, another potential NMDA receptor agonist (Fig. 32, A). Despite these observations, I found that I was able to evoke inward currents with D-aspartate (Fig. 32, A), at roughly half the amplitudes of those evoked by NMDA. L-homocysteate (HCA) also evoked inward currents, this time with amplitudes comparable to NMDA-evoked responses. HCA-evoked currents were appreciably reduced by 10 μM D-APV, indicating that HCA acts through NMDA receptors (Fig. 32, B). To rule out the possibility that L-glutamate acts as an antagonist or partial agonist I examined responses to NMDA before and after application of 1 mM L-glutamate. Again, the presence of glutamate had no effect (Fig. 32, C).

Figure 25: Responses to NMDA in differentiated cells of an immortalized mouse podocyte cell line. ***A***: Whole-cell recordings from two different podocytes. A micropipette filled with 100 µM NMDA placed adjacent to the recorded cells was used to deliver NMDA in response to brief pressure pulses shown by the lines above the traces. Once the pipette was placed, responses to NMDA in a given cell were very consistent, as shown by response to three separate NMDA applications in each of the two cells. The holding potential in these experiments was -60 mV. ***B***: Responses to NMDA do not desensitize or fade during prolonged application. This record shows a response to a continuous 60-sec application of 100 µM NMDA to a podocyte at a holding potential of -60 mV. ***C***: Concentration-response curve for NMDA in podocytes. Data points show mean ± S.E.M of currents evoked by a given NMDA concentration applied to groups of four cells. The superimposed curve is a non-linear least squared fit to the logistic equation with an EC_{50} of 36 µM NMDA and a Hill coefficient of 1.98 (R^2 = 0.96413).

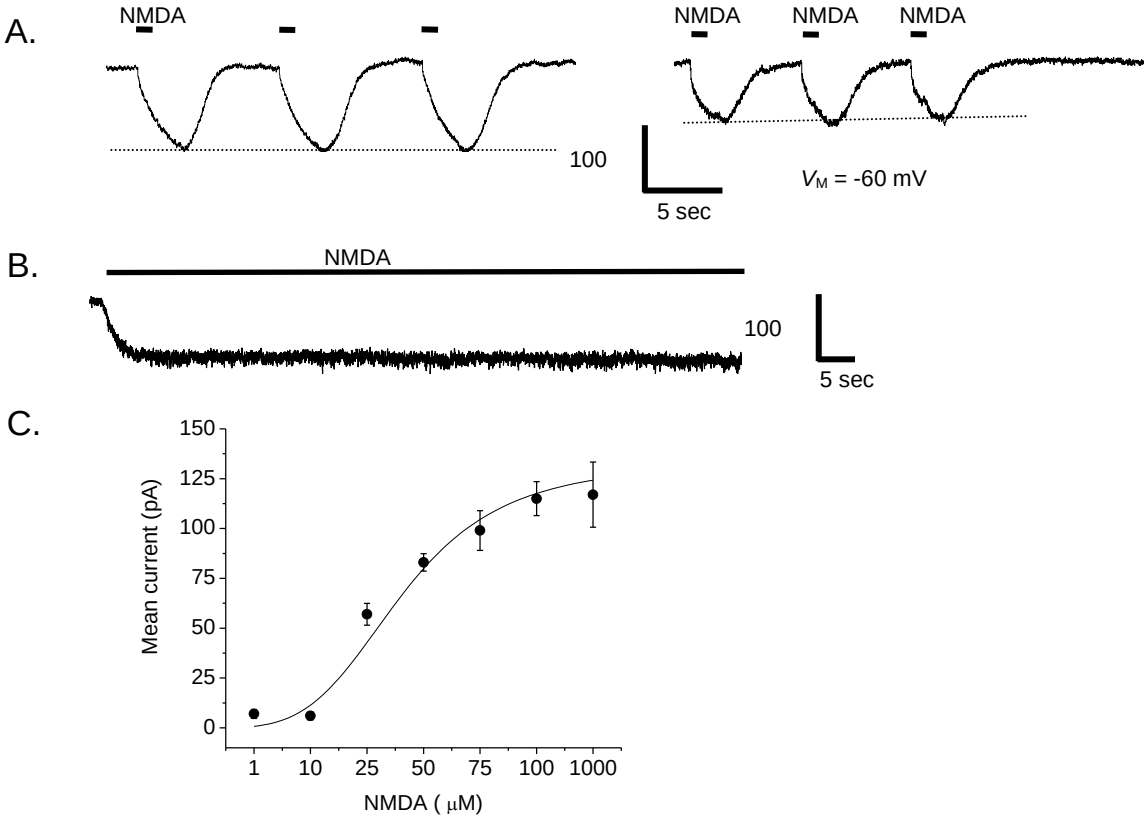

Figure 25.

Figure 26: Reversal potentials of NMDA-evoked currents in mouse podocyte cell lines. ***A***: NMDA-evoked currents in a podocyte at the holding potentials indicated to the left of each trace. ***B***: Current-voltage plot of the data shown in A. ***C***: Current voltage-plots for NMDA-evoked currents in podocytes in 10 mM external Ca^{2+} and in the same cells after perfusion with nominally Ca^{2+}-free external solution. Note decrease in inward currents in Ca^{2+}-free solutions at holding potentials negative to -20 mV and increase in outward currents at positive holding potentials. ***D***: A similar experiment in a different group of cells. Here NMDA-evoked currents were evoked at membrane potentials that more closely bracketed the reversal potentials. Note negative shift in reversal potential after switching to Ca^{2+}-free external salines. Data in C and D represent mean ± S.E.M. from four cells.

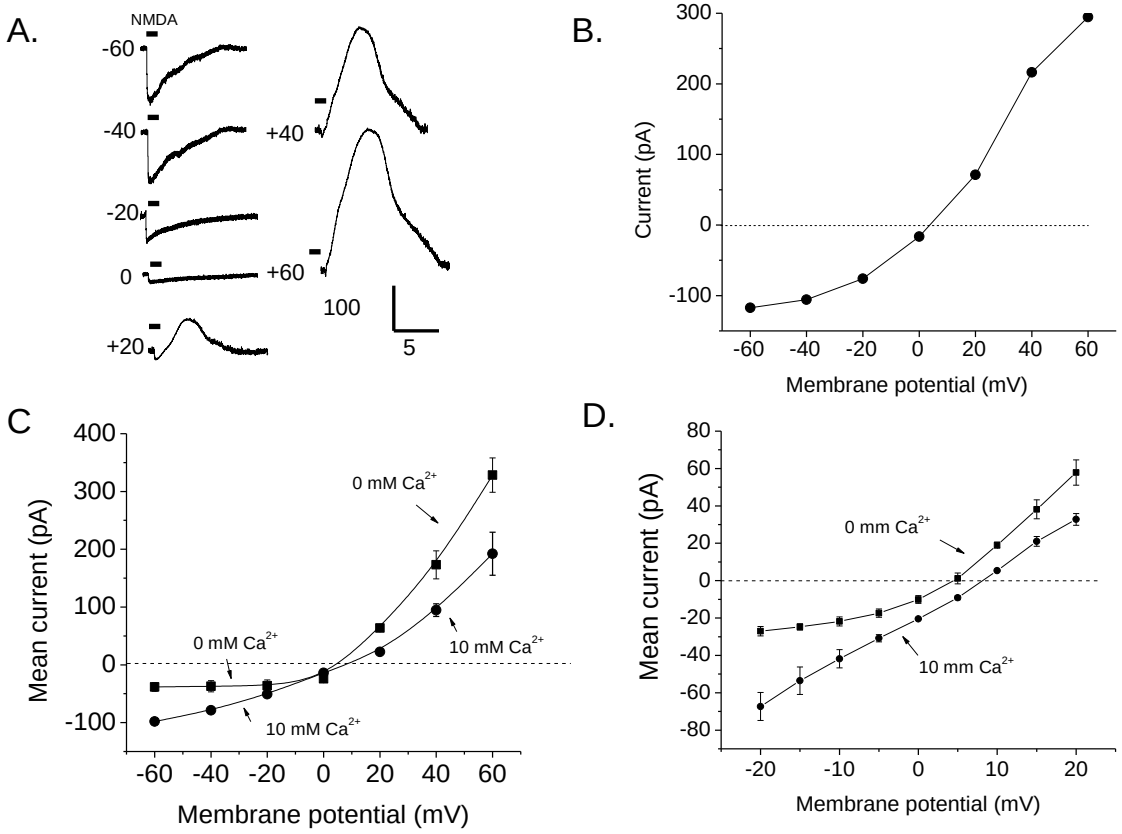

Figure 26.

Figure 27: Example of NMDA-evoked current from a podocyte in primary cell culture. Whole-cell recordings of cells with visible primary processes were made 72 hr after isolation from a 6-week old mouse. ***A***: Example of NMDA-evoked current from cell held at -60 mV and ***B***: current-voltage characteristic constructed in the same cell using the same methods shown in Fig. 2A.

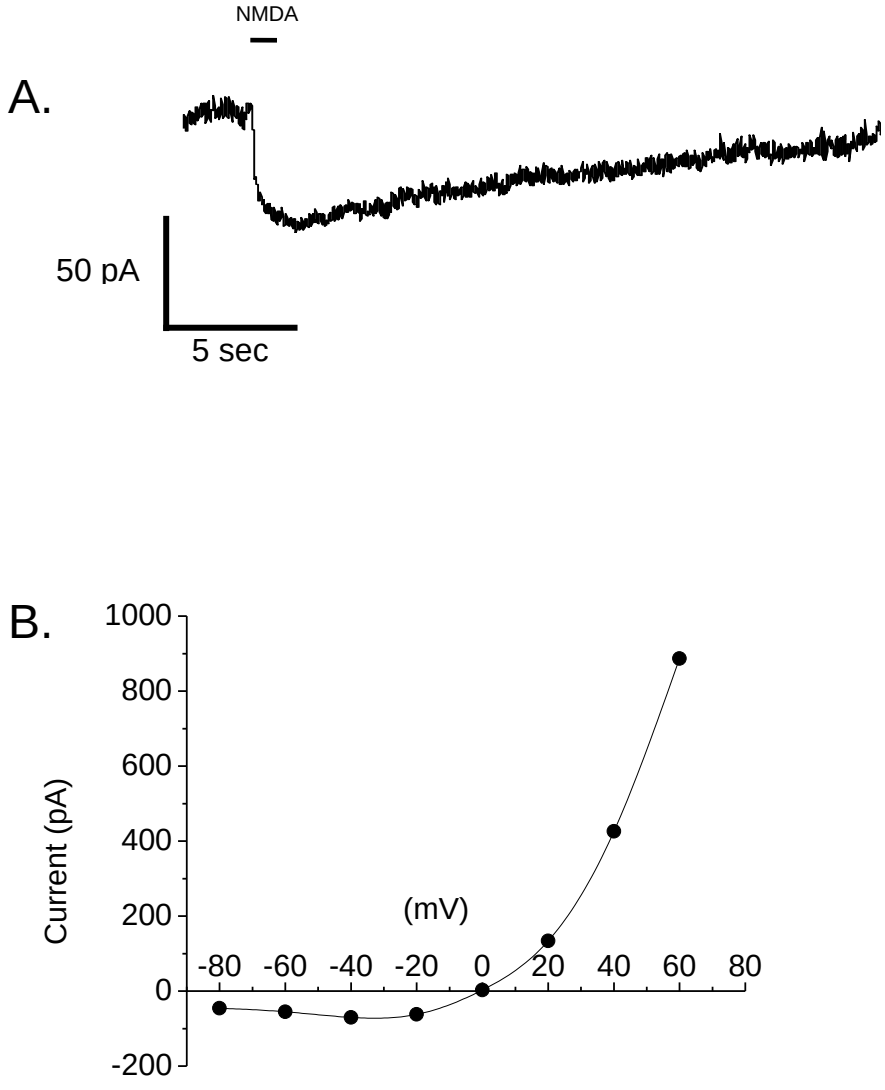

Figure 27.

Figure 28: Responses to NMDA in podocytes are blocked by external or internal Mg^{2+} ions. ***A***: NMDA-evoked current in an immortalized podocyte before and after application of a solution containing 5 mM Mg^{2+} as indicated. The holding potential in this experiment was -60 mV. ***B***: Bar-graph showing mean ± S.E.M. of six repetitions of this experiment. Asterisk indicates $P < 0.0001$ (Student's paired *t*-test). ***C***: NMDA did not evoke detectable currents in recordings made using pipettes filled with a solution containing 5 mM Mg^{2+} at a holding potential of -60 mV.

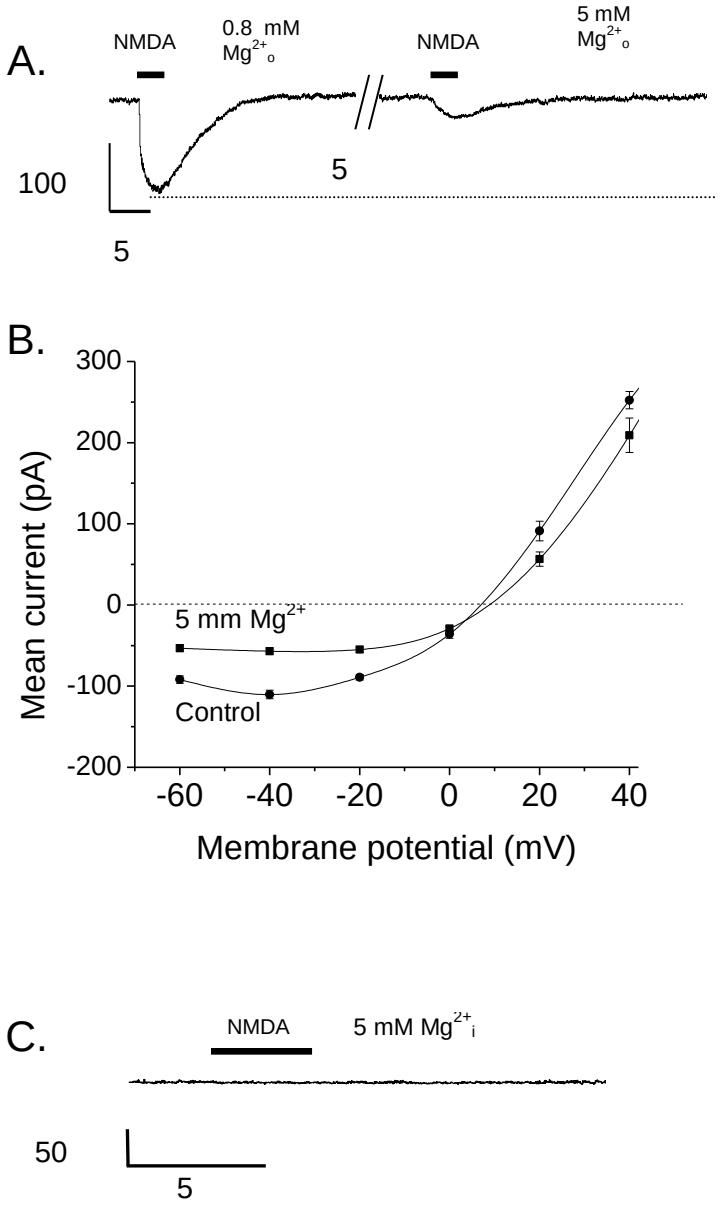

Figure 28.

Figure 29: Inhibition of NMDA-evoked currents in podocytes by prototypical antagonists. ***A***: NMDA-evoked currents in an immortalized podocyte were reduced after application of MK-801. These currents were evoked at a holding potential of -60 mV. MK-801 inhibition did not recover after 30 min of washing in control solutions. ***B***: Inhibition of NMDA-evoked currents by D-APV. Note that inhibition was at least partially reversible with a 20-min wash. ***C*** and ***D*** show mean ± S.E.M. of several repetitions of these experiments as indicated. Asterisks indicate $P < 0.0001$ (Student's paired *t*-test).

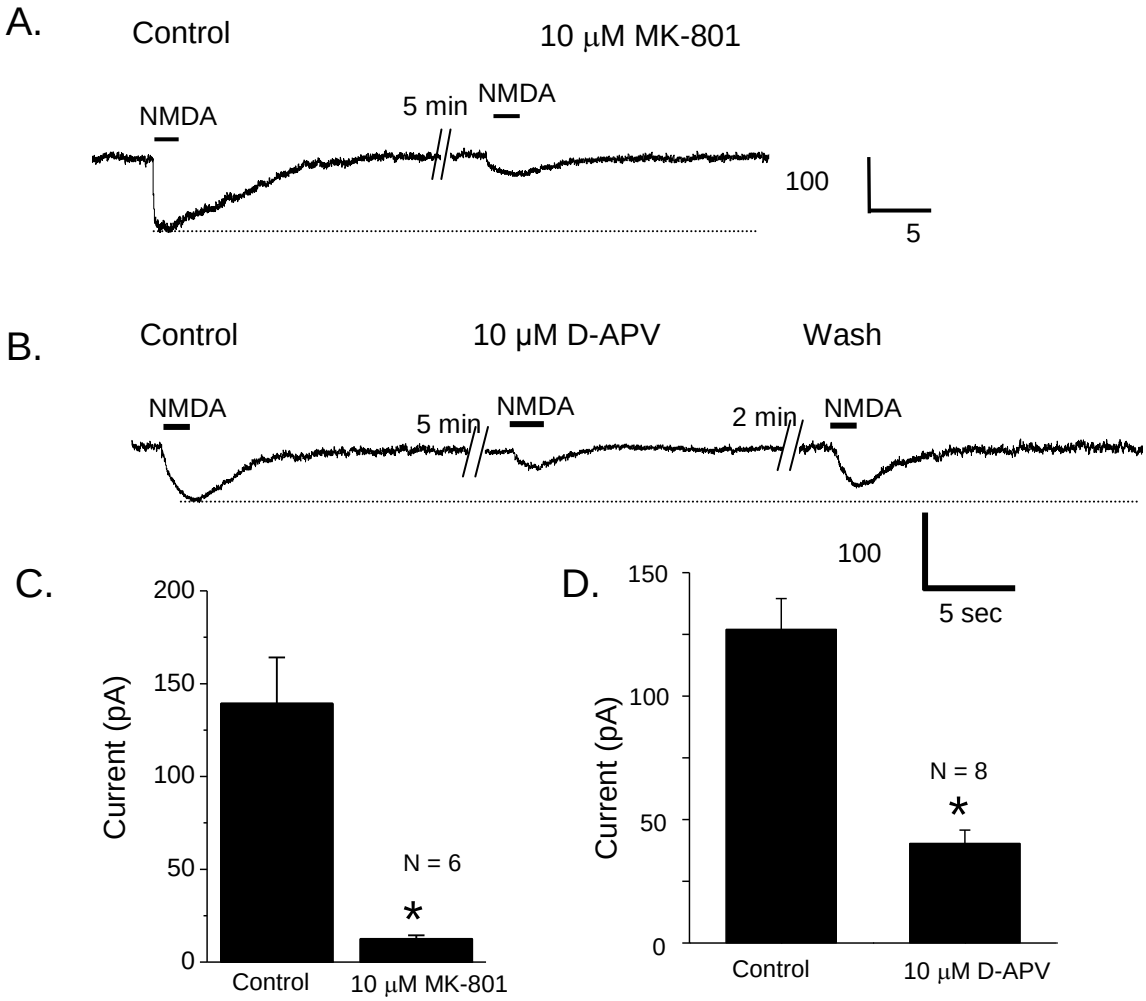

Figure 29.

Figure 30: Bath application of glycine does not increase NMDA-evoked currents in immortalized podocytes. ***A***: Examples of NMDA-evoked currents before and after 5 min exposure to 1 mM glycine. The holding potential was -60 mV. ***B***: Mean ± S.E.M. of six repetitions of this experiment. Mean currents are not significantly different after application of 1 mM glycine. ***C***: Application of 10 mM glycine by pressure injection did not evoke membrane currents in podocytes.

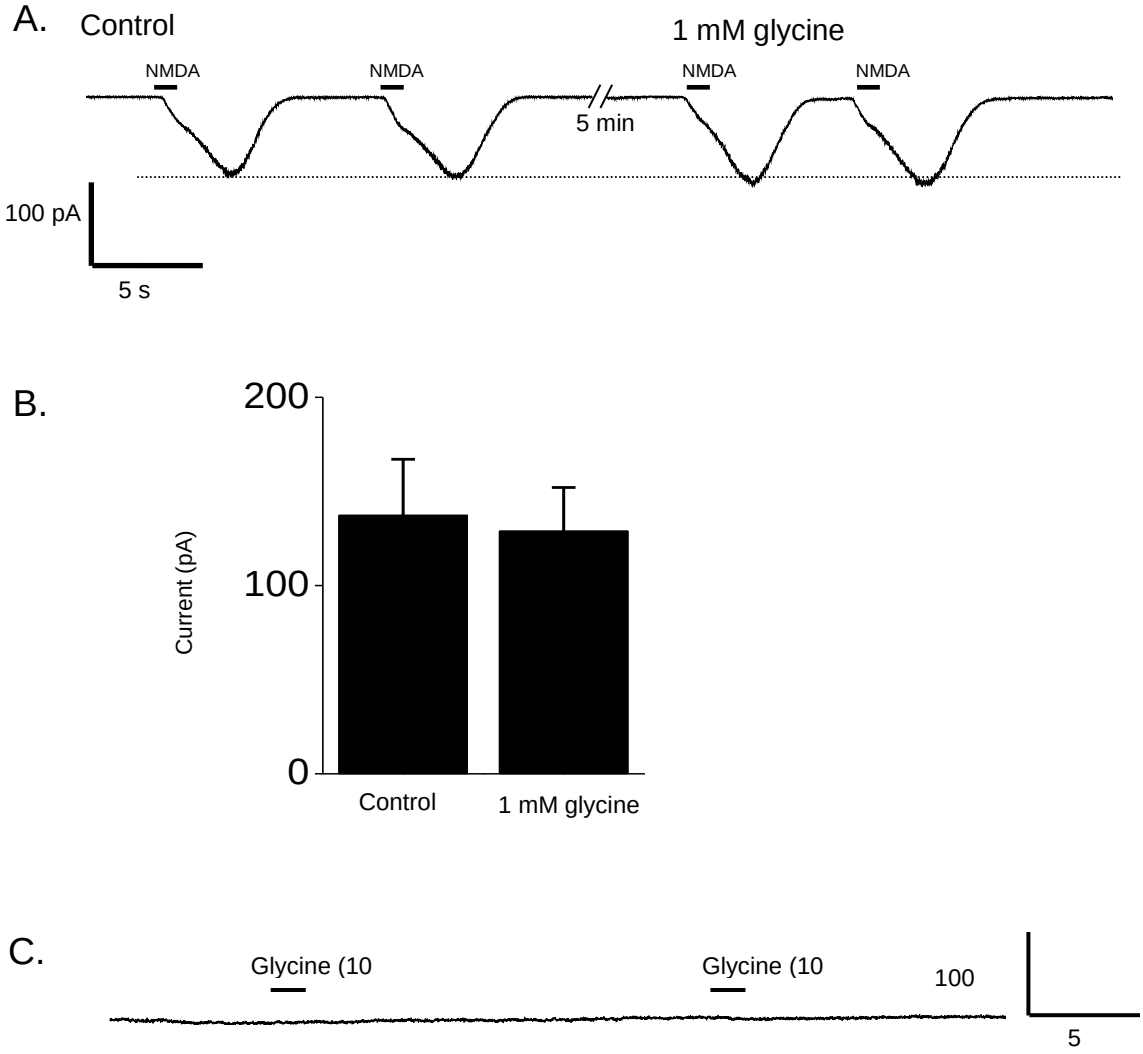

Figure 30.

Figure 31: Bath application of D-serine potentiates NMDA-evoked currents in immortalized podocytes. ***A***: Examples of currents before and 5 min after bath perfusion of 1 mM D-serine at a holding potential of -60 mV. ***B***: Mean ± S.E.M. of six repetitions of this experiment. ***C***: Inhibition of NMDA-evoked currents by an inhibitor of the D-serine allosteric site of NMDA receptors. Examples of NMDA-evoked currents are shown before and after application of 1 mM D-serine, which caused its usual potentiation of current. After exposure of the same cell to external solutions containing 1 mM D-serine and 100 nM L689560, NMDA responses were nearly completely inhibited.

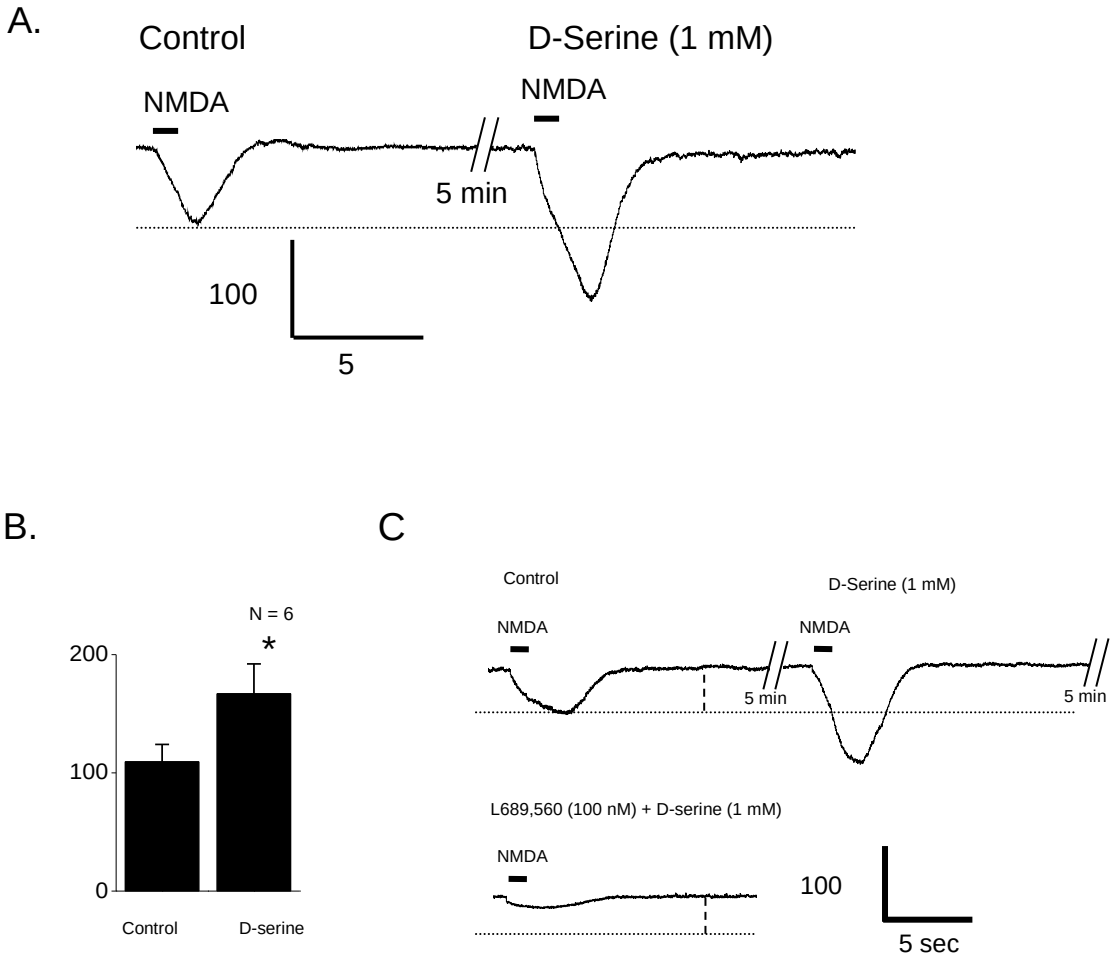

Figure 31.

Figure 32. Responses to other potential NMDA receptor ligands in immortalized podocytes. ***A***: Pressure application of 1 mM L-glutamate or 1 mM L-aspartate evoked very small currents, whereas application of 1 mM D-aspartate evoked readily detectable inward currents. These traces represent recordings made from different cells, but all were made at a holding potential of -60 mV. ***B***: Application of 100 µM L-homocysteic acid (HCA) before and after application of external solutions containing 10 µM D-APV at a holding potential of -60 mV. Note in this cell that D-APV inhibited the initial peak current to a greater extent than the more sustained component of current. This pattern was seen in most of the cells tested. ***C***: Bath superfusion of 1 mM L-glutamate did not affect responses to pressure injection of NMDA indicating that L-glutamate is not an antagonist.

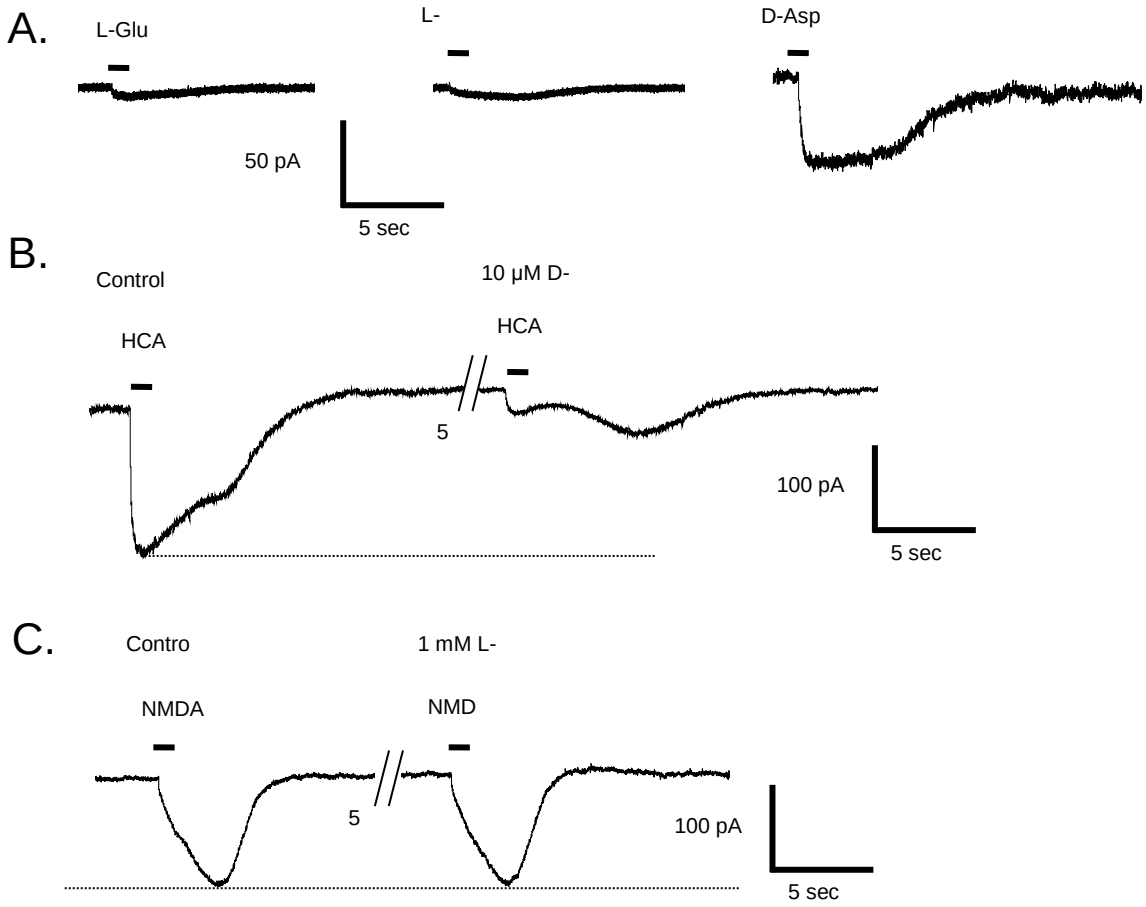

Figure 32.

4 DISCUSSION

Within the glomerulus, podocyte function is largely dependent on cellular structure; disruption of podocyte foot processes results in breakdown of the glomerular filtration barrier (4, 24, 34). Because podocytes reside in a dynamic fluid environment, maintaining their structure requires an equally dynamic, but carefully regulated actin cytoskeleton. This is evidenced by the fact that many familial glomerular diseases are linked to mutations in actin-regulatory and actin-binding proteins, and foot process effacement is preceded by alterations of actin filaments (34). Many signaling cascades converge on the actin cytoskeleton, and often Ca^{2+}-influx initiates and participates in these same cascades. Ca^{2+}-permeable ion channels therefore play a critical role in the regulation of actin within podocytes (83). The discovery that mutations in TRPC6 channels are associated with a subset of familial FSGS underscores their importance in controlling Ca^{2+} flux and ultimately, podocyte functionality (98). My work has focused on multiple aspects of the regulation of TRPC6 channels in podocytes. I have shown that podocyte TRPC6 channels are activated by both receptors and membrane-stretch, and I have further elucidated the signaling cascades and other mechanisms that are involved in TRPC6 activation (Illustration 4 and 5).

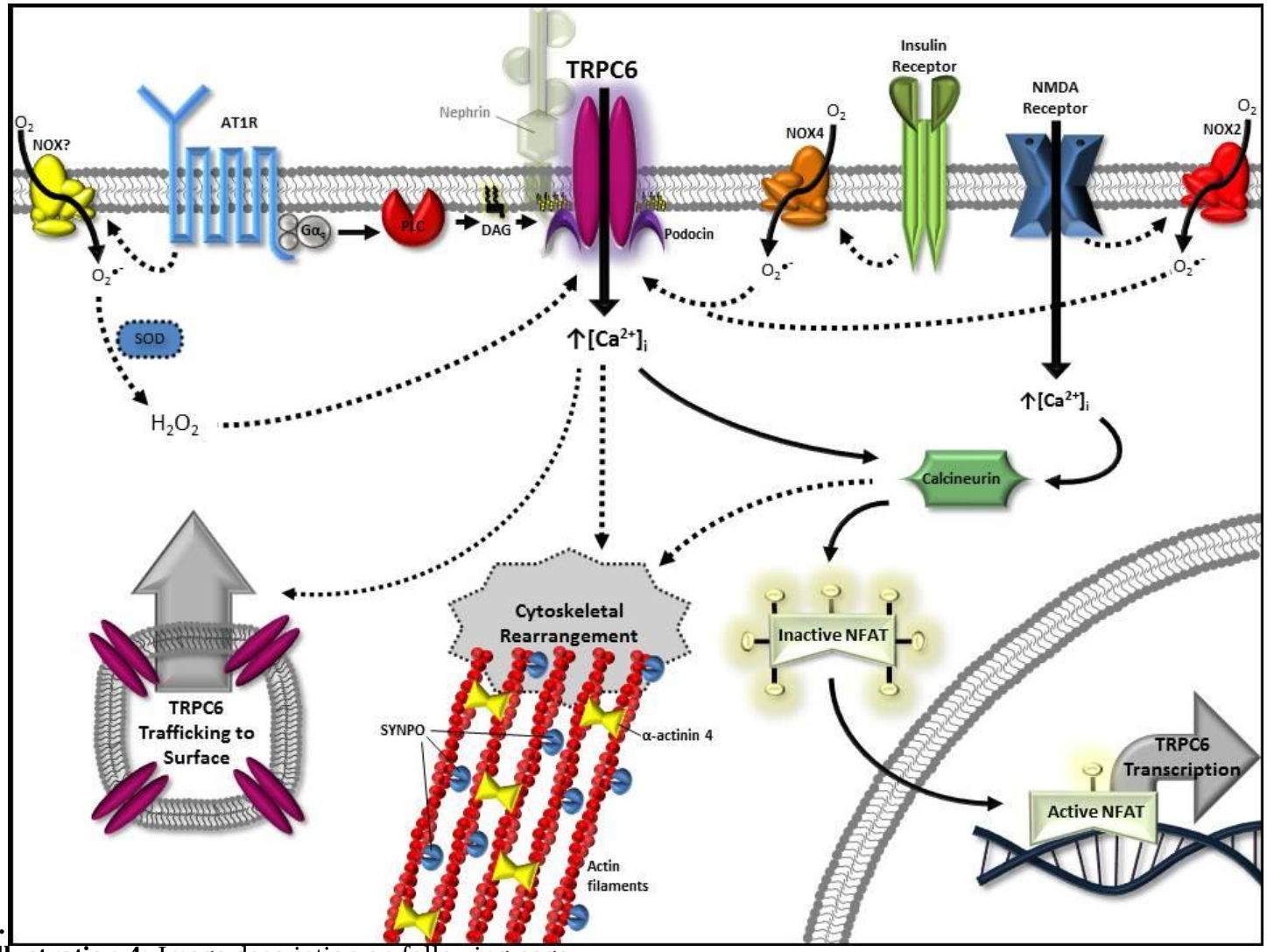

4.

Illustration 4: Image description on following page.

Illustration 4: Diagram of pathways involved in receptor-mediated activation of TRPC6 in podocytes. Multiple receptor types have signaling pathways that converge on TRPC6 activation. Solid-line arrows represent direct pathways. Dashed-line arrows represent indirect pathways or pathways that have not been fully characterized. TRPC6 channels are Ca^{2+} permeable and are located at the slit-diaphragm on podocyte foot processes. There, TRPC6 channels associated with nephrin (shown faded green) and podocin, a cholesterol-binding protein with a hairpin-like structure. Podocin is necessary for chemical activation of TRPC6 channels in podocytes.The angiotensin II type 1 receptor (AT1R) signals is Gαq coupled, and can activate phospholipase C (PLC). PLC cleaves phosphatidylinositol into diacylglycerol (DAG) and inositol 1,4,5-trisphosphate (IP3). DAG directly activates TRPC6. In addition, AT1R activates NADPH-oxidase (NOX), although the NOX isoform in podocytes remains unknown. NOX generates reactive oxygen species which can activate the redox-sensitive TRPC6 channel. Superoxide dismutase (SOD) may be involved in converting superoxide ($O_2^{\cdot-}$) into peroxide (H_2O_2). Both insulin receptor and NMDA receptor-mediated signaling occurs via NOX activation. Insulin mobilizes NOX4 to the cell surface, where it produces reactive oxygen species. NMDA receptor signaling occurs via NOX2 and Ca^{2+}-influx. TRPC6 channel activation also causes Ca^{2+}-influx. Increased intracellular Ca^{2+} activates calcineurin, a protein phosphatase that dephosphorylates the transcription factor known as nuclear factor of activated T-cells (NFAT). Dephosphorylated NFAT moves from the cytosol to the nucleus, where it causes gene transcription including the TRPC6 gene. Calcineurin can also influence actin filament dynamics through its effect on synaptopodin (SNYPO). Calcineurin dephosphorylates synaptopodin and renders it susceptible to cathepsin L-mediated degradation. Without synapotpodin, RhoA is degraded, leading to loss of stress fibers and to cytoskeletal rearrangement.In addition, α-actinin 4 plays a role in actin filament bundling, and can stabilize stress fibers. Finally, increased intracellular [Ca^{2+}] can lead to trafficking of TRPC6 channels to the surface.

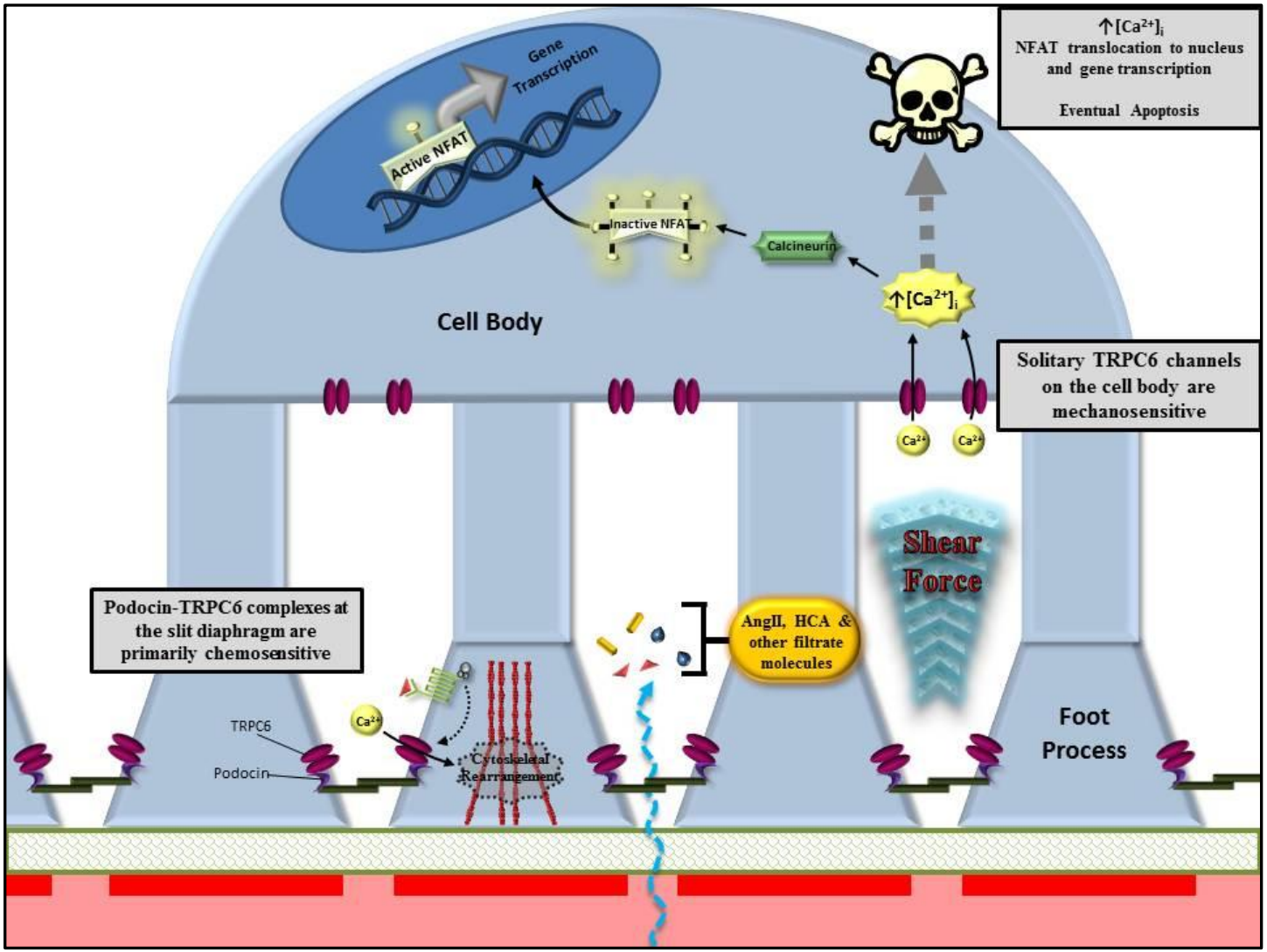

5.

Illustration 5: Image description on following page.

Illustration 5: Model of podocyte cell with emphasis on TRPC6 channels located in the cell body and in the foot processes; differential effects of podocin on TRPC6 activation. At the slit diaphragm, TRPC6 channels associate with podocin and nephrin. The TRPC6-podocin complex is sensitive to chemical activation mediated by G-protein coupled receptors, such as the angiotensin II type 1 receptor (AT1R). Activation of TRPC6 channels allows for Ca^{2+}-influx that can influence actin dynamics and cytoskeletal rearrangement within the foot processes. At the same time, TRPC6 channels at the slit diaphragm are resistant to mechanical activation due to the presence of podocin. A mutation of the podocin gene would result in a gain of mechanosensitivity of TRPC6 and could potentially lead to Ca^{2+}-overload and eventual foot process effacement. On the cell body, podocin is absent. As a result, the TRPC6 channels located there are resistant to chemical activation but are mechanosensitive. This population of TRPC6 channels can respond to mechanical stimuli such as shear force that occurs in the subpodocyte space. Ca^{2+}-influx in the cell body results in activation of calcineurin which then causes translocation of the transcription factor NFAT to the cell nucleus and subsequent gene transcription. Prolonged activation of TRPC6 channels in the cell body could result in Ca^{2+}-overload and eventual apoptosis. Evidently, TRPC6 channels in the cell body are involved in more long term regulatory changes, as opposed to the more rapid changes mediated by the TRPC6-podocin complex in the foot processes.

The interaction between TRPC6 and angiotensin was already recognized prior to my work, but it remained unclear the how angiotensin signaling causes acute activation of TRPC6 channels in podocytes (25, 49, 88). Furthermore, there was still some debate whether angiotensin induced Ca^{2+}-influx was in fact mediated by TRPC6 rather than TRPC5 (41, 109). My findings indicate that angiotensin specifically activates TRPC6, and this activation is mediated via both a $G\alpha_q$-PLC pathway and a NOX-ROS pathway.

Because there is no TRPC6 specific blocker currently available, verifying that angiotensin's affects TRPC6 was accomplished using a combination of methods. First, the nonspecific TRPC blocker, SKF-96365 was used, and I found that it inhibited the angiotensin-activated current. Micromolar concentrations of lanthanum inhibit most TRPC channels, but it activates TRPC4 and TRPC5 (64). Application of lanthanum ruled out the speculated role of TRPC5, because I found that angiotensin-activated current was lanthanum sensitive. Final evidence was provided by siRNA knockdown of TRPC6. In the podocytes with TRPC6 knocked down, I found that there was little increase in current after application of angiotensin. The fact that my recordings were obtained from glomerular attached podocytes gives further credence that the same effects occur *in vivo*.

The AT1R is $G\alpha_q$-coupled and typically activates PLCβ (25, 49, 88). As predicted, my results indicate that angiotensin in part activates TRPC6 channels by this pathway. Inhibiting either $G\alpha_q$ or PLC prevented TRPC6 activation by angiotensin, while inhibition of PKC had no effect. This is consistent with the fact that TRPC6 is sensitive to DAG, while TRPC5 is not.

In conjunction with $G\alpha_q$-PLC signaling, the AT1R can activate NADPH-oxidase that can then generate ROS. There are multiple isoforms of NOX, and angiotensin is

capable of activating NOX1, NOX2, and NOX4, depending on cell type (10). Using MnTBAP, a membrane permeable mimetic of superoxide dismutase and catalase, I was first able to establish a role for ROS in angiotensin activation of TRPC6. Next using either apocynin or DPI, I found that TRPC6 activation is partly mediated by NOX activity. Both apocynin and DPI are rather nonspecific in regards to the NOX isoforms they inhibit, so precise identification of which NOX is involved in angiotensin mediated TRPC6 activation remains unknown.

The results from this first set of experiments provide insight into previous studies that found that TRPC6 enhances angiotensin II-induced albuminuria (88). It is theorized that prolonged activation of TRPC6 by angiotensin results in an increased Ca^{2+} load that has deleterious effects on podocytes. Specifically, elevated Ca^{2+} levels can lead to increased expression of the TRPC6 channel itself, thereby creating a feedback loop that results in even greater Ca^{2+}-influx. At the same time, this excess Ca^{2+} can induce cytoskeletal rearrangement that precedes foot process effacement and disruption of the filtration barrier. A gain of function mutation in the TRPC6 channel would exacerbate the effects of angiotensin and hasten the demise of functional podocytes. While my work does not address the long term effects of angiotensin induced activation of TRPC6, it identifies the signaling pathways that contribute to the more immediate effects of angiotensin and verifies the identity of the TRPC6 channel as the likely culprit in angiotensin evoked Ca^{2+}-influx.

Prior to the work of Dryer and coworkers, a functional link between the insulin receptor and TRPC6 channel in podocytes was not yet identified. My research contributed to the discovery that insulin modulates TRPC6 activity in cultured podocytes,

and this effect was NOX4-ROS mediated. Surface biotinylation assays conducted by Eun Young Kim revealed that insulin causes acute increases in steady-state surface expression of TRPC6. I showed that this is functionally relevant by recording from podocytes that were treated with insulin for 12 hours. The currents measured from these cells were significantly elevated compared to the control group. As with the angiotensin experiments, I used multiple methods to establish that the increased current was attributable to TRPC6. Inhibition of the current by SKF-96365, indicates a member of the TRPC family, while sensitivity to lanthanum precludes TRPC4 or TRPC5. Additionally, siRNA knockdown of TRPC6 eliminated the effects of insulin on whole-cell current. The insulin signaling cascade can initiate the formation of ROS such as H_2O_2, and it is known that TRPC6 channels are redox sensitive (40). We first established that podocytes generate H_2O_2 in response to insulin. Dr. Kim used a fluorometric assay to show that there is an increase in H_2O_2 generation in podocytes after insulin treatment of 0.25, 6, and 24-hr exposure times. The same assay showed that the generation of insulin evoked H_2O_2 was inhibited by pretreating the cells with MnTBAP, a free radical scavenger. Dr. Kim conducted additional surface biotinylation assays that revealed that the insulin evoked increase in surface expression of TRPC6 is inhibited by pretreatment with MnTBAP, indicating that insulin induced TRPC6 trafficking is dependent on ROS. My results show that peroxide increases the activity of TRPC6 channels, and this effect could also be inhibited by MnTBAP pretreatment. Dr. Kim identified the likely source of endogenous H_2O_2 by showing that insulin mobilizes NOX4 to the cell surface, and that siRNA knockdown of NOX4 inhibited an increase in TRPC6 surface expression in response to insulin. These findings provide evidence that insulin signaling may in part

regulate podocyte contractility and maintenance of the filtration barrier. As to why such a role would be necessary, it is known that glomerular filtration rate (GFR) increases after intravenous infusions of glucose (27, 66, 68). Increased GFR corresponds to an increase in transmural pressure across the filtration barrier and therefore greater mechanical strain on the slit diaphragm. The circulating insulin that is released in response to the glucose load can upregulate TRPC6 channels on podocyte foot processes, thereby causing an increased Ca^{2+}-influx. As has already been discussed, Ca^{2+}-influx can initiate cytoskeletal rearrangement and contraction, enabling the podocytes to counteract the increase in transmural pressure. If sustained for prolonged periods of time, this same process could become pathological in individuals with type 2 diabetes, and may in part explain the development of diabetic proteinuria. Owing to their resistance to insulin, circulating levels of insulin are higher in type 2 diabetics. This could cause excessive upregulation of TRPC6 channels in podocytes that leads to greater than normal Ca^{2+}-influx. At the same time aberrant insulin signaling in podocytes may generate a detrimental amount of ROS. The end results would be foot process effacement and potential Ca^{2+}/ROS-induced apoptosis in podocytes. Once again the difference between a normal and diseased state is a matter of degree; normal insulin facilitation of TRPC6 is necessary to maintain the integrity of the filtration barrier, but excessive insulin levels may induce TRPC6-mediated Ca^{2+}-overload and eventual breakdown of the filtration barrier.

Previous studies have indicated that podocytes express the necessary cellular components for functional glutamatergic signaling, including glutamate transporters, vesicular structures and both metabotropic and ionotropic glutamate receptor subunits (38, 96). It has been observed that blockade of NMDA receptors leads to proteinuria in

both mice and humans (116). In addition, antagonizing NMDA receptors in cultured podocytes induces cytoskeletal remodeling and redistribution of nephrin (38). Apart from these studies, little is known about the precise nature of the NMDA receptor mediated signaling pathways in podocytes. In the present study I have shown that functional NMDA receptors are expressed in both mouse and human podocyte cell lines, as well as in primary cultures of mouse podocytes. In addition, I found the NMDA receptors can activate TRPC6 channels in an ROS dependent manner. Using both surface biotinylation assays and fluormetric assays, Dr. Kim identified NOX2 as the likely source of NMDA receptor induced ROS. Contrasted with the finding that insulin receptors trigger NOX4 activation, it becomes apparent that multiple signaling pathways converge upon TRPC6 channels. This underscores the possibility that disregulation of TRPC6 activity is the common factor in many forms of glomerular disease.

Despite sharing many of the pharmacological and functional characteristics of neuronal NMDA receptors, the receptors I identified in podocytes displayed several distinct properties. Of particular importance is the fact that podocyte NMDA receptors displayed essentially no response to either L-glutamate or L-aspartate. Considering that the NMDA receptor almost by definition is a glutamatergic ion channel, this property is unusual to say the least. It also calls in to question the significance of the previously identified cellular machinery found in podocytes that typifies functional glutamate-mediated signaling. It was found that mouse glomeruli express NMDA receptors, mGluR7, vesicular glutamate transporter 1 and a vacuolar proton pump. In additional to these, cultured podocytes possess glutamate containing vesicles and can be induced to release glutamate with α-latrotoxin (38). While our study seems to rule out a role for the

NMDA receptor in such a signaling pathway, it does not exclude that possibility that metabotropic glutamatergic receptors (mGluRs) are the endogenous target for glutamate release in podocytes. The resistance to glutamate indicates the presence of a novel form of the NR2 subunit, one that has subtle alterations to the agonist binding site and is specially suited for signaling in podocytes. It has been shown that the substitution of tyrosine residue with a tryptophan residue within the ABD of the NR2 subunit prevents glutamate binding by steric hindrance (78, 90). It is possible that a similar substitution occurs in the NR2 subunit expressed by podocytes, but this remains to be determined.

While unresponsive to L-glutamate and L-aspartate, I found that podocyte NMDA receptors were activated by homocysteate (HCA), displaying evoked inward currents similar to those seen with NMDA application. HCA is formed from the oxidation of homocysteine, an amino acid that participates in numerous metabolic pathways and is usually found in the blood at low levels (5). Both HC and HCA have been found to be neurotoxins, and this effect is mediated, at least in part, by NMDA receptors (5, 70, 106). It has been noted that neurons are significantly more sensitive to HCA than HC (5), and I found that podocytes responded only to HCA and not HC. The fact that elevated serum HC levels are correlated with proteinuria in humans and glomerulersclerosis in rats seems to indicate that these effects may largely be caused by HCA (36).

I found that podocyte NMDA receptors also responded to D-aspartate. In this case the implications are not as clear. While D-aspartate is produced by the enzyme aspartate racemase and is found both in the serum and brain, its role, if any, in the kidneys has not been identified. It is known that depletion of aspartate racemase, and correspondingly D-aspartate, in mice results in severe developmental defects in neuronal dendrites and a

marked reduction in neurons survival (19, 76). It has also been identified as a player in an alternative pathway for thyroid hormone synthesis (19). It follows that it is not outside the realm of possibility that D-aspartate has a physiological role in the kidneys as well and deserves further investigation.

Another distinguishing characteristic of podocyte NMDA receptors is that are not potentiated by glycine. Previously viewed as the obligatory co-agonist for NMDA receptor activation, glycine typically acts in a regulatory fashion to both increase the receptor's affinity for glutamate and decrease receptor desensitization (6, 31). In some rare instances, specifically receptors comprised of NR1/NR3 diheteromers, glycine alone can activate NDMA receptors (12). In addition, glycine site antagonists essentially abolish NMDA receptor mediated current (90). I found that podocytes show no change in evoked current when glycine is added to the bath solution and do not respond at all when glycine alone is applied to the cells. However, the addition of the glycine site antagonist L689,560 nearly eliminated any evoked inward current, indicating that the co-agonist site is present and can be occupied (42). Previous studies have shown that D-serine can act in place of glycine as a co-agonist, and in at least some instances, is a stronger potentiator of NMDA receptor mediated current (18, 90). As is the case with D-aspartate, D-serine is found in appreciable levels in the mammalian brain and serum and is endogenously produced by a racemase enzyme (113, 114). Of particular physiological importance, serine racemase is expressed in proximal tubule cells of the kidney (100, 114). I found that podocytes display inward currents with significantly increased amplitude when D-serine is supplied in the bath solution. D-serine has been shown to act as a nephrotoxin

and illicit proteinuria by damaging the proximal tubule, and D-serine may have further deleterious effects on podocytes (43).

Apart from their unusual agonist binding profile, podocyte NMDA receptors display many of the characteristics of typical, neuronal NMDA receptors. Specifically, they are calcium permeable, albeit at a lesser extent that neuronal receptors (79). This has potential physiological implications that will be discussed later. Never the less, podocyte receptors are blocked by magnesium and respond appropriately to the NMDA receptor antagonists MK-801 and D-APV. As MK-801 is a pore blocker, its ability to antagonize NMDA receptor mediated current is expected regardless of glutamate's efficacy at eliciting a response. D-APV, however, acts at the ABD of the NR2 subunit (78, 90). Due to the fact that the NR2 subunit appears to be of a novel subtype, as indicated by its resistance to glutamate, it is somewhat surprising that D-APV acts as an antagonist for podocyte NMDARs . Recently, it has been suggested that small antagonists such as D-APV only bind in the immediate vicinity of the glutamate binding site and display limited NR2 subtype selectivity (90). This then accounts for our findings of D-APV's effects despite the receptor's resistance to glutamate.

Dr. Eun Young Kim of our group found that application of NMDA at concentrations and durations that cause excitotoxicity in cultured neurons did not cause a noticeable loss of cultured podocytes (15, 67). This may be do to the fact that podocyte NMDA receptors display somewhat reduced Ca^{2+}-permeability (79), and this may render them more resistant to acute toxicity mediated by NMDA receptor activation. Also of importance, podocytes lack voltage-activated Ca^{2+} channels (27). As a result, NMDA receptor activation would not trigger additional Ca^{2+}-influx and may prevent Ca^{2+} levels

from reaching levels that are excitotoxic in neuronal cells (15). Although, NMDA application below the 72 hour mark did not result in any apparent cell death, podocytes exposed to sustained levels of 50 μM NMDA showed reduced expression of nephrin. As nephrin is a vital component of glomerular slit diaphragms (47, 56, 95), NMDA receptor mediated disruptions of nephrin could potentially lead to compromised glomerular function.

The observed interaction between NMDA receptors and TRPC6 channels has some important physiological implications. As stated, elevated serum levels of HCA are associated with proteinuria, and I found that the NMDA receptors expressed by podocytes are activated by HCA. This activation would trigger an upregulation of TRPC6 activity, as indicated by my other findings. TRC6 activation could contribute to cytoskeletal rearrangement and foot process effacement. It is also worth noting that at normal neuronal resting potential NMDA receptors are blocked by Mg^{2+} ions at the pore site. A depolarizing event is necessary to remove this block and permit ligand-gated opening of the NMDA receptor. However, at the podocyte resting potential of ≈ -40 mV there would be much less of a Mg^{2+} block. In addition, TRPC6 channels themselves could instigate the necessary localized depolarization, and close proximity NMDA receptors would be responsive to this. Again, another feedback loop could exist where TRPC6 channels allow for NMDA receptor function, which then increases the activity of TRPC6 channels, leading to a snowball effect. In this event podocyte injury becomes even more likely, given that both NMDA receptors and TRPC6 channels are Ca^{2+} permeable (27, 67).

There is little question that TRPC6 channels expressed in podocytes are regulated by receptor mediated signaling cascades. Greater uncertainty surrounds the possibility that podocyte TRPC6 channels are mechanosensitive as well (39). My findings indicated that TRPC6 channels respond to multiple forms of membrane deformation. Moreover, the TRPC6 associated protein podocin determines the preferred mode of channel activation. Again, these findings may help to explain the pathologies associated with mutations in the TRPC6 and podocin genes.

TRPC6 channels respond to hypoosmotic stretch, surface-applied pressure pulses, changes in shear force, and chemically induced membrane deformation. Stretch response is abolished with the addition of GsMTx4, a peptide that interferes with TRPC6's ability to directly interact with the lipid bilayer (9, 108). Furthermore, stretch response does not require an intact cytoskeleton. In fact, I found that treating the cells with cytochalasin resulted in an enhanced hypoosmotic stretch response. Taken together, these findings indicate that mechanical forces are transmitted to TRPC6 channels directly through the cell membrane, and actin filaments actually seem to constrain deformation of the membrane. Mechanosensitivity persists in the presence of PLC and PLA inhibitors, strongly suggesting that the stretch response is not mediated by the activation of internal signaling cascades. The fact that inhibiting PLC often prevents receptor mediated activation of TRPC6 indicates that the channels are independently regulated by chemical and mechanical stimuli.

Either addition or depletion of cholesterol can alter membrane fluidity and affect the gating of mechanosensitive channels. Cholesterol depletion is thought to increase membrane fluidity, and my results seem to support this theory. TRPC6 stretch sensitivity

was markedly enhanced in cells subjected to 24-hr cholesterol depletion. As expected, addition of cholesterol reduced TRPC6 mechanosensitivity, ostensibly by increasing membrane rigidity (14, 101).

Cholesterol's effect on membrane fluidity may only partially explain the observed alterations of TRPC6 mechanosensitivity. Podocin binds cholesterol and can associate with TRPC6 channels, and podocin homologues such as MEC-2 regulate channel mechanosensitivity in *C. elegans* (58). Cholesterol binding is essential for MEC-2 function, and a similar requirement is thought to exist for podocin function. This may explain why cholesterol depletion has such a pronounced effect on TRPC6 mechanosensitivity. By recruiting cholesterol to the lipid domain surrounding the TRPC6 channel complex, podocin creates a more rigid membrane environment. In essence this isolates the TRPC6 –podocin complex from more fluid areas of the membrane, rendering TRPC6 less responsive to membrane stretch (Illustration 6B). In podocyte cell lines that do not express podocin, stretch sensitivity is significantly greater than wild-type cells, further suggesting that podocin has a repressive effect. At the same time, knockdown of podocin has an unexpected effect on TRPC6 sensitivity to OAG. Without podocin there is no increase in TRPC6 activity after treatment with OAG (Illustration 6C). In this case it appears that podocin is required for DAG mediated activation of TRPC6 channels in podocytes (Illustration 6A). Initially, podocin's dual function appears to suggest that TRPC6 stretch sensitivity plays only a minor role in podocyte physiology. However, protein-protein interactions often depend on cellular location. In the foot process, specifically at the slit diaphragm, TRPC6 channels associate with podocin. In the cell body however, podocin is absent. Having two distinct populations of TRPC6 channels

may allow for increased chemical sensitivity in the foot processes while enhancing mechanosensitivity in the podocyte cell body. Of course the corollary of this is that TRPC6 channels in the foot processes would be less sensitive to mechanical stimulation. Because podocyte foot processes are exposed to high frequency mechanical stimulation arising from changes in capillary pressure, excessive mechanical activation of TRPC6 could potentially lead to Ca^{2+} overload and subsequent foot process effacement. The suppressant effects of podocin would be essential for preventing TRPC6 over-activation, and may explain why podocin mutations cause such severe and early onset nephrotic syndrome. In the podocyte cell body and major processes, the lack of podocin may allow TRPC6 channels that are expressed in these locations to be especially sensitive to mechanical activation. As a result, these areas of the cell would be well suited to detect sustained changes in glomerular filtration rates such as those resulting from tubuloglomerular regulation of renal blood flow (27).

6.

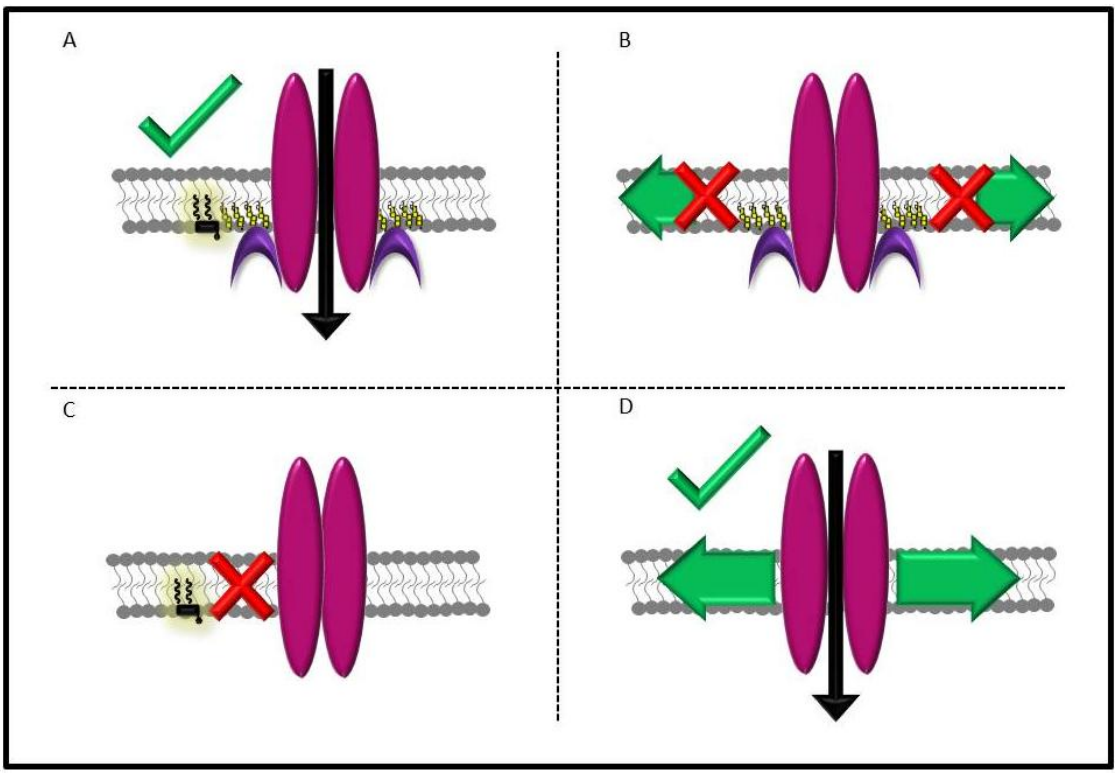

Illustration 6: Role of podocin in determining the mode of TRPC6 activation. ***A:*** Podocin is necessary for DAG-mediated activation of TRPC6 channels. ***B:*** Podocin suppresses mechanosensitivity of TRPC6 channels. Podocin associates with TRPC6 at the slit diaphragm, thereby favoring chemical activation of TRPC6 channels. ***C:*** Without podocin, TRPC6 channels are resistant to DAG activation. ***D:*** The absence of podocin allows for mechanical activation of TRPC6 channels. Podocin is absent from the podocyte cell body, and the TRPC6 channels located there are more responsive to mechanical stimuli.

Ultimately, my work shows that TRPC6 channels in podocytes can be regulated by multiple forms of chemical and mechanical stimuli. Angiotensin activates TRPC6 channels through Gαq-PLC signaling and its effects are in part dependent on the formation of ROS. Podocyte TRPC6 channels are activated by insulin receptor signaling via NOX4 and ROS. Similarly, NMDA receptors mediate TRPC6 activation in a NOX2-ROS dependent manner. In the process of studying receptor mediated TRPC6 activation I found that podocytes express NMDA receptors with several unique characteristics. Podocyte NMDA receptors show no response to the canonical agonists L-glutamate and

L-aspartate. The receptors are nevertheless functional in that NMDA, HCA, and D-aspartate all generate a robust inward current. While AT1Rs, insulin receptors, and NMDA receptors all utilize different signaling pathways, they converge on TRPC6 activation. The implication is that TRPC6 channels are at the crux of normal podocyte function and disregulation of TRPC6 may underlie many forms of nephrotic disease. Furthermore, I have shown that TRPC6 channels in podocytes are mechanosensitive and that stretch sensitivity is modulated by podocin. Podocin reduces TRPC6 sensitivity to mechanical stimulation. At the same time, podocin is required for at least one form of chemical activation of the TRPC6 channel. This suggests that podocin acts as a molecular determinate of the preferred mode of TRPC6 activation in podocytes, and may explain why mutations in either podocin or TRPC6 result in glomerular disease. Without podocin, TRPC6 channels would be overly sensitive to mechanical stimulation, potentially leading to Ca^{2+}-overload and foot process effacement. Gain of function mutations of TRPC6 can also provide an avenue for excessive Ca^{2+}-influx that could then trigger aberrant cytoskeletal rearrangement. The fact that the podocin-TRPC6 interaction only occurs in podocyte foot processes suggests that an increase in channel mechanosensitivity may trigger remodeling of the actin cytoskeleton that foreshadows foot process effacement. Drugs that selectively target and suppress TRPC6 mechanosensitivity could potentially serve as treatments for glomerular diseases. The discovery of such a clear delineation between chemical and mechanical activation of TRPC6 may prove to be a genuine turning point in renal medicine.

5 REFERENCES

1. **Anderson M, Suh JM, Kim EY, Dryer SE.** Functional NMDA receptors with atypical properties are expressed in podocytes. *Am J Physiol Cell Physiol.* 300(1): C22-32, 2011.
2. **Appel D, Kershaw DB, Smeets B, Yuan G, Fuss A, Frye B, Elger M, Kriz W, Floege J, Moeller MJ.** Recruitment of podocytes from glomerular parietal epithelial cells. *J Am Soc Nephrol* 20: 333–343, 2009.
3. **Bao L, Rapin AM, Holmstrand EC, Cox DH.** Elimination of the BK_{Ca} channel's high-affinity Ca^{2+} sensitivity. *J Gen Physiol* 120: 173–189,2002.
4. **Benzing, T**. Signaling at the slit diaphragm. *J Am So. Nephrol* 15:1382-1391, 2004.
5. **Boldyrev AA.** Molecular Mechanisms of Homocysteine Toxicity. *Biochem (Moscow)* 74: 589-598, 2009.
6. **Boulay G.** Ca^{2+}-calmodulin regulates receptor-operated Ca^{2+} entry activity of TRPC6 in HEK-293 cells. *Cell Calcium* 32: 201–207, 2002.
7. **Boulay G, Zhu X, Peyton M, Jiang M, Hurst R, Stefani E, Birnbaumer L.** Cloning and expression of a novel mammalian homolog of *Drosophila* transient receptor potential (Trp) involved in calcium entry secondary to activation of receptors coupled by the Gq class of G protein. *J Biol Chem.* 272(47): 29672-29680, 1997.
8. **Boute N, Gribouval O, Roselli S, Benessy F, Lee H, Fuchshuber A, Dahan K, Gubler MC, Niaudet P, Antignac C.** NPHS2, encoding the glomerular protein podocin, is mutated in autosomal recessive steroidresistant nephrotic syndrome. *Nat Genet* 24: 349–354, 2000.
9. **Bowman CL, Gottlieb PA, Suchyna TM, Murphy YK, Sachs F.** Mechanosensitive ion channels and the peptide inhibitor GsMTx-4: history, properties, mechanisms and pharmacology. *Toxicon.* 49(2): 249-70, 2006.
10. **Brown DI, Griendling KK**. Nox proteins in signal transduction. *Free Radic Biol Med.* 47(9): 1239-1253, 2009.
11. **Butler JN.** The thermodynamic activity of calcium ion in sodium chloride-calcium chloride electrolytes. *Biophys J* 8: 1426-1433, 1968.
12. **Cavara NA, Hollmann M**. Shuffling the Deck Anew: How NR3 tweaks NMDA receptor function. *Mol Neurobiol* 38: 16-26, 2008.
13. **Cayouette S, Lussier MP, Mathieu EL, Bousquet SM, Boulay G.** Exocytotic insertion of TRPC6 channel into the plasma membrane upon Gq protein-coupled receptor activation. *J Biol Chem* 279: 7241–7246, 2004.

14. **Chang HM, Reitstetter R, Mason RP, Gruener R.** Attenuation of channel kinetics and conductance by cholesterol: an interpretation using structural stress as a unifying concept. *J Membr Biol* 143: 51–63, 1995.
15. **Choi DW.** Excitotoxic cell death. *J Neurobiol* 23: 1261-1276, 1992.
16. **Chrissobolis S, Banfi B, Sobey CG, Faraci FM.** Role of Nox isoforms in angiotensin II-induced oxidative stress and endothelial dysfunction in brain. *J Appl Physiol* 113(2): 184-191, 2012.
17. **Clapham, DE.** TRP Channels. http://clapham.tch.harvard.edu/publications/pdf/TRP%20WEB%2003.pdf. *Clapham Website*, 2003.
18. **Danysz W, Parsons CG.** Glycine and N-methyl-D-aspartate receptors: Physiological Significance and Possible Therapeutic Applications. *Pharmacological Reviews* 50: 597-650, 1998.
19. **Deng A, Thomson SC.** Renal NMDA receptors independently stimulate proximal reabsorption and glomerular filtration. *Am J Physiol Renal Physiol* 296: F976-982, 2009.
20. **Dietrich A, Chubanov V, Gudermann T.** Renal TRPathies. *J Am Soc Nephrol* 21: 736-744, 2010.
21. **Dietrich A, Kalwa H, Rost BR, Gudermann T.** The diacylgylcerolsensitive TRPC3/6/7 subfamily of cation channels: functional characterization and physiological relevance. *Pflügers Arch* 451: 72–80, 2005.
22. **Dietrich A, Mederos y Schnitzler M, Emmel J, Kalwa H, Hofmann T, Gudermann T.** N-linked protein glycosylation is a major determinant for basal TRPC3 and TRPC6 channel activity. *J Biol Chem* 278: 47842–47852, 2003.
23. **Dietrich A, Mederos Schnitzler MY, Gollasch M, Gross V, Storch U, Dubrovska G, Obst M, Yildirim E, Salanova B, Kalwa H, Essin K, Pinkenburg O, Luft FC, Gudermann T, Birnbaumer L.** Increased vascular smooth muscle contractility in TRPC6-/- mice. *Mol Cell Biol* 25: 6980–6989, 2005.
24. **Dijkman H, Assmann KJM, Steenbergen EJ.** The podocyte and parietal epithehial cell in proteinuria and glomerulosclerosis. *Nephrol Iss Exper Research* 12: 42-46, 2007.
25. **Ding G, Reddy K, Kapasi AA, Franki N, Gibbons N, Kasinath BS, Singhal PC.** Angiotensin II induces apoptosis in rat glomerular epithelial cells. *Am J Physiol Renal Physiol* 283: F173–F180, 2002.
26. **Drenckhahn D, Franke RP.** Ultrastructural organization of contractile and cytoskeletal proteins in glomerular podocytes of chicken, rat, and man. *Lab Invest* 59: 673–682, 1988.

27. **Dryer SE, Reiser J.** TRPC6 channels and their binding partners in podocytes: role in glomerular filtration and pathophysiology. *Am J Physiol Renal Physiol* 299: F689-701, 2010.
28. **Dunlop DS, Neidle A, McHale D, Dunlop DM, Lajtha A.** The presence of free D-aspartic acid in rodents and man. *Biochem Biophys Res Commun* 141: 27-32, 1986.
29. **Dyachenko V, Husse B, Rueckschloss U, Isenberg G.** Mechanical deformation of ventricular myocytes modulates both TRPC6 and Kir2.3 channels. *Cell Calcium* 45: 38–54, 2009.
30. **Eid SR, Cortright DN.** Transient receptor potential channels on sensory nerves. *Handb Exp Pharmacol* 194: 261–281, 2009.
31. **Endlich N, Endlich K.** Stretch, tension and adhesion - adaptive mechanisms of the actin cytoskeleton in podocytes. *Eur J Cell Biol.* 85(3-4): 229-234, 2006.
32. **Endlich N, Kress KR, Reiser J, Uttenweiler D, Kriz W, Mundel P, Endlich K.** Podocytes respond to mechanical stress in vitro. *J Am Soc Nephrol* 12: 413–422, 2001.
33. **Estacion M, Sinkins WG, Jones SW, Applegate MA, Schilling WP.** Human TRPC6 expressed in HEK 293 cells forms non-selective cation channels with limited Ca^{2+} permeability. *J Physiol* 572: 359–377, 2006.
34. **Faul C, Asanuma K, Yanagida-Asanuma E, Kim K, Mundel P.** Actin up: regulation of podocyte structure and function by components of the actin cytoskeleton. *Trends Cell Biol* 17: 428–437, 2007.
35. **Fogo AB, Kon V.** The glomerulus-a view from the inside-the endothelial cell. *Int J Biochem Cell Biol.* 42(9): 1388-1397, 2010.
36. **Francis ME, Eggers PW, Hostetter TH, Briggs JP.** Association between serum homocysteine and markers of impaired kidney function in adults in the United States. *Kidney Int* 66: 303-312, 2004.
37. **Friedrich C, Endlich N, Kriz W, Endlich K.** Podocytes are sensitive to fluid shear stress in vitro. *Am J Physiol Renal Physiol* 291: F856–F865, 2006.
38. **Giardino L, Armelloni S, Corbelli A, Mattinzoli D, Zennaro C, Guerrot D, Tourrel F, Ikehata M, Li M, Berra S, Carraro M, Messa P, Rastaldi MP.** Podocyte glutamatergic signaling contributes to the function of the glomerular filtration barrier. *J Am Soc Nephrol* 20: 1929-1940, 2009.
39. **Gottlieb P, Folgering J, Maroto R, Raso A, Wood TG, Kurosky A, Bowman C, Bichet D, Patel A, Sachs F, Martinac B, Hamill OP, Honoré E.** Revisiting TRPC1 and TRPC6 mechanosensitivity. *Pflügers Arch* 455: 1097–1103, 2008.
40. **Graham S, Ding M, Ding Y, Sours-Brothers S, Luchowski R, Gryczynski Z, Yorio T, Ma H, Ma R.** Canonical transient receptor potential 6 (TRPC6), a redox-regulated cation channel. *J Biol Chem* 285(30):23466-23476, 2010.

41. **Greka A, Mundel P.** Balancing Calcium Signals through TRPC5 and TRPC6 in Podocytes. *J Am Soc Nephrol* 22: 1969 –1980, 2011.
42. **Grimwood S, Moseley AM, Carling RW, Leeson PD, Foster AC.** Characterization of the binding of [^{3}H]L-689,560, an antagonist for the glycine site on the *N*-methyl-D-aspartate receptor, to rat brain membranes. *Mol Pharmacol* 41: 923-930, 1992.
43. **Gruden G, Perin PC, Camussi G.** Insight on the pathogenesis of diabetic nephropathy from the study of podocyte and mesangial cell biology. *Curr Diabetes Rev* 1: 27-40, 2005.
44. **Gudermann T, Hofmann T, Mederos y Schnitzler M, Dietrich A.** Activation, subunit composition and physiological relevance of DAG sensitive TRPC proteins. *Novartis Found Symp* 258: 103–118, 2004.
45. **Gu L, Liang X, Wang L, Yan Y, Ni Z, Dai H, Gao J, Mou S, Wang Q, Chen X, Wang L, Qian J.** Functional metabotropic glutamate receptors 1 and 5 are expressed in murine podocytes. *Kidney Int* 81(5): 458-468, 2012.
46. **Haraldsson B, Nyström J, Deen WM.** Properties of the glomerular barrier and mechanisms of proteinuria. *Physiol Rev* 88: 451–487, 2008.
47. **Harita Y, Kurihara H, Kosako H, Tezuka T, Sekine T, Igarashi T, Ohsawa I, Ohta S, Hattori S**. Phosphorylation of Nephrin Triggers Ca2+ Signaling by Recruitment and Activation of Phospholipase C-γ 1. *J Biol Chem* 284(13): 8951-8962, 2009.
48. **Heeringa SF, Möller CC, Du J, Yue L, Hinkes B, Chernin G, Vlangos CN, Hoyer PF, Reiser J, Hildebrandt F.** A novel TRPC6 mutation that causes childhood FSGS. *PLoS One* 4: e7771, 2009.
49. **Henger A, Huber T, Fischer KG, Nitschke R, Mundel P, Schollmeyer P, Greger R, Pavenstädt H.** Angiotensin II increases the cytosolic calcium activity in rat podocytes in culture. *Kidney Int* 52: 687–693, 1997.
50. **Hisatsune C, Kuroda Y, Nakamura K, Inoue T, Nakamura T, Michikawa T, Mizutani A, Mikoshiba K.** Regulation of TRPC6 channel activity by tyrosine phosphorylation. *J Biol Chem* 279: 18887–18894, 2004.
51. **Hofmann T, Obukhov AG, Schaefer M, Harteneck C, Gudermann T, Schultz G.** Direct activation of human TRPC6 and TRPC3 channels by diacylglycerol. *Nature* 397: 259–263, 1999.
52. **Hsu YJ, Hoenderop JG, Bindels RJ.** TRP channels in kidney disease. *Biochim Biophys Acta* 1772(8): 928-936, 2007.
53. **Huang M, Gu G, Ferguson EL, Chalfie M.** A stomatin-like protein necessary for mechanosensation in *C. elegans. Nature* 378: 292–295, 1995.
54. **Huber TB, Benzing T.** The slit diaphragm: a signaling platform to regulate podocyte function. *Curr Opin Nephrol Hypertens* 14: 211–216, 2005.

55. **Huber TB, Gloy J, Henger A, Schollmeyer P, Greger R, Mundel P, Pavenstädt H.** Catecholamines modulate podocyte function. *J Am Soc Nephrol* 9: 335-345, 1998.
56. **Huber TB, Kottgen M, Schilling B, Walz G, Benzing T.** Interaction with podocin facilitates nephrin signaling. *J Biol Chem* 276: 41543–41546, 2001.
57. **Huber TB, Kwoh C, Wu H, Asanuma K, Gödel M, Hartleben B, Blumer KJ, Miner JH, Mundel P, Shaw AS.** Bigenic mouse models of focal segmental glomerulosclerosis involving pairwise interaction of CD2AP, Fyn, and synaptopodin. *J Clin Invest* 116: 1337–1345, 2006.
58. **Huber TB, Schermer B, Müller RU, Höhne M, Bartram M, Calixto A, Hagmann H, Reinhardt C, Koos F, Kunzelmann K, Shirokova E, Krautwurst D, Harteneck C, Simons M, Pavenstädt H, Kerjaschki D, Thiele C, Walz G, Chalfie M, Benzing T.** Podocin and MEC-2 bind cholesterol to regulate the activity of associated ion channels. *Proc NatlAcad Sci USA* 103: 17079–17086, 2006.
59. **Hunt JL, Pollak MR, Denker BM.** Cultured podocytes establish a size-selective barrier regulated by specific signaling pathways and demonstrate synchronized barrier assembly in a calcium switch model of junction formation. *J Am Soc Nephrol* 16: 1593–1602, 2005.
60. **Ichimura K, Kurihara H, Sakai T.** Actin filament organization of foot processes in vertebrate glomerular podocytes. *Cell Tissue Res* 329:541–557, 2007.
61. **Inoue R, Jensen LJ, Jian Z, Shi J, Hai L, Lurie AI, Henriksen FH, Salomonsson M, Morita H, Kawarabayashi Y, Mori M, Mori Y, Ito Y.** Synergistic activation of vascular TRPC6 channel by receptor and mechanical stimulation via phospholipase C/diacylglycerol and phospholipase A2/omega-hydroxylase/20-HETE pathways. *Circ Res.* 104(12): 1399-1409, 2009.
62. **Jahr CE, Stevens CF.** Calcium permeability of the *N*-methyl-D-aspartate receptor channel in hippocampal neurons in culture. *Proc Natl Acad Sci USA* 90: 11573-11577, 1993.
63. **Johnson JW, Ascher P.** Glycine potentiates the NMDA response in cultured mouse brain neurons. *Nature* 325: 529-531, 1987.
64. **Jung S, Mühle A, Schaefer M, Strotmann R, Schultz G, Plant TD.** Lanthanides potentiate TRPC5 currents by an action at extracellular sites close to the pore mouth. *J Biol Chem.* 278(6): 3562-3571, 2003.
65. **Kim EY, Alvarez-Baron CP, Dryer SE.** Canonical transient receptor potential channel (TRPC) 3 and TRPC6 associate with large-conductance Ca^{2+}-activated $^{K+}$ (BK_{Ca}) channels: role in BK_{Ca} trafficking to the surface of cultured podocytes. *Mol Pharmacol* 75(3): 466–477, 2009.

66. **Kim EY, Anderson M, Dryer SE.** Insulin increases surface expression of TRPC6 channels in podocytes: role of NADPH oxidases and reactive oxygen species. *Am J Physiol Renal Physiol* 302: F298-F307, 2012.
67. **Kim EY, Anderson M, Dryer SE.** Sustained activation of N-methyl-D-aspartate receptors in podoctyes leads to oxidative stress, mobilization of transient receptor potential canonical 6 channels, nuclear factor of activated T cells activation, and apoptotic cell death. *Mol Pharmacol.* 82(4): 728-737, 2012.
68. **Kim EY, Dryer SE.** Effects of insulin and high glucose on mobilization of slo1 BK_{Ca} channels in podocytes. *J Cell Physiol.* 226(9): 2307-2315, 2011.
69. **Kim EY, Suh JM, Chiu YH, Dryer SE.** Regulation of podocyte BK(Ca) channels by synaptopodin, Rho, and actin microfilaments. *Am J Physiol Renal Physiol* 299(3): F594-604, 2010.
70. **Kim JP, Koh JY, Choi DW.** L-homocysteate is a potent neurotoxin on cultured cortical neurons. *Brain Res* 437: 103-110, 1987.
71. **Kim PM, Duan X, Huang AS, Liu CY, Ming GL, Song H, Snyder SH.** Aspartate racemase, generating neuronal D-aspartate, regulates adult neurogenesis. *Proc Natl Acad Sci USA* 107: 3175-3179, 2010.
72. **Krall P, Canales CP, Kairath P, Carmona-Mora P, Molina J, Carpio JD, Ruiz P, Mezzano SA, Li J, Wei C, Reiser J, Young JI, Walz K.** Podocyte-specific overexpression of wild type or mutant trpc6 in mice is sufficient to cause glomerular disease. *PLoS One.* 5(9): e12859, 2010.
73. **Kriz W, Elger M, Mundel P, Lemley KV.** Structure stabilizing forces in the glomerular tuft. *J Am Soc Nephrol* 5: 1731-1739, 1995.
74. **Kriz W, Hackenthal E, Nobiling R, Sakai T, Elger M, Hähnel B.** A role for podocytes to counteract capillary wall distension. *Kidney Int* 45: 369–376, 1994.
75. **Kriz W, Hosser H, Hahnel B, Simons JL, Provoost AP.** Development of vascular pole-associated glomerulosclerosis in the fawn-hooded rat. *J Am Soc Nephrol* 9: 381-396, 1998.
76. **Makhro A, Wang J, Vogel J, Boldyrev AA, Gassmann M, Kaestner L, Bogdanova A.** Functional NMDA receptors in rat erythrocytes. *Am J Physiol Cell Physiol* 298: C1315-C1325, 2010.
77. **Mashkina AP, Cizkova D, Vanicky I, Boldyrev AA**. NMDA receptors are expressed in lymphocytes activated both in vitro and in vivo. *Cell Mol Neurobiol* 30(6): 901-907, 2010.
78. **Mayer ML, Armstrong N**. Structure and function of glutamate receptor ion channels. *Annu Rev Physiol* 66: 161-181, 2004.
79. **Mayer ML, Westbrook GL.** Permeation and block of *N*-methyl-D-aspartic acid receptor channels by divalent cations in mouse cultured central neurones. *J Physiol* 394: 501-527, 1987.

80. **Mayer ML, Westbrook GL, Guthrie PB.** Voltage-dependent block by Mg^{2+} of NMDA responses in spinal cord neurones. *Nature* 309: 261-263, 1984.
81. **Merritt JE, Armstrong WP, Benham CD, Hallam TJ, Jacob R, Jaxa-Chamiec A, Leigh BK, McCarthy SA, Moores KE, Rink TJ.** SK&F 96365, a novel inhibitor of receptor-mediated calcium entry. *Biochem J.* 15;271(2): 515-522, 1990.
82. **Möller CC, Wei C, Altintas MM, Li J, Greka A, Ohse T, Pippin JW, Rastaldi MP, Wawersik S, Schiavi S, Henger A, Kretzler M, Shankland SJ, Reiser J.** Induction of TRPC6 channel in acquired forms of proteinuric kidney disease. *J Am Soc Nephrol* 18: 29-36, 2007.
83. **Morton MJ, Hutchinson K, Mathieson PW, Witherden IR, Saleem MA, Hunter M.** Human podocytes possess a stretch-sensitive, Ca^{2+}-activated K^+ channel: potential implications for the control of glomerular filtration. *J Am Soc Nephrol* 15: 2981–2987, 2004.
84. **Mothet JP, Parent AT, Wolosker H, Brady RO Jr, Linden DJ, Ferris CD, Rogawski MA, Snyder SH.** D-serine is an endogenous ligand for the glycine site of the *N*-methyl-D-aspartate receptor. *Proc Natl Acad Sci USA* 97: 4926-4931, 2000.
85. **Müller A, Kukley M, Uebachs M, Beck H, Dietrich D.** Nanodomains of single Ca^{2+} channels contribute to action potential repolarization in cortical neurons. *J Neurosci* 27: 483–495, 2007.
86. **Neal CR, Crook H, Bell E, Harper SJ, Bates DO.** Three-dimensional reconstruction of glomeruli by electron microscopy reveals a distinct restrictive urinary subpodocyte space. *J Am Soc Nephrol* 16(5): 1223–1235, 2005.
87. **Neal CR, Muston PR, Njegovan D, Verrill R, Harper SJ, Deen WM, Bates DO.** Glomerular filtration into the subpodocyte space is highly restricted under physiological perfusion conditions. *Am J Physiol Renal Physiol* 293(6): F1787–F1798, 2007.
88. **Nijenhuis T, Sloan AJ, Hoenderop JG, Flesche J, van Goor H, Kistler AD, Bakker M, Bindels RJ, de Boer RA, Möller CC, Hamming I, Navis G, Wetzels JF, Berden JH, Reiser J, Faul C, van der Vlag J.** Angiotensin II contributes to podocyte injury by increasing TRPC6 expression via an NFAT-mediated positive feedback signaling pathway. *Am J Pathol.* 179(4): 1719-1732, 2011.
89. **Olney JW, Price MT, Salles KS, Labruyere J, Ryerson R, Mahan K, Frierdich G, Samson L.** L-homocysteic acid: an endogenous excitotoxic ligand of the NMDA receptor. *Brain Res Bull.* 19(5):597-602, 1987.
90. **Paoletti P, Neyton J.** NMDA receptor subunits: function and pharmacology. *Curr Opinion in Pharma* 7: 39-47, 2007.

91. **Patel A, Sharif-Naeini R, Folgering JR, Bichet D, Duprat F, Honoré E.** Canonical TRP channels and mechanotransduction: from physiology to disease states. *Pflugers Arch.* 460(3): 571-581, 2010.
92. **Patneau DK, Mayer ML.** Structure-activity relationships for amino acid transmitter candidates acting at *N*-methyl-D-aspartate and quisqualate receptors. *J Neurosci* 10: 2385-2399, 1990.
93. **Patton K, Thibodeau GA.** Anatomy and physiology, 7th edition. *Elsevier Inc* 952-963, 2010.
94. **Priestley T, Woodruff GN, Kemp JA.** Antagonism of responses to excitatory amino acids on rat cortical neurones by the spider toxin, argiotoxin 636. *Br J Pharmacol* 97: 1315-1323 1989.
95. **Putaala H, Soininen R, Kilpeläinen P, Wartiovaara J, Tryggvason K.** The murine nephrin gene is specifically expressed in kidney, brain and pancreas: inactivation of the gene leads to massive proteinuria and neonatal death. *Hum Mol Genet* 10: 1-8, 2001.
96. **Rastaldi MP, Armelloni S, Berra S, Calvaresi N, Corbelli A, Giardino LA, Li M, Wang GQ, Fornasieri A, Villa A, Heikkila E, Soliymani R, Boucherot A, Cohen CD, Kretzler M, Nitsche A, Ripamonti M, Malgaroli A, Pesaresi M, Forloni GL, Schlöndorff D, Holthofer H, D'Amico G.** Glomerular podocytes contain neuron-like functional synaptic vesicles. *FASEB J* 20: 976-978, 2006.
97. **Rebola N, Srikumar BN, Mulle C.** Activity-dependent synaptic plasticity of NMDA receptors. *J Physiol* 588: 93-99 2010.
98. **Reiser J, Polu KR, Möller CC, Kenlan P, Altintas MM, Wei C, Faul C, Herbert S, Villegas I, Avila-Casado C, et al.** TRPC6 is a glomerular slit diaphragm-associated channel required for normal renal function. *Nature Genetics* 37: 739-744, 2005.
99. **Schaefer M, Plant TD, Obukhov AG, Hofmann T, Gudermann T, Schultz G.** Receptor-mediated regulation of the nonselective cation channels TRPC4 and TRPC5. *J Biol Chem* 275: 17517–17526, 2000.
100. **Schell MJ.** The N-methyl-D-aspartate receptor glycine site and D-serine metabolism: an evolutionary perspective. *Phil Trans R Soc Lond* 359: 943-964, 2004.
101. **Schermer B, Benzing T.** Lipid-protein interactions along the slit diaphragm of podocytes. *J Am Soc Nephrol*. 20(3): 473-478, 2009.
102. **Schlöndorff J, Del Camino D, Carrasquillo R, Lacey V, Pollak MR.** TRPC6 mutations associated with focal segmental glomerulosclerosis cause constitutive activation of NFAT-dependent transcription. *Am J Physiol Cell Physiol.* 296(3):C558-C569, 2009.

103. **Sen U, Munjal C, Qipshidze N, Abe O, Gargoum R, Tyagi SC.** Hydrogen sulfide regulates homocysteine-mediated glomerulosclerosis. *Am J Nephrol*. 31(5): 442-455, 2010.

104. **Shirato I.** Podocyte process effacement in vivo. *Microsc Res Tech* 57: 241-246, 2002.

105. **Shirato I, Sakai T, Kimura K, Tomino Y, Kriz W.** Cytoskeletal changes in podocytes associated with foot process effacement in Masugi nephritis. *Am J Pathol.* 148(4): 1283-1296, 1996.

106. **Shu Q, Savage JE, Hufeisen SJ, Rauser L, Grajkowska E, Ernsberger P, Wroblewski JT, Nadeau JH, Roth BL.** L-Homocysteine sulfonic acid and other acidic homocysteine derivatives are potent and selective metabotropic glutamate receptor agonists. *J Pharma and Experim Therap* 305: 131-142, 2003.

107. **Spassova MA, Hewavitharana T, Xu W, Soboloff J, Gill DL.** A common mechanism underlies stretch activation and receptor activation of TRPC6 channels. *Proc Natl Acad Sci U S A*. 103(44): 16586-16591, 2006.

108. **Suchyna TM, Johnson JH, Hamer K, Leykam JF, Gage DA, Clemo HF, Baumgarten CM, Sachs F.** Identification of a peptide toxin from Grammostola spatulata spider venom that blocks cation-selective stretch-activated channels. *J Gen Physiol.* 115(5): 583-598, 2000.

109. **Tian D, Jacobo SM, Billing D, Rozkalne A, Gage SD, Anagnostou T, Pavenstädt H, Hsu HH, Schlondorff J, Ramos A, and Greka A.** Antagonistic regulation of actin dynamics and cell motility by TRPC5 and TRPC6 channels. *Sci Signal* 3(145): ra77, 2010.

110. **Truesdell AH.** Activity coefficients of aqueous sodium chloride from 15° to 50°C measured with a glass electrode. *Science* 161: 884–886, 1968.

111. **Wang Z, Wei X, Zhang Y, Ma X, Li B, Zhang S, Du P, Zhang X, and Yi F.** NADPH oxidase-derived ROS contributes to upregulation of TRPC6 expression in puromycin aminonucleoside-induced podocyte injury. *Cell Physiol Biochem* 24: 619-626, 2009.

112. **Winn MP, Conlon PJ, Lynn KL, Farrington MK, Creazzo T, Hawkins AF, Daskalakis N, Kwan SY, Ebersviller S, Burchette JL, et al.** A mutation in the TRPC6 cation channel causes familial focal segmental glomerulosclerosis. *Science* 308: 1801-1804, 2005.

113. **Wolosker H.** NMDA receptor regulation by D-serine: new findings and perspectives. *Mol Neurobiology* 36: 152-164, 2007.

114. **Wolosker H, Blackshaw S, Snyder SH.** Serine racemase: a glial enzyme synthesizing D-serine to regulate glutamate-*N*-methyl-D-aspartate neurotransmission. *Proc Natl Acad Sci USA* 96: 13409-13414, 1999.
115. **Xia M, Liu Y, Figueroa DJ, Chiu CS, Wei N, Lawlor AM, Lu P, Sur C, Koblan KS, Connolly TM.** Characterization and localization of a human serine racemase. *Brain Res Mol Brain Res* 125: 96-104, 2004.
116. **Yang CC, Chien CT, Wu MH, Ma MC, Chen CF.** NMDA receptor blocker ameliorates ischemia-reperfusion-induced renal dysfunction in rat kidneys. *Am J Physiol Renal Physiol* 294: F1433-F1440, 2008.
117. **Yashiro K, Philpot BD.** Regulation of NMDA receptor subunit expression and its implications for LTD, LTP, and metaplasticity. *Neurophrama* 55: 1081-1094, 2008.
118. **Yi F, dos Santos EA, Xia M, Chen QZ, Li PL,and Li N**. Podocyte injury and glomerulosclerosis in hyperhomocysteinemic rats. *Am J Nephrol* 27: 262-268, 2007.
119. **Zhang C, Yi F, Xia M, Boini KM, Zhu Q, Laperle LA, Abais JM, Brimson CA, and Li PL.** NMDA receptor-mediated activation of NADPH oxidase and glomerulosclerosis in hyperhomocysteinemic rats. *Antioxid Redox Signal* 13: 975-986, 2010.
120. **Zhang C, Hu JJ, Xia M, Boini KM, Brimson C, and Li PL.** Redox signaling via lipid raft clustering in homocysteine-induced injury of podocytes. *Biochim Biophys Acta* 1803: 482-491, 2010.